INVESTIGATIONS INTO THE ROLE OF STRESS GRANULE FORMATION DURING RESPIRATORY SYNCYTIAL VIRUS INFECTION

By

Michael Edward Lindquist

Dissertation

Submitted to the Faculty of the

Graduate School of Vanderbilt University

in partial fulfillment of the requirements

for the degree of

DOCTOR OF PHILOSOPHY

In

Microbiology and Immunology

May, 2011

Nashville, Tennessee

Approved:

Terence Dermody

Mark Denison

James Goldenring

Christopher Aiken

James Crowe

ACKNOWLEDGEMENTS

I would like to extend my heartfelt gratitude to the many people I have had the pleasure of working with while at Vanderbilt University. First, I thank my mentor, Dr. James Crowe, for the insight, encouragement, and enthusiasm he has provided to me. His love and passion for excellent science is unrivaled and I hope that I can carry on that tradition. I would also like to thank Jim for providing me with such an excellent work environment. I owe many debts to my coworkers, both present and past, who have taken the time to help me with the development and execution of all of my experiments. I would also like to thank the Department of Microbiology and Immunology, especially Dr. Jacek Hawiger for assembling such an amazing collection of bright scientists.

I would like to thank the members of my thesis committee, Drs. Terence Dermody, Mark Denison, Chris Aiken, and James Goldenring. Their guidance and suggestions have been instrumental in the development of my project and my development as a scientist. I would also like to thank my wonderful collaborators. Dr. Philip Santangelo at the Georgia Institute of Technology has shared countless reagents and ideas with us. Drs. Bernardo Mainou and Elena Kolobova have also given considerable time and reagents to my work. I also thank my funding sources, including the Burroughs Wellcome Fund and a research grant from the March of Dimes.

Most of all I want to thank my friends and family for their unending support. Especially my parents, who have always encouraged me to do what I believe in. I am incredibly lucky to have been blessed with such undying support.

TABLE OF CONTENTS

LIST OF TABLES

LIST OF FIGURES

LIST OF ABBREVIATIONS

2-AP	2-aminopurine
dsRNA	double-stranded RNA
eIF	eukaryotic initiation factor
F	fusion protein
G	attachment protein
G3BP	ras-GAP SH3 domain binding protein
GCN2	general control nonrepressed 2
HCV	hepatitis C virus
HPF	high-powered field
HRI	heme-regulated inhibitor
HSP	heat shock protein
IFN	interferon
IL	interleukin
L	polymerase protein
M	matrix protein
MEF	mouse embryo fibroblast
MOI	multiplicity of infection
N	nucleoprotein
NS	nonstructural
P	phosphoprotein
PKR	protein kinase r

PERK	PKR-like ER-localized eIF2α kinase
RSV	respiratory syncytial virus
RIG-I	retinoic acid-inducible gene I
RRV	rhesus rotavirus
shRNA	short-hairpin RNA
SH	Small hydrophobic protein
siRNA	small-interfering RNA
TIA-1	T-cell intracytoplasmic antigen
TLR	Toll-Like Receptor

CHAPTER I

INTRODUCTION

Thesis Overview

The experiments described in this thesis were designed to elucidate the role that stress granule formation plays in respiratory syncytial virus (RSV) infection. In Chapter I, I provide a brief background of RSV, host stress granules, and interactions between RSV and the innate immune system. In Chapter II, I present my research examining the kinetics of stress granule formation during RSV infection. I demonstrate that stress granules form during RSV infection and they may play an important role in viral replication. In Chapter III, I examine the upstream signaling pathways utilized by RSV to initiate stress granule formation. I show that RSV infection induces the activation of PKR, which in turn phosphorylates eIF2α and is responsible stress granules formation. I then show that reduction of PKR protein levels by shRNA does not affect RSV replication. However, the PKR inhibitor, 2-aminopurine, significantly impairs RSV replication. Chapter IV summarizes our observations and offers potential future experiments that will be useful to continue this work.

Respiratory syncytial virus

Human respiratory syncytial virus (RSV) represents a leading cause of serious lower respiratory tract illness in infants, the elderly, and immunocompromised individuals worldwide. First discovered in 1956, the virus remains a prime target for

vaccine development due to the frequency of infection and the potential for severe disease. Disease associated with RSV infection ranges from mild to severe and typical symptoms include runny nose, fever, and coughing while in more severe cases wheezing and difficulties in breathing may occur

RSV belongs to the subfamily *Pneumovirinae* of the *Paraxmyxoviridae* family and is a member of the *Mononegavirales* order. The virion consists of a host-derived lipid membrane containing three virally derived surface proteins that surrounds the viral nucleocapsid. Viral particles are typically observed as small pleomorphic particles around 200 nm in diameter, or as long filamentous particles reaching up to 10 μM in length (Roberts et al., 1995). An illustration of a virion particle can be found in Figure 1-1. The RSV genome comprises 15,222 bases that encode nine structural and two nonstructural proteins. The two nonstructural proteins, NS1 and NS2, function as interferon antagonists. The viral genome, nucleoprotein (N), phosphoprotein (P), and polymerase protein (L) assemble to form the viral ribonucleoprotein complex that is responsible for transcription of viral genes and replication of the viral genome. The glycoprotein (G) and fusion protein (F) are virion surface proteins responsible for

attachment and entry of the virion into host cells, respectively (Levine et al., 1987). The small hydrophobic (SH) protein is also expressed on the surface of virion particles and has been predicted to function in enhancing membrane permeability (Carter et al., 2010). The matrix (M) protein is found inside the virion particle and is necessary for particle morphogenesis. Finally, the M2-1 and M2-2 proteins play important roles in transcription processivity and replication initiation, respectively (Fearns and Collins, 1999) (Bermingham and Collins, 1999). See Table 1-1 for a list of the viral proteins

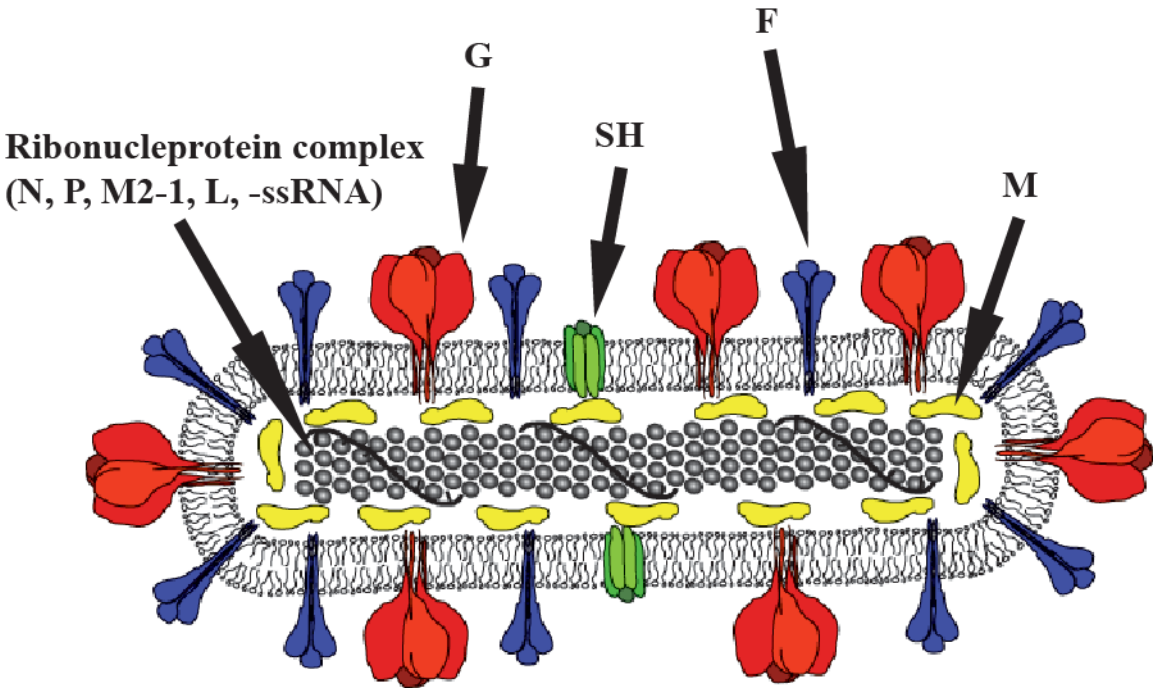

Figure 1-1. The RSV virion. RSV surface proteins (G, SH, and F) are shown on the membrane of the particle while the internal proteins associate with the genome. Figure provided by Tom Utley.

and their functions.

The first step in the viral life cycle involves the virion particle attaching to host cells through an interaction between the viral G protein and cellular glycosaminoglycans, particularly heparan sulfate and chondroitin sulfate B (Feldman et al., 2000). RSV F then mediates fusion between the virion envelope and the plasma membrane. Following fusion, the nucleocapsid is released into the cytoplasm where transcription of viral genes begins using the RNA-dependent viral RNA polymerase. Transcription occurs in a polar gradient with genes proximal to the 3′ terminus of the genome produced in greater abundance than those located closer to the 5′ terminus. Transcription and translation of viral proteins likely begins immediately upon release of the nucleocapsid into the cytoplasm. In contrast, replication of the viral genome is delayed following infection. The three surface proteins are glycosylated and can be detected within the endoplasmic reticulum and Golgi apparatus as well as at the plasma membrane. The N, P, L, M, and M2-1 proteins localize to cytoplasmic viral inclusion bodies. Figure 1-2 is a confocal image showing inclusion bodies and filaments in RSV infected cells.

For replication to occur, the RNA-dependent viral RNA polymerase must produce an antigenomic intermediate that is then used as a template for progeny genomes. The components of the virion assemble at the host plasma membrane and budding of new infectious virions occurs. In polarized cells, assembly and budding occur exclusively at the apical surface of infected cells. Interestingly, the majority of newly formed particles do not bud from the host cell but instead remain cell associated. Figure 1-3 provides an illustration of the viral life cycle.

Table 1-1. The RSV proteins and their functions.

	Gene	Protein	Size (kD)	Function
Nonstructural	NS1	Non-structural 1	13.8	Inhibitor of IFN
	NS2	Non-structural 2	14.5	Inhibitor of IFN
Polymerase complex	N	Nucleoprotein	45	Binds vRNA
	P	Phosphoprotein	29-33	Binds N and L
	M2	Matrix 2 (Orf 1&2)	22/11	Transcription processivity
	L	Polymerase	250	Major polymerase subunit
Matrix	M	Matrix	25	Filament formation
Surface protein	SH	Small Hydrophobic	7.5-60	Unknown
	G	Glycoprotein	90	Attachment
	F	Fusion	70	Fusion

Interactions between RSV and cellular proteins

The interactions between host proteins and RSV proteins have thus far been poorly defined. Multiple proteins have been shown to bind or colocalize with RSV proteins; however, the exact functions or roles for the majority of these proteins on infection are unknown. The chaperone protein heat shock protein 70 (HSP70) colocalizes with viral inclusion bodies during infection. Additionally, an interaction between the viral polymerase complex and HSP70 was demonstrated through immunoprecipitation (Brown et al., 2005). Another HSP, HSP90, colocalizes with RSV F in viral filaments. In experiments in which HSP90 expression of function was inhibited, RSV transmission and filament formation were reduced, suggesting HSP90 is important in either viral assembly or egress (Radhakrishnan et al., 2010). The Rab11a family interacting protein 2 (Rab11-FIP2) is essential for proper RSV budding. Deletion of the N-terminal C2 domain resulted in a block to viral egress and the wild-type protein colocalized with viral inclusion bodies and viral filaments (Utley et al., 2008). In addition to Rab11-FIP2, the integral membrane protein caveolin-1 is known to associate with viral particles (Brown et al., 2002).

Experiments examining RNA transcription *in vitro* indicate that the cellular cytoskeleton protein actin is important for viral transcription (Burke et al., 1998).When chemical inhibitors of actin or microtubule assembly were used, viral egress and budding were negatively affected, respectively (Kallewaard et al., 2005). Inhibition of the actin-associated protein, profilin, also resulted in a decrease in viral transcription (Burke et al., 2000). Actin also associates with viral inclusion bodies (Brown et al., 2005). Actin binds the N protein-encapsidated viral RNA, and profilin then binds the actin-RNA structure.

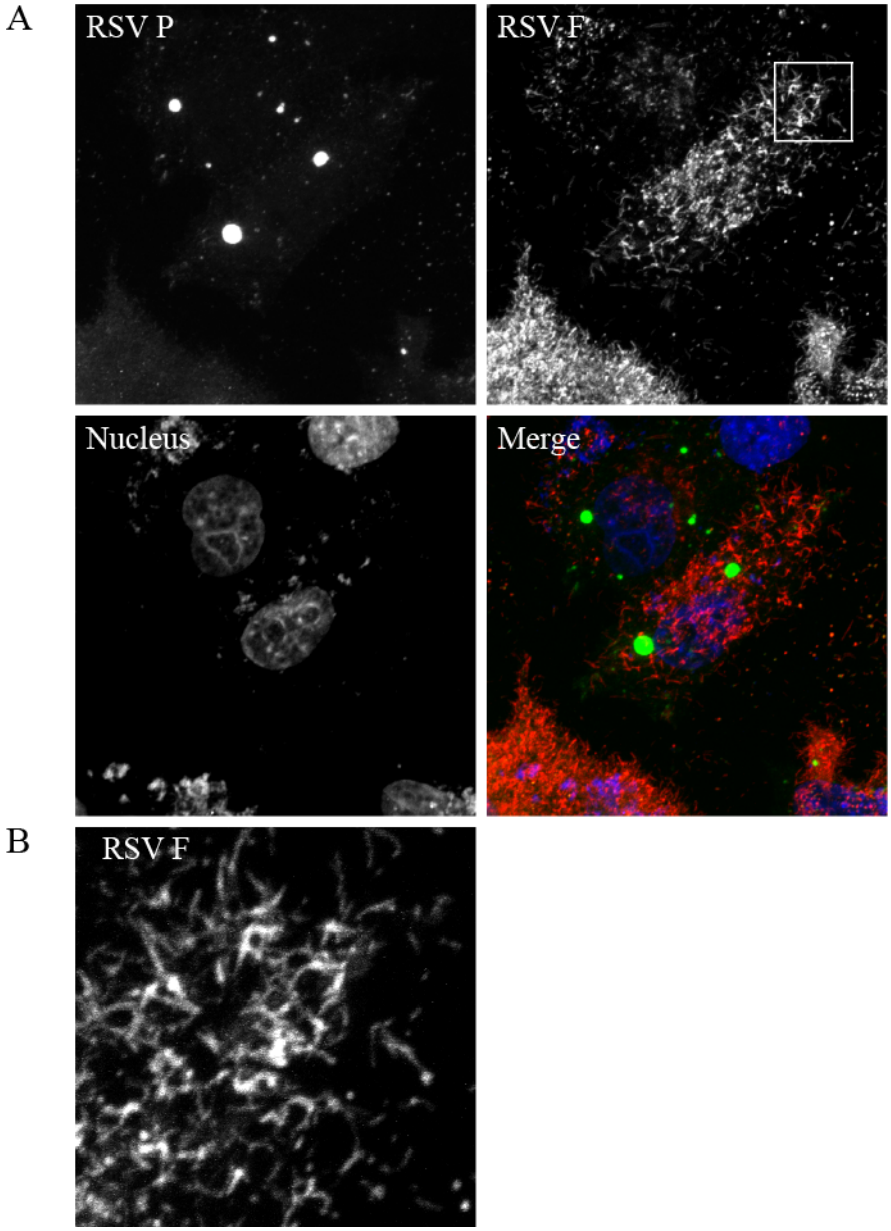

Figure 1-2. Confocal images of the major RSV structures in infected cells. Cells were infected with RSV (MOI=5.0) for 48 hours. Cells were fixed and processed for immunofluorescence. (A) Anti-RSV P (green in merge) was used to detect viral inclusion bodies and anti-RSV F (red in merge) was used to detect viral filaments. A fluorescent dye was used to stain the nuclei (blue in merge). (B) The inset from (A) showing a close-up of viral filaments. The collapsed Z-sections are shown for each image.

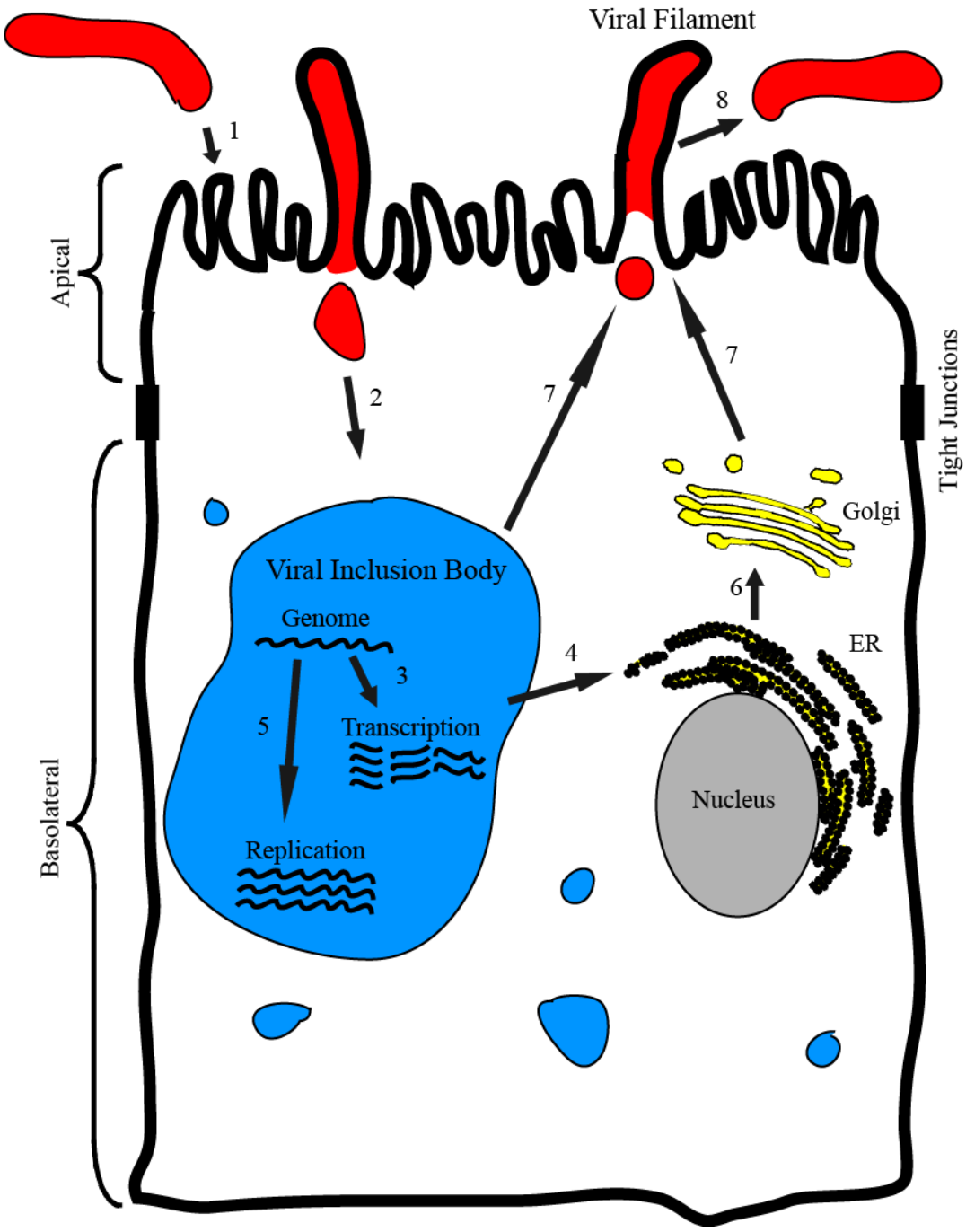

Figure 1-3. Diagram of the RSV life cycle. (1) The RSV virion attaches to the cell. (2) The viral ribonucleoprotein complex is delivered to the cytoplasm. (3) The genome is transcribed into viral mRNAs, which are then translated on host ribosomes (4) either at the endoplasmic reticulum for the glycoproteins, or free cytoplasmic ribosomes. (5) A switch occurs from transcription to replication of the viral genome. (6) glycoproteins are trafficked from the ER to the Golgi apparatus where they are modified. (7) All the virion components must be trafficked to the apical membrane. (8) Assembled virions bud from the infected cell. Image provided by Tom Utley.

Interestingly, deletion of the divalent-cation-binding domain of actin resulted in an inhibition of viral transcription. Deletion mutants where the functional domains necessary for actin polymerization were removed had no effect on RSV transcription (Harpen et al., 2009). These results show that while actin is a critical protein for cytoskeletal rearrangement, its importance in RSV gene transcription is independent of this role.

The cellular GTPase, RhoA, was identified as a potential interacting partner with RSV F by yeast two-hybrid and immunoprecipitation studies. RhoA has a function in cytoskeletal reorganization and cell motility, among other processes. Overexpression of RhoA in stably transfected cells increases syncytium formation upon RSV infection (Pastey et al., 1999). RSV infection induces activation of RhoA as well as relocalization of the protein to the plasma membranes of infected cells (Gower et al., 2001). Treatment with specific inhibitors of RhoA signaling during viral infection results in reduced syncytia formation as well as altered morphology of viral filaments. Interestingly, in RhoA inhibitor treated cells, RSV titers were unaffected, suggesting that RhoA signaling is not necessary for efficient viral replication (Gower et al., 2005). In addition to RhoA, phosphatidyl-3-kinase (PI3K) and Rac1 appear to be important in viral filament formation, as treatment with inhibitors to either of these molecules resulted in altered filament morphology during infection (Jeffree et al., 2007).

Stress granules

Stress granules are host RNA cytoplasmic granules formed in cells in response to multiple types of environmental stress (Kedersha and Anderson, 2007). The most fully characterized pathway for stress granule formation involves phosphorylation of the

translation initiation factor eIF2α, leading to accumulation of stalled translation pre-initiation complexes (Kedersha et al., 1999). Untranslated RNA transcripts are bound by mRNA-binding proteins, such as TIA-1, G3BP, and HuR. Translation factors such as eIF4E and eIF3 are recruited to stress granules, resulting in protein-RNA complexes that are the contents of the granules (Kedersha and Anderson, 2007). Stress granules can also be induced by an alternate mechanism that is independent of eIF2α phosphorylation via inactivation of the translation factors eIF4A or eIF4G (Dang et al., 2006) and (Mokas et al., 2009). Figure 1-4 shows confocal images of cells mock-treated or treated with a cellular stressor, sodium arsenite, and stained for stress granules.

eIF2α phosphorylation is mediated by four known kinases: protein kinase R (PKR), PKR-like ER-localized eIF2α kinase (PERK), general control nonrepressed 2 (GCN2) kinase, and heme-regulated inhibitor (HRI). Each kinase is activated in response to a specific stress. PKR is activated by the presence of double-stranded RNA intermediates during viral infection. PERK is activated during ER stress, typically by the unfolded protein response. GCN2 is typically activated in response to amino acid deprivation and HRI is activated by low intracellular heme levels.

There is much debate about the function of stress granules. Compositionally, stress granules are made up of untranslated mRNA, mRNA-binding proteins, and translation factors. Originally it was proposed that stress granules function as an mRNA sorting facility, targeting mRNAs for degradation, storage, or translation reinitiation (Anderson and Kedersha, 2002). However, live-cell imaging analysis of mRNAs revealed that a given mRNA only spends a short amount of time, generally less than a minute, in a stress granule. In addition, the vast majority of translationally repressed mRNA in cells remains

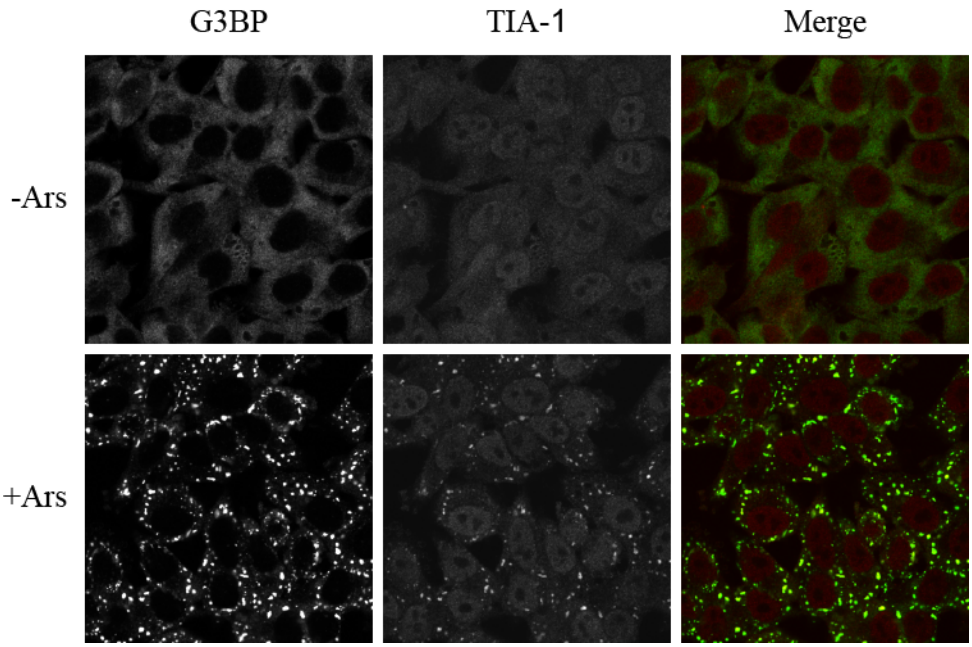

Figure 1-4. Stress granule formation in response to sodium arsenite. HEp-2 cells were mock treated (top row) or arsenite treated (bottom row) for 30 minutes. Cells then were stained for the stress granule markers G3BP (green in merge) or TIA-1 (red in merge).

cytoplasmic (Mollet et al., 2008). These data suggest stress granules do not modify or store mRNA. Another possibility is that stress granules are important for delaying apoptosis. A number of apoptotic regulatory factors are found in stress granules and cells that are for impaired stress granule formation exhibit faster rates of apoptosis induction after stress (Arimoto et al., 2008), (Ohn et al., 2008), (Eisinger-Mathason et al., 2008), (Kolobova et al., 2009), and (Buchan and Parker, 2009).

Virus and stress granule interactions.

Many viruses are known to modulate host translation in order to facilitate viral protein production. In recent years several viruses have been studied to monitor their effect on the host stress response. Viruses known to induce host stress granules include the paramyxovirus Sendai virus, the coronavirus mouse hepatitis virus, the alphavirus Semliki Forest virus, reovirus, and poliovirus (Iseni et al., 2002), (McInerney et al., 2005), (Raaben et al., 2007), (Smith et al., 2006), and (White et al., 2007). In addition, West Nile virus prevents stress granule formation throughout infection (Emara and Brinton, 2007). While it is reasonable to think that stress granules may play a role in infection for these viruses, the specific role or function of stress granules during infection has not been well defined.

Specific strains of mammalian orthoreovirus can induce stress granule formation both early (Qin et al., 2009) and late times after infection (Smith et al., 2006). Using a non-phosphorylatable eIF2α mutant expressing cell line, it was shown that eIF2α phosphorylation is essential for stress granule formation following reovirus infection. Interestingly, in experiments using PKR -/-, PERK -/-, HRI -/- and GCN2 -/- mouse

embryo fibroblast (MEF) cell lines, reovirus infection continued to induce stress granules, indicating that at least two of these kinases are activated by reovirus during infection and are responsible for stress granule formation (Qin et al., 2009).

Poliovirus induces stress granules as early as two hours post-infection, with many infected cells staining positively for stress granules (Mazroui et al., 2006) and (White et al., 2007). These reports, using G3BP as a marker for stress granules, appeared to show that although poliovirus induced stress granules at early times post infection, cleavage of G3BP mediated by a viral protease prevented stress granule formation at later times after infection (White et al., 2007). Subsequent characterization of this process revealed that although several stress granule proteins are degraded during poliovirus infection, stress granules that stain positively for TIA-1 can be found in infected cells throughout the course of infection, with as many as 90% of infected cells staining positively for stress granules at 6 hours post-infection (Piotrowska et al., 2010).

Stress granule proteins can interact directly with viral processes. Sindbis virus and vaccinia virus recruit the stress granule protein G3BP to viral structures (Cristea et al., 2006) and (Katsafanas and Moss, 2007) while West Nile virus interacts with the host stress granule proteins TIA-1 and TIAR (Emara and Brinton, 2007). Sendai virus trailer RNA binds TIAR (Iseni et al., 2002), and the poliovirus 3C proteinase can cleave G3BP (White et al., 2007). HuR associates with regions of the hepatitis C virus RNA and the human immunodeficiency virus reverse transcriptase (Rivas-Aravena et al., 2009) and (Spangberg et al., 2000).

PKR signaling

PKR is a well-characterized protein kinase that is activated by double-stranded RNA (dsRNA) during viral infection and often is associated with antiviral host cell responses. Upon binding to dsRNA, PKR dimerizes and autophosphorylates, resulting in an active state of the protein (Garcia et al., 2007). As previously mentioned, phosphorylated PKR is one of the four known kinases that regulates the activation of the translation initiation factor eukaryotic initiation factor 2 (eIF2α). Phosphorylated eIF2α is not able to mediate the delivery of initiator Met-tRNA to host translation complexes, resulting in a reduction of protein synthesis in virus-infected cells.

In addition to eIF2α phosphorylation, PKR plays a role in a number of other host signaling pathways. Most of these studies have been carried out in MEF cells that lack PKR expression (PKR -/- MEF). PKR -/- MEFs are deficient in activation of the MAP kinases JNK and p38 in response to a number of cellular stresses (Goh et al., 2000). STAT1 activation is impaired in PKR -/- MEFs in response to interferon treatment (Ramana et al., 2000). PKR binds directly to the tumor suppressor p53 (Cuddihy et al., 1999) and PKR knockdown cells are more prone to tumor formation (Yoon et al., 2009). PKR also plays an important role in NF-κB activation in response to viral infection. PKR appears to stabilize the IKK complex which is essential for allowing NF-κB to translocate to the nucleus (Garcia et al., 2006).

Many viruses have evolved molecular mechanisms to prevent PKR activation, presumably in order to inhibit the type I interferon response or to ensure host translation machinery remains sufficiently active for synthesis of viral proteins. Viral strategies to prevent PKR activation include expression of viral products that interact directly with

PKR and prevent activation, expression of viral proteins that bind and sequester dsRNA, or activation of host proteins that inhibit or counteract PKR activation (Garcia et al., 2007). In virtually every case studied to date, the activation of PKR in infected cells is associated with induction of an antiviral state. However, activation of PKR during hepatitis C virus (HCV) infection may enhance viral replication because of the resulting lack of translation of specific antiviral interferon-stimulated genes during infection (Garaigorta and Chisari, 2009).

RSV infection leads to increased levels of expression of total PKR. RSV infection also can induce the phosphorylation and activation of PKR (Groskreutz et al., 2010). These studies also suggest a direct interaction between PKR and the RSV nucleoprotein (N)

Induction of PKR is often associated with an antiviral state. For example, both vesicular stomatitis virus and influenza virus grew to higher viral titers in PKR-/- mice in comparison to wild-type mice (Balachandran et al., 2000). Similarly, PKR-/- mice exhibited faster mortality rates when infected with Bunyamwera virus in comparison to wild-type mice (Streitenfeld et al., 2003). There are cases, however, in which PKR plays only a minor or no role in inhibition of replication. Severe acute respiratory syndrome coronavirus replication is unaffected in cells that had been treated with phosphorodiamidate morpholino oligomers (PMO) specific for PKR mRNA (Krahling et al., 2009). In cells treated with siRNA for PKR, adenovirus or reovirus replication (Zhang and Samuel, 2007), or rotavirus protein translation (Rojas et al., 2010), is unaffected. Likewise, Rift Valley fever virus replication was not altered in PKR -/- MEFs (Habjan et al., 2009).

Innate immune signaling during RSV infection

As previously mentioned, infection with RSV can result in severe lower respiratory tract disease. A significant portion of disease is thought to be due to improper activation of the innate immune system during infection. Currently, RSV is known to both activate and inactivate several key signaling pathways involved in early viral detection.

Toll-like receptors (TLR) function to recognize general viral or bacterial markers and are expressed on a variety of respiratory epithelial cells. TLR activation is essential for rapid activation of the innate immune response. However, improper TLR signaling can result in acute or chronic lung inflammation (Lafferty et al., 2010). RSV is known to upregulate TLR4 expression and membrane localization in airway epithelial cells after infection. Increased expression of TLR4 then results in greater sensitivity to endotoxin in comparison to uninfected cells (Monick et al., 2003). IL-6 and IL-8 expression are also increased as a result of TLR4 upregulation, implicating this pathway as a major cause of disease during infection (Xie et al., 2009). Other studies have shown that expression of RSV F alone can mediate the upregulation of TLR4 (Kurt-Jones et al., 2000). Interestingly, severe respiratory disease has been linked to two polymorphisms of TLR4. Infants expressing an Asp299Gly or Thr399Ile mutation in TLR4 exhibited a much greater risk of severe RSV bronchiolitis (Tal et al., 2004) and (Awomoyi et al., 2007).

In addition to TLR4, TLR3 and TLR2 are activated in RSV-infected cells. Expression of TLR3 is increased in RSV infected cells, likely due to the presence of viral dsRNA intermediate products. TLR3 also undergoes a change in subcellular localization, switching from primarily being localized to endosomal membranes to being found at the

plasma membrane of infected cells. Subsequent exposure to dsRNA resulted in increased NF-κB activation and IL-8 production, suggesting that RSV primes epithelial cells for hyperreactivity following infection (Groskreutz et al., 2006). Further experiments showed that TLR3 upregulation is due to the activation of the retinoic acid-inducible gene I (RIG-I). RIG-I bound and was activated by RSV transcripts within 12 hours after infection. Knockdown of RIG-I expression prevented RSV-mediated activation of TLR3 and subsequent NF-κB activation (Liu et al., 2007). TLR2 is essential for TNF-α production in macrophages infected with RSV. Additionally, TLR2 signaling appears to be an important step in viral clearance, as TLR2 knockout mice contained higher viral titers in comparison to wild-type mice up to four days after infection (Murawski et al., 2009).

RSV induces the activation of several cytokines and chemokines during infection. Cytokines are a family of secreted proteins that are induced in response to a variety of stimuli and function in regulating the immune response, inflammation, and hematopoiesis. Chemokines are a subset of cytokines that function to attract leukocytes to sites of viral or bacterial infection. RSV infection of airway epithelial cells results in the expression of proinflammatory cytokines and chemokines that include RANTES, MCP, eotaxin, IL-9, TNF-α, IL-6, IL-1, and CX3CL1 (Oshansky et al., 2009). Some or all of these signaling molecules may be responsible for enhanced pathogenesis of RSV infection. For example, mice infected with RSV that were treated with an anti-RANTES antibody exhibited significantly reduced signs of airway hyperreactivity (Tekkanat et al., 2002). Similar experiments were performed with an anti-eotaxin antibody, these results again showed a decrease in disease in comparison to untreated mice (Matthews et al., 2005).

Several studies have examined the impact of specific RSV proteins on immune signaling. Expression of RSV F alone stimulates TLR4 production. The RSV SH protein functions as a TNF-α antagonist protein (Fuentes et al., 2007). TNF-α is an important signaling molecule involved in NF-κB activation, cell proliferation, and induction of apoptosis (Gaur and Aggarwal, 2003). Cells infected with a viral construct lacking the SH gene produced a greater amount of TNF-α in response to infection. In addition, expression of SH alone by transfection prevented activation of NF-κB upon exogenous addition of TNF-α to transfected cells. Structural studies have shown that RSV G contains a domain that is homologous with a portion of the TNF receptor. It is possible that the secreted form of RSV G can bind to TNF-α and prevent the molecule from properly signaling through its receptor (Langedijk et al., 1998).

Type I interferon is essential for mounting a complete innate response to viral infection. IFN is responsible for inducing a number of key antiviral proteins in both infected cells and uninfected neighboring cells (Boo and Yang, 2010). Interestingly, RSV infection appears to be largely resistant to IFN signaling (Atreya and Kulkarni, 1999). Early studies attempting to identify the mechanism by which RSV inhibits IFN induction showed that the nonstructural proteins, NS1 and NS2, are essential for this function. RSV gene deletion viruses that lack the NS1 and NS2 genes induce much higher levels of IFN in infected airway epithelial cells when compared to wild-type virus (Spann et al., 2004). Further experiments revealed that NS1 and NS2 target the IFN intermediate signaling molecule, STAT2, for degradation (Lo et al., 2005). NS1 is capable of acting like an E3 ligase, causing the ubiquitination and subsequent degradation of STAT2 during infection, initiating binding of the E3 ubiquitin ligase to STAT2 (Elliott et al., 2007).

CHAPTER II

RESPIRATORY SYNCYTIAL VIRUS INDUCES HOST RNA STRESS GRANULES TO FACILITATE VIRAL REPLICATION

Introduction

I began these studies with the intention of determining a role for RSV inclusion bodies. Previously, these structures had been proposed to be either viral replication factories or simply nonfunctional aggregates of excess viral protein. We were first introduced to stress granules by Dr. James Goldenring at Vanderbilt University. Dr. Goldenring encouraged us to delineate the differences between viral inclusion bodies and host stress granules. As I performed my initial studies to identify sites of viral RNA production using in situ hybridization, we began collaborating with Dr. Philip Santangelo at the Georgia Institute of Technology. Dr. Santangelo provided us with much more sensitive RNA probes that were easier to work with and made much of this work possible. Thus, our work expanded greatly and we began to study the relationship between inclusion bodies, viral RNA, and stress granules.

This section begins by confirming the presence of stress granules in virally infected cells. These structures are separate and distinct from viral inclusion bodies, save for one shared component, HuR. I found that viral replication is greatly reduced in cells that cannot form stress granules. Finally I found that although viral RNA can be found in stress granules, the vast majority is found in inclusion bodies.

Materials and Methods

Cells. HEp-2 cells (ATCC CCL-23) were maintained in OPTI-MEM I medium (Invitrogen) containing 5% (v/v) fetal calf serum, 1% (v/v) L-glutamine, 2.5 μg/mL amphotericin B, and 50 μg/mL gentamicin. MA104 cells (ATCC CRL 2738.1), which were used to prepare rotavirus, and RGD3 and U2OS cells (kindly provided by Paul Anderson, Brigham and Women's Hospital) were maintained in DMEM containing 5% (v/v) fetal calf serum, 1% (v/v) sodium pyruvate, 1% (v/v) L-glutamine, 1% (v/v) non-essential amino acids, 2.5 μg/mL amphotericin B, and 50 μg/mL gentamicin.

Viruses. A suspension of RSV wild-type strain A2 prepared in HEp-2 cells (1×10^6 pfu/mL) was used to infect HEp-2 cell monolayer cultures. Infectious virus was adsorbed to the cells for one hour in a 37 °C incubator in 5% CO_2. Following adsorption, the inoculum was removed and fresh medium added. Cells then were incubated at 37 °C in 5% CO_2 for the duration of the infection period. UV inactivated virus was prepared from the same virus stock by irradiation in a UV crosslinker for 15 minutes. Rhesus rotavirus (RRV) was a kind gift from Susana Lopez.

Fixation and immunostaining. Cells were fixed with 3.7% (w/v) paraformaldehyde in phosphate buffered saline (PBS) for 10 minutes at room temperature. Cells were permeabilized with 0.2% (w/v) Triton X-100 and 3.7% paraformaldehyde in PBS for ten minutes at room temperature. Following fixation, cells were blocked in 5% (w/v) BSA in PBS for one hour followed by addition of primary antibody for one hour. Cells then were washed three times in PBS and species-specific IgG Alexa Fluor (Molecular Probes) was

added at a dilution of 1:1,000 in block solution for detection of primary antibodies. Cells were washed 3 times in PBS and fixed on glass slides using Prolong Antifade kit (Molecular Probes). Images were obtained on a Zeiss inverted LSM510 confocal microscope using a 40X Plan-Neofluar oil objective lens. Polyclonal anti-G3BP (ab37906) antibody was obtained from Abcam and used for immunostaining. The following antibodies were obtained from Santa Cruz for immunostaining: polyclonal anti-TIA-1 (sc-1751), polyclonal anti-HuR (sc-20694), and polyclonal anti-eIF3η (sc-16377). Anti-RSV P protein (clone 3_5) and anti-RSV N protein (clone B130) monoclonal antibodies were a kind gift of Earling Norrby and Ewa Bjorling. An anti-RSV F protein humanized mouse monoclonal antibody (palivizumab; MedImmune) was obtained from the Vanderbilt Pharmacy. Imaging of the RNA with G3BP and RSV N protein was performed using a 63X, NA=1.4 Plan-Apochromat objective using a Zeiss LSM 510 confocal microscope. For images where 3-dimensional z-stacks were obtained, we collapsed the series of fields into an extended view using Volocity imaging software.

RT-PCR. HEp-2 cells were grown on 48-well plates and infected with RSV for indicated times. RNA was extracted using the RNeasy mini kit (Qiagen). RT-PCR was performed using the OneStep RT-PCR kit (Qiagen) and primer-probe combinations for RSV F, rotavirus VP3 or human GAPDH. Normalized cycle threshold (ΔCt) was calculated for each time point using the following formula: ΔCt=RSV F Ct – GAPDH Ct. Change in normalized Ct over time (ΔΔCt) was calculated for each condition using the ΔCt of wild-type cells two hours post infection as the initial point of reference for relative amount of

viral RNA: ΔΔCt= [ΔCt at X hour PI (+/-) shRNA] – [ΔCt 2 hour PI wild-type], where X equals each specific time point.

shRNA reagents. A stable cell line exhibiting knockdown of HuR expression was generated using a set of three SMARTvector lentiviral shRNA particles (Dharmacon), along with cells treated with non-targeting shRNA particles. HEp-2 cells were plated into 48-well plates at approximately 50% confluency and transduced with the lentiviral particles according to the manufacturer's protocol. A panel of stable cell lines exhibiting knockdown of G3BP expression was generated using MISSION shRNA Lentiviral Transduction Particles (Sigma). HEp-2 cells were plated onto 6-well plates and transduced with lentiviral particles according to the manufacturer's protocol. For selection of each target, cells containing integrated lentivirus sequences were selected using puromycin (5 μg/mL) diluted in medium. Medium containing puromycin was replaced every three days until resistant colonies were observed. Puromycin-resistant colonies were isolated using cloning cylinders (Sigma) and tested for target protein expression.

Western blots. HEp-2 cells were grown on 6-well plates and harvested for protein. Cell lysates were obtained using lysis buffer (50 mM Tris-HCl, 150 mM NaCl, 1% Triton X-100, pH 8.0) containing 0.5% (v/v) of protease inhibitor cocktail (Sigma) and 1.0% (v/v) of phosphatase inhibitors (Sigma). Lysates were separated on 4-12% NuPAGE Bis-Tris gels (Invitrogen) and transferred to nitrocellulose membranes using an iBlot dry blotting system (Invitrogen). Membranes were blocked for one hour using Odyssey blocking

buffer (Li-Cor) diluted 1:1 in PBS. Primary antibodies were diluted in blocking buffer and incubated overnight at 4 °C. Membranes then were washed four times in Tris buffered saline + 0.2% Tween (TBST) for five minutes each. Li-Cor IRDye 680CW or IRDye 800CW secondary antibodies were diluted 1:5,000 in blocking buffer and added to each membrane for one hour. Membranes were washed four times in TBST. Bands were imaged and quantitated using the Odyssey Infrared Imaging System. G3BP protein was detected using a monoclonal antibody from BD Biosciences (611127). GAPDH was detected using a monoclonal antibody from Millipore (MAB374). HuR was detected using a monoclonal antibody from Santa Cruz Biotechnology (sc-5261).

RNA probe and live cell delivery. Single RNA sensitive probes (Santangelo et al., 2009) designed to target the gene-start-intergenic region of the genomic RNA of hRSV were delivered at 30 nM via reversible-permeabilization with streptolysin O into separate sets of infected or mock-infected HEp-2 cells at 1, 6, 12, 18, and 24 hours PI. Delivery took approximately 10 minutes, and 15 minutes after delivery the cells were fixed with 3.7% (w/v) paraformaldehyde in PBS for 10 minutes at room temperature. The cells then could be immunostained for G3BP and the RSV N protein as discussed above.

Quantification of imaging. To determine quantitative features of stress granule induction by RSV, HEp-2 cells were plated onto coverslips placed in wells of a 24-well plate. Cells were grown to approximately 75% confluency and were infected with RSV for 0, 6, 12, 16, 20 or 24 hours (MOI=1). Cells were fixed as above. Cells were stained with anti-G3BP antibody (BD Transduction Laboratories) diluted 1:1,000 in block

solution, the anti-RSV F protein antibody palivizumab (MedImmune) diluted 1:10,000 in blocking solution and the nuclear stain TO-PRO-3 iodide (Invitrogen) diluted 1:1000 in block solution for one hour. Twenty high-powered fields (HPFs) were obtained for each time point. Images were examined using Volocity imaging software (version 5.1, Improvision). Each HPF was quantified for total number of cells by counting the number of nuclei. We also quantified the number of infected cells by staining for the presence of RSV F protein, the number of cells containing stress granules by staining for the presence G3BP protein, and number of infected cells that also contained stress granules per HPF. To calculate stress granule size in wild-type or G3BP-deficient cells, cells were plated onto coverslips placed in wells of a 24-well plate. Cells then were treated with 0.5 mM arsenite for 15 minutes. Cells were fixed and stained for G3BP (1:500) and TIA-1 (1:250). Images for 10 HPFs were obtained for each cell line. We then used Volocity imaging software to determine the percentage of cells per HPF with stress granules and the size of each stress granule for those cells containing stress granules. To determine inclusion body number and volume, HEp-2 cells were placed on coverslips in 24-well plates. Cells were infected with RSV for 24 hours (MOI=1.0) and fixed. Cells were stained for inclusion bodies using anti-RSV P protein antibody and stress granules using anti-G3BP antibody. At least 10 cells containing or not containing stress granules were analyzed for inclusion bodies. Volocity imaging software was used to determine the number of and volume of individual inclusion bodies per cell. Volocity also was used to quantify the colocalization of the viral genomic RNA with inclusion bodies (marked by the RSV N protein) or with stress granules, in addition to colocalization of inclusion

bodies with stress granules. Manders overlap coefficients were calculated using voxels generated from three-dimensional reconstructions.

Results

RSV infection induces stress granule formation. We first tested whether RSV infection of epithelial cells induced stress granules. HEp-2 cell monolayer cultures were inoculated with RSV wild-type strain A2 at an MOI of 1 pfu/cell and incubated in liquid medium for 24 hours. We then fixed and immunostained the cells for the stress granule proteins G3BP, eIF3η, or TIA-1. Figure 2-1 (first column) shows that each of these markers frequently relocalized into dense cytoplasmic foci that are characteristic of stress granules. We noted that the host stress granules appeared similar in size, shape, and location to previously described viral inclusion bodies that form during RSV infection. To investigate whether the granules containing stress granule associated proteins were viral inclusion bodies, we co-stained infected cells with antibodies to stress granule markers and one of the viral proteins found in inclusion bodies (RSV P protein) (Figure 2-1 middle column). The results indicate that viral inclusion bodies are separated spatially from stress granules and represent distinct structures in the cytoplasm. We next performed a time course of infection to determine the kinetics of stress granule formation in RSV-infected cells. We inoculated cells with RSV (MOI=1 pfu/cell), then incubated for varying time points (0-24 hours). We fixed and immunostained cells for RSV F protein and the stress granule protein marker G3BP. After 12 hours, stress granules formed and the number of infected cells containing stress granules increased

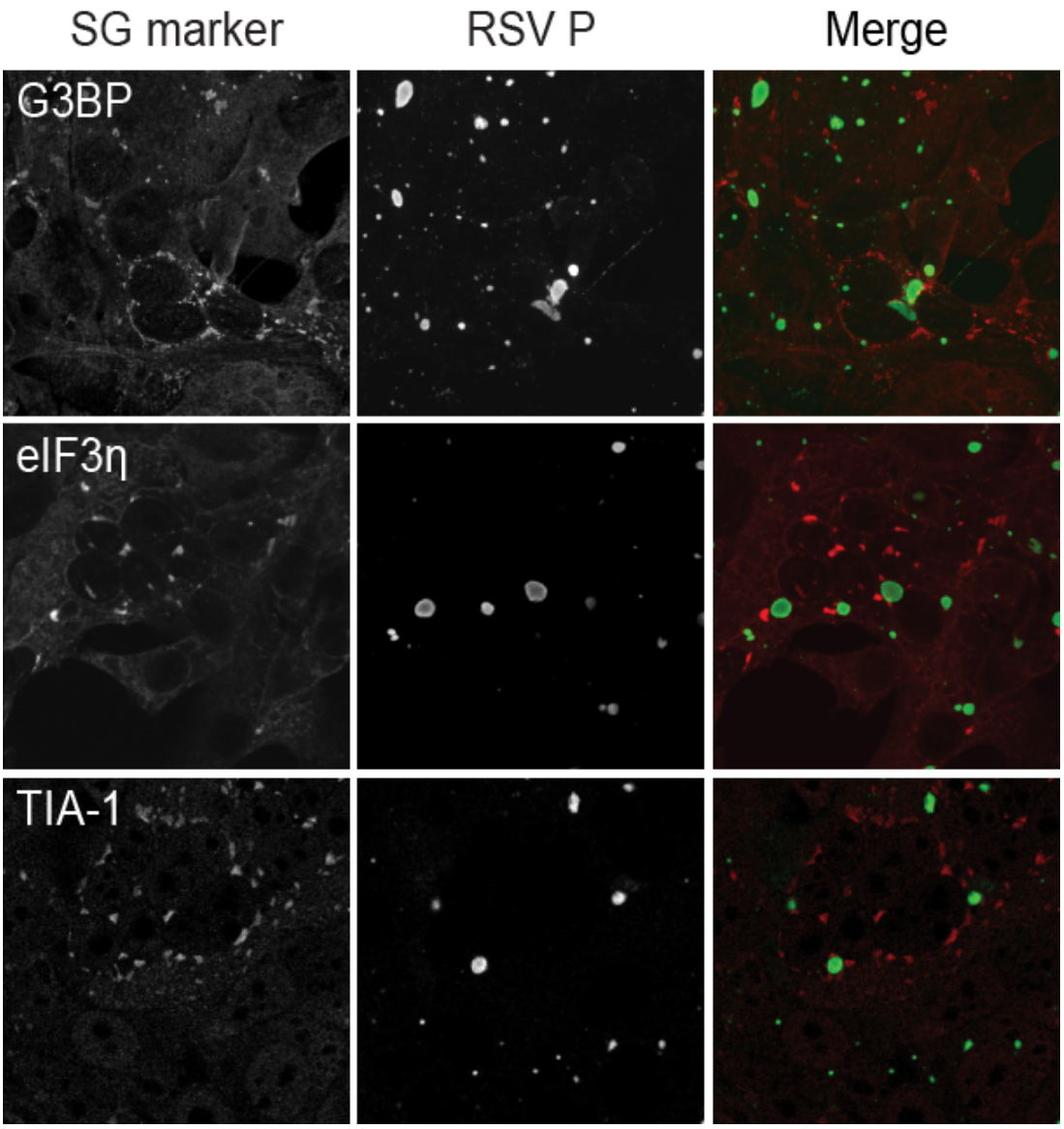

Figure 2-1. Stress granules are induced during RSV infection. HEp-2 cells were infected with RSV (MOI=1.0) for 24 hours, fixed and processed for immunofluorescence. Anti-G3BP, anti-eIF3η, and anti-TIA-1 were used as stress granule markers and appear red in the merge panel. Anti-RSV P was used as the viral inclusion body marker and appears green in the merge panel. The collapsed z-sections are shown for each image.

incrementally throughout the 24-hour period of observation (Figure 2-2). We did not observe stress granules in mock-infected cells over the time course. In addition, in the cultures in which RSV was added, we did not observe stress granules in cells that did not stain for RSV protein. These results demonstrated that RSV induces a potent stress granule response beginning at about 12 hours after inoculation and continuing throughout the viral life cycle.

Stress granule formation is dependent on RSV replication. In order to verify that RSV replication is necessary for stress granule formation, we mock inoculated, inoculated with replication competent RSV (MOI=1.0 pfu/cell), or inoculated with an equivalent volume of UV-inactivated RSV for 48 hours, then fixed and immunostained for RSV F and G3BP. RSV infection once again induced robust stress granule formation (Figure 2-3 bottom row) while we did not observe stress granules in mock inoculated or UV-inactivated RSV inoculated samples (Figure 2-3 top and middle rows). These results confirmed that RSV replication, and not simply the presence of RSV protein is required for stress granule formation. We next compared RSV protein levels between cells with and without stress granules. HEp-2 cells were inoculated with RSV (MOI=1.0) for 24 hours, then fixed and immunostained for RSV P and G3BP. We used RSV inclusion body size and number as a measure to compare the amount of viral protein present in cells. Interestingly, the results indicated that infected cells that have formed stress granules contain more inclusion bodies than cells that have not formed inclusion bodies (Figure 2-4A). In addition, individual inclusion bodies were larger in cells that had formed stress granules (Figure 2-4B) and the total amount of protein contained in inclusion bodies was

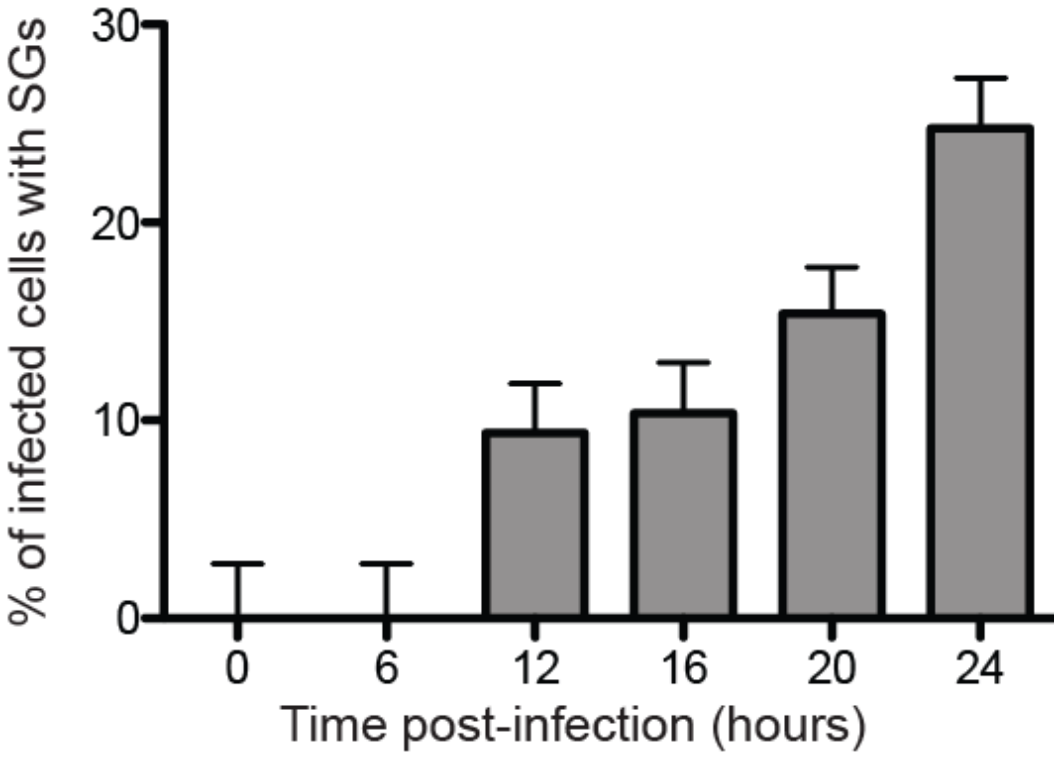

Figure 2-2. Stress granule formation increases throughout infection. HEp-2 cells were infected with RSV (MOI=1.0) for indicated times. The percentage of infected cells and cells containing stress granules per HPF was quantified as described in Materials and Methods.

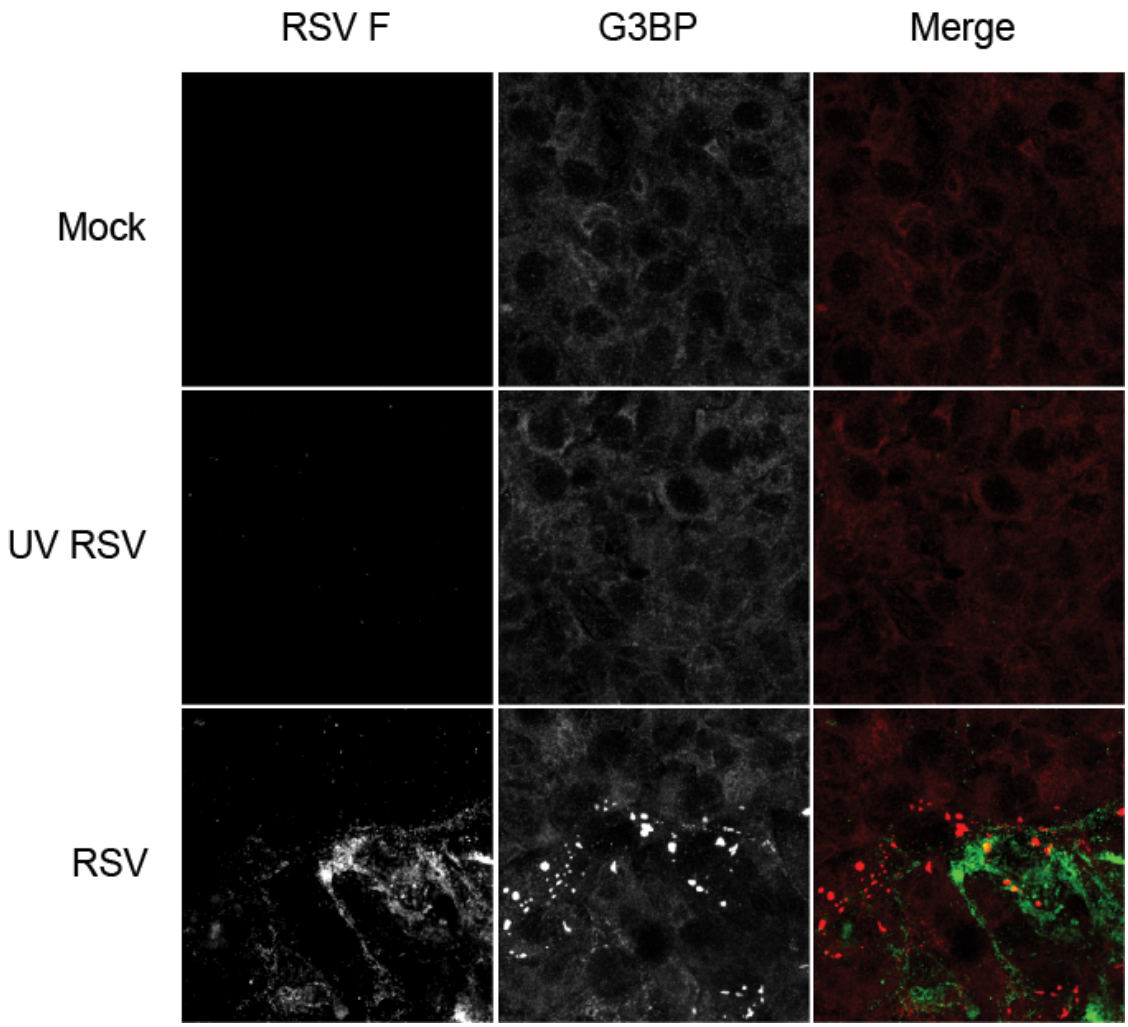

Figure 2-3. RSV-induced stress granule formation is dependent on virus replication. HEp-2 cells mock infected (top row), inoculated with UV-inactivated RSV (middle row), or inoculated with replication competent RSV (MOI=1.0) (bottom row) for 48 hours were fixed and processed for immunofluorescence. Anti-G3BP was used as a marker for stress granules and appears red in the merge. Anti-RSV F was used as a marker for viral infection and appears green in the merge. The collapsed z-sections are shown for each image.

greater (Figure 2-4C). Although the quantification of size and number of inclusion bodies in infected cells in the cultures clearly showed larger and more inclusion bodies in cells with stress granules, we also did observe some individual cells without stress granules that contained high amounts of RSV protein (for example, two cells with high N expression in Figure 2-11, at 12 hours post-infection). These data suggested that stress granules enhance viral protein production and inclusion body formation, but are not absolutely required for these viral processes.

Inhibition of host stress granule formation reduces RSV replication. To investigate whether stress granule formation is beneficial to the virus or host, we inoculated MEF lines derived from TIA-1 or TIAR deficient mice (kindly provided by Paul Anderson), however, RSV did not establish a productive infection in these cells. It is well-established that human RSV strains do not infect murine cells efficiently. Next, we created human cell lines deficient for stress granule formation by transducing HEp-2 cells with lentiviral shRNA transduction particles to induce stable knockdown of G3BP expression. When analyzed by western blot, G3BP was not detected in the knockdown cells (Figure 2-5A). However, when these cells were compared with wild-type cells by immunofluorescence, we could still observe a small amount of G3BP in fixed and permeabilized knockdown cells. The G3BP-deficient cells expressed normal amounts of other stress granule proteins, such as TIA-1 (Figure 2-5B). G3BP-deficient cells were treated with 0.5 mM arsenite for 15 minutes to determine if they were capable of forming stress granules. Stress granules were detected using anti-TIA-1 antibodies (Figure 2-6A). We compared

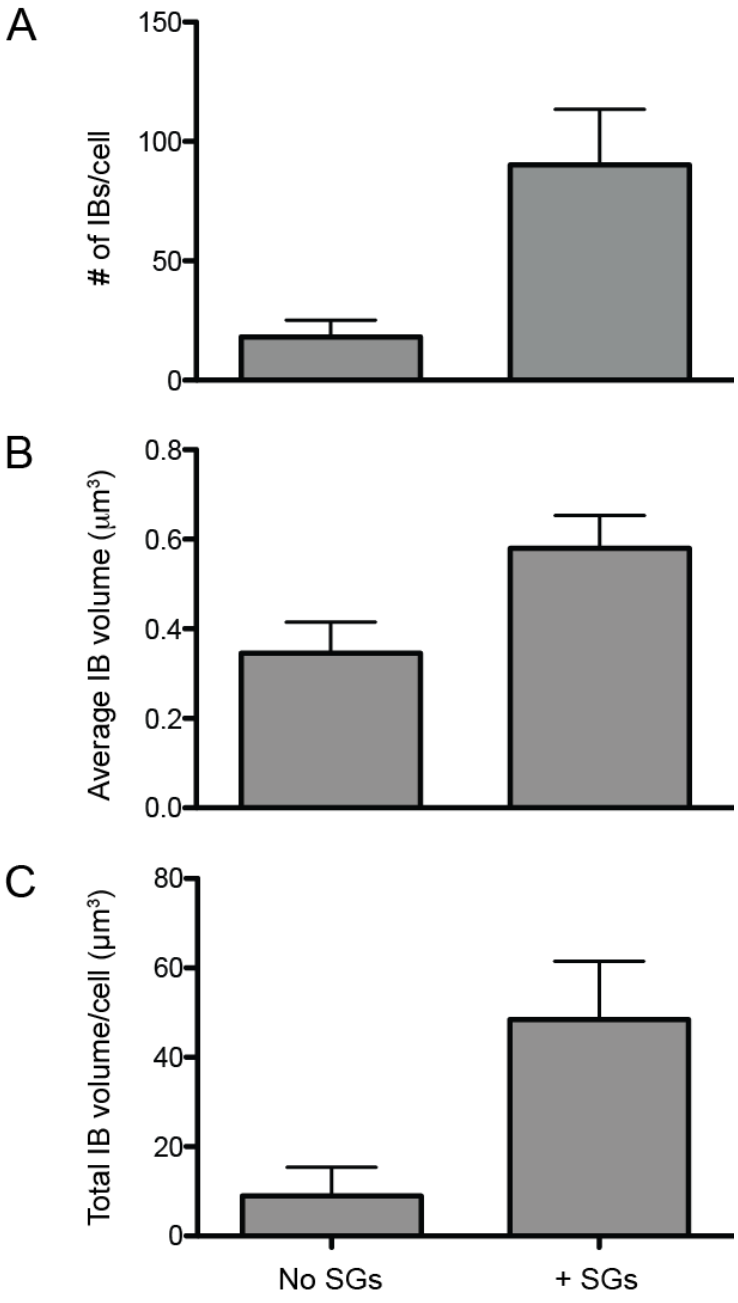

Figure 2-4. RSV protein levels are higher in cells with stress granules. HEp-2 cells were infected with RSV (MOI=1.0) for 24 hours. At least 10 infected cells containing or not containing stress granules were analyzed. (A) Total average number of inclusion bodies per cell was determined as described in the Materials and Methods for cells containing stress granules (+SGs) or not containing stress granules (No SGs). (B) The average volume (μm^3) of individual inclusion bodies was determined for cells containing or not containing stress granules. (C) The volumes for all of individual inclusion bodies in single cells containing or not containing stress granules were totaled on a per cell basis to determine average total inclusion body volume per cell.

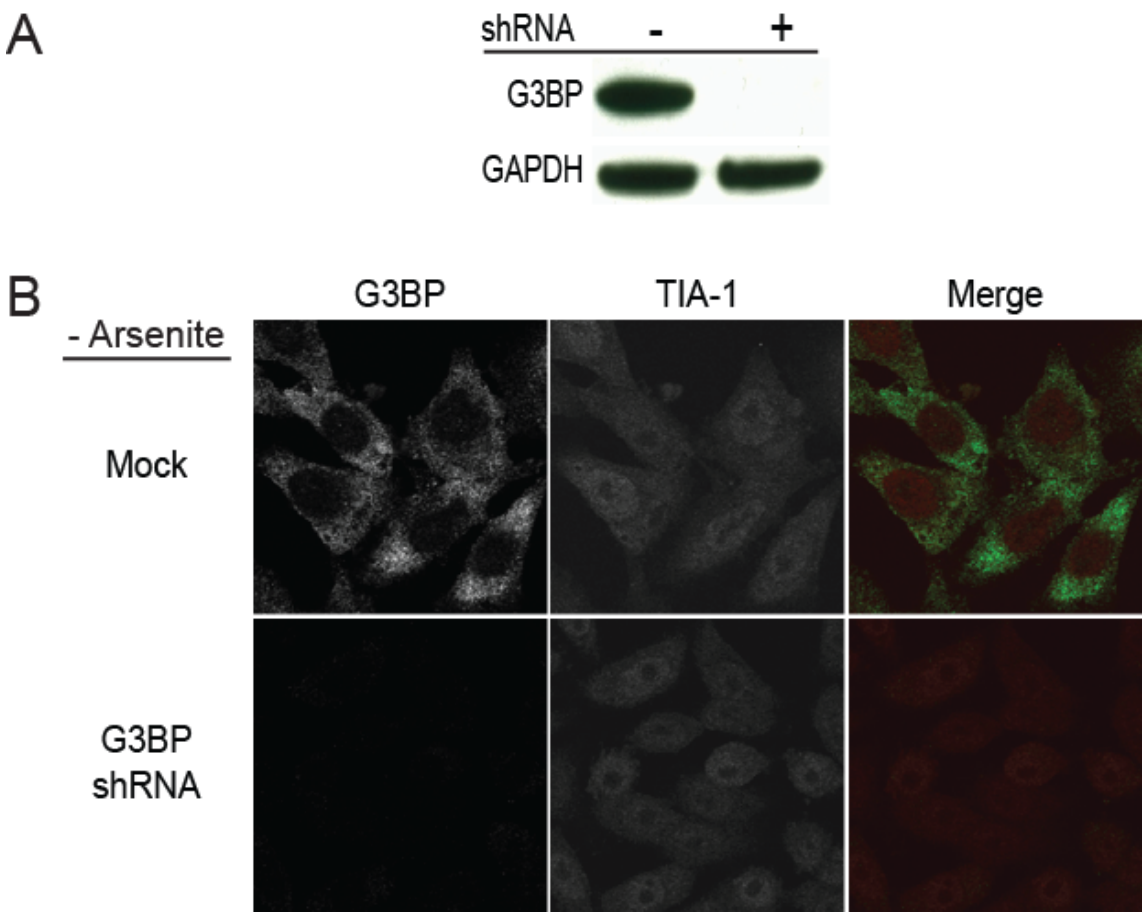

Figure 2-5. shRNA knockdown of G3BP expression. (A) Wild-type or representative G3BP-deficient HEp-2 cells were analyzed for G3BP expression via (A) western blot or (B) for G3BP (green in merge) and TIA-1 (red in merge) expression using indirect immunofluorescence. (C) Each cell type was treated with arsenite, fixed, and processed for immunofluorescence. Stress granule proteins were stained using anti-G3BP (green in merge) and TIA-1 (red in merge) antibodies and then examined (D) for percentage of cells containing stress granules per HPF and size of stress granules per cell using TIA-1 as a marker for stress granules, as described in Materials and Methods.

the percentage of cells with stress granules per high-powered field. In G3BP-deficient cells, approximately 75% fewer cells formed stress granules per HPF. We also examined individual G3BP-knockdown cells that did form stress granules and noted that there was also a slight decrease in stress granule size when compared to those in wild-type HEp-2 cells (Figure 2-6B). These results indicated that G3BP-deficient cells are impaired for stress granule formation.

We next determined whether RSV replication was altered in the G3BP-deficient cell line. Wild-type or G3BP-deficient cells were infected with RSV (MOI=1 pfu/cell) for 1, 2, or 4 days. Cell-associated and supernatant virus was collected separately and viral titer was determined using plaque assays. The G3BP-deficient cells consistently demonstrated a ten-fold reduction in viral titer when comparing supernatant- or cell-associated virus with titers collected from wild-type cells (Figure 2-7A). In addition, RSV infection was associated with death of most wild-type HEp-2 cells after 2 days, while in contrast the G3BP-deficient cells consistently remained viable for 4 days after infection. We also determined the effects of G3BP overexpression on RSV replication using RGD3 cells, a U2OS osteosarcoma cell line selected to express GFP-G3BP. We inoculated RGD3 or parental U2OS cells with RSV (MOI=1.0) and harvested cell-associated virus for plaque assays at time points spanning 0-4 days after inoculation. RSV replication remained largely unaltered in cells overexpressing G3BP (Figure 2-7B). Interestingly, although G3BP levels are higher in RGD3 cells, stress granule formation is largely unaltered (Kedersha et al., 2008). These data indicated that the presence of artificially elevated levels of G3BP do not enhance replication.

We next sought to determine if reduction of G3BP expression and stress granule

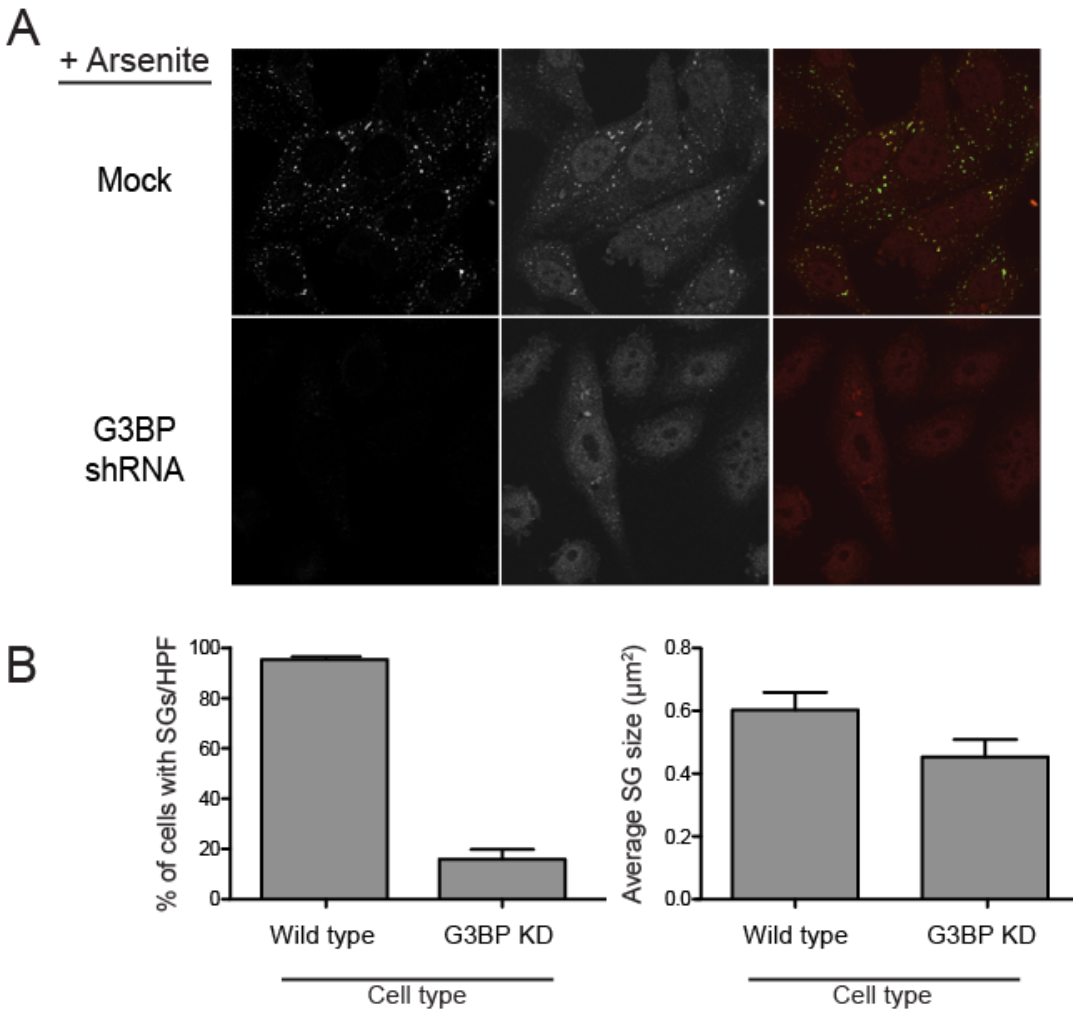

Figure 2-6. Decreased levels of G3BP inhibit stress granule formation. (A) Wild-type or G3BP-deficient cells were treated with arsenite, fixed, and processed for immunofluorescence. Stress granule proteins were stained using anti-G3BP (green in merge) and TIA-1 (red in merge) antibodies and then examined (B) for percentage of cells containing stress granules per HPF and size of stress granules per cell using TIA-1 as a marker for stress granules, as described in Materials and Methods.

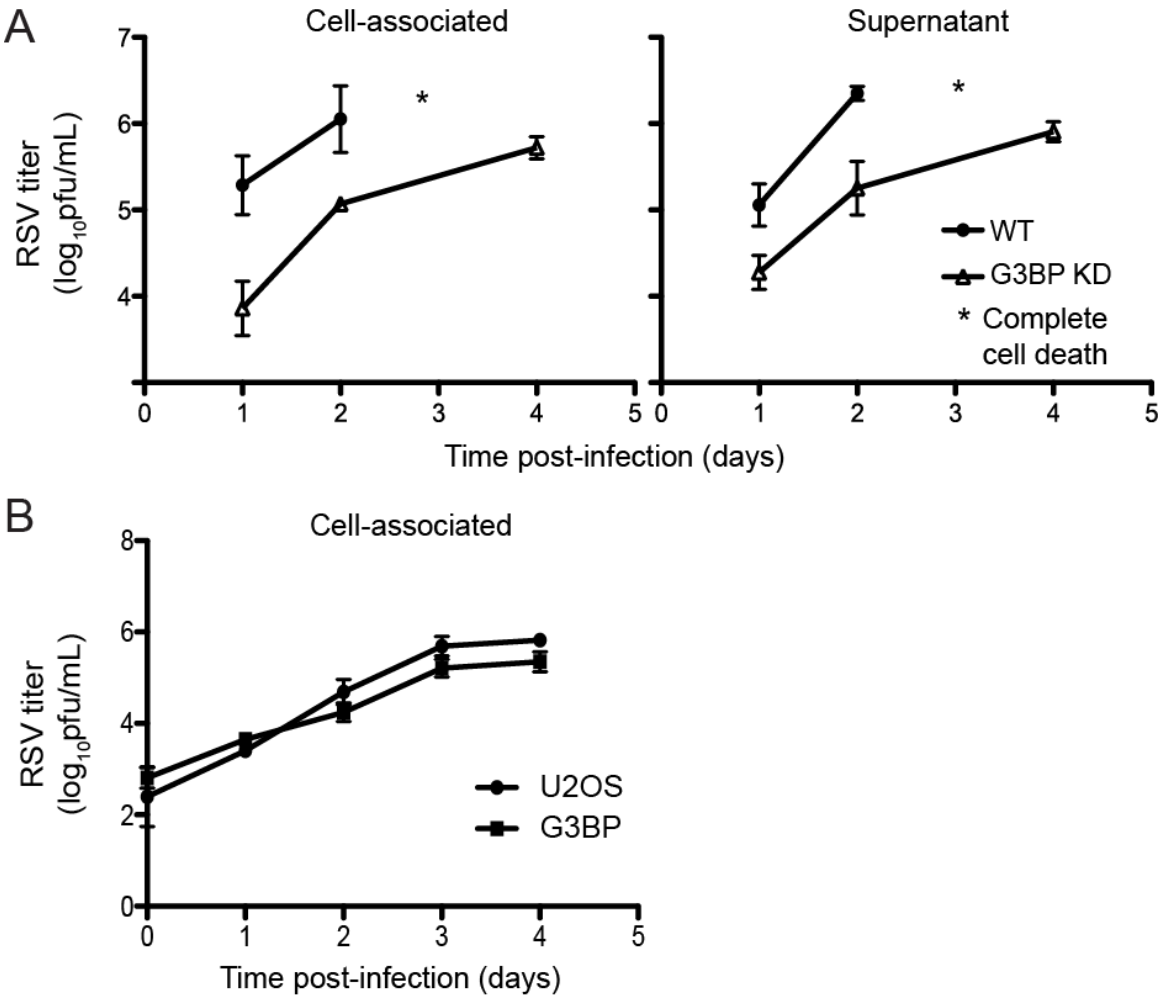

Figure 2-7. RSV replication is inhibited in G3BP-deficient cells. (A) Wild-type or representative G3BP-deficient cells were infected with RSV (MOI=1.0) for indicated times. Cell-associated or supernatant virus was collected at each time point. Viral titer for each sample was determined by plaque assay. (B) Wild-type or G3BP-overexpressing cells derived from U2OS cells (RGD3) were infected with RSV (MOI=1.0) for indicated times. Cell-associated virus was collected at each time point, and viral titer for each sample was determined by plaque assay.

formation affected the efficiency of replication of viral RNA. We inoculated wild-type or G3BP-deficient cells for 0, 2, 12, 24, or 48 hours and then harvested total RNA from cell lysates. We performed reverse transcriptase-PCR and normalized RNA levels to that of host GAPDH and compared with levels found at 2 hours post-infection in the wild-type HEp-2 cells. We observed a decrease in RSV RNA in the G3BP-deficient cell line at each time point tested after infection (Figure 2-8). Interestingly, when these cells were infected with rhesus rotavirus, a virus that does not induce stress granule formation (Montero et al., 2008), replication of rotavirus was unaffected. These data indicate that stress granule formation may play an important role in the RSV life cycle even at very early time points after infection.

The stress granule marker HuR is recruited to RSV inclusion bodies. We examined other markers of stress granules and found a non-classical feature involving the mRNA-binding stress granule protein HuR. In cells infected with RSV, HuR was recruited to stress granules during infection but the protein also was largely associated with structures that were not marked by other stress granule proteins. When cells were inoculated with RSV (MOI=1) and co-stained for G3BP and viral proteins in RSV inclusion bodies, we noted that HuR was present both in host stress granules and in RSV inclusion bodies (Figure 2-9). Thus, HuR protein is a shared component between the two structures.

HuR expression is not required for efficient RSV replication. Using RNA interference, we sought to determine the effect of decreased HuR expression on RSV replication. shRNA knockdown of HuR resulted in an approximately 70% reduction of

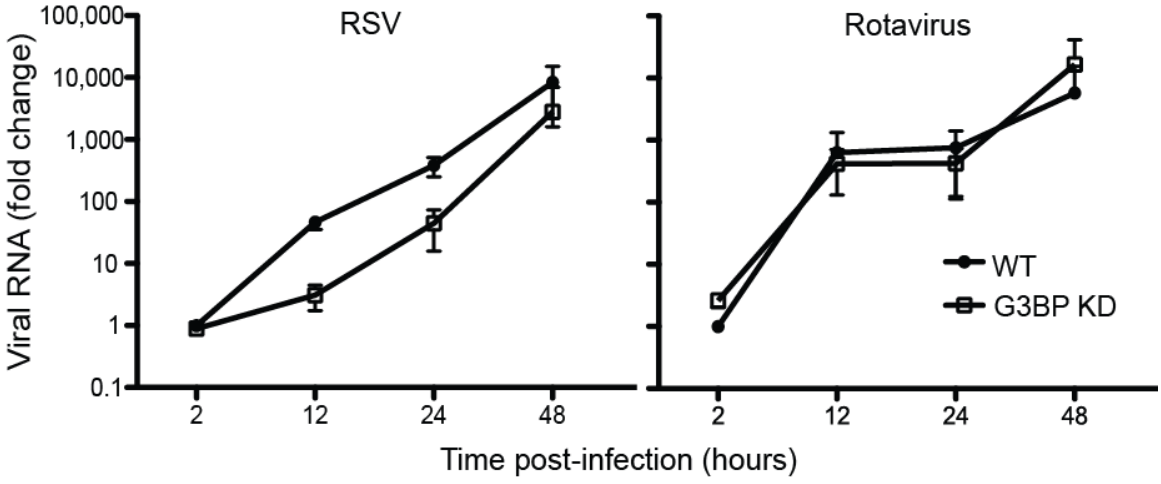

Figure 2-8. RSV replication is inhibited in G3BP-deficient cells. Wild-type or G3BP-deficient cells were infected with RSV or rotavirus for indicated times. Viral RNA was collected and assayed for fold change of RNA during infection using RT-PCR.

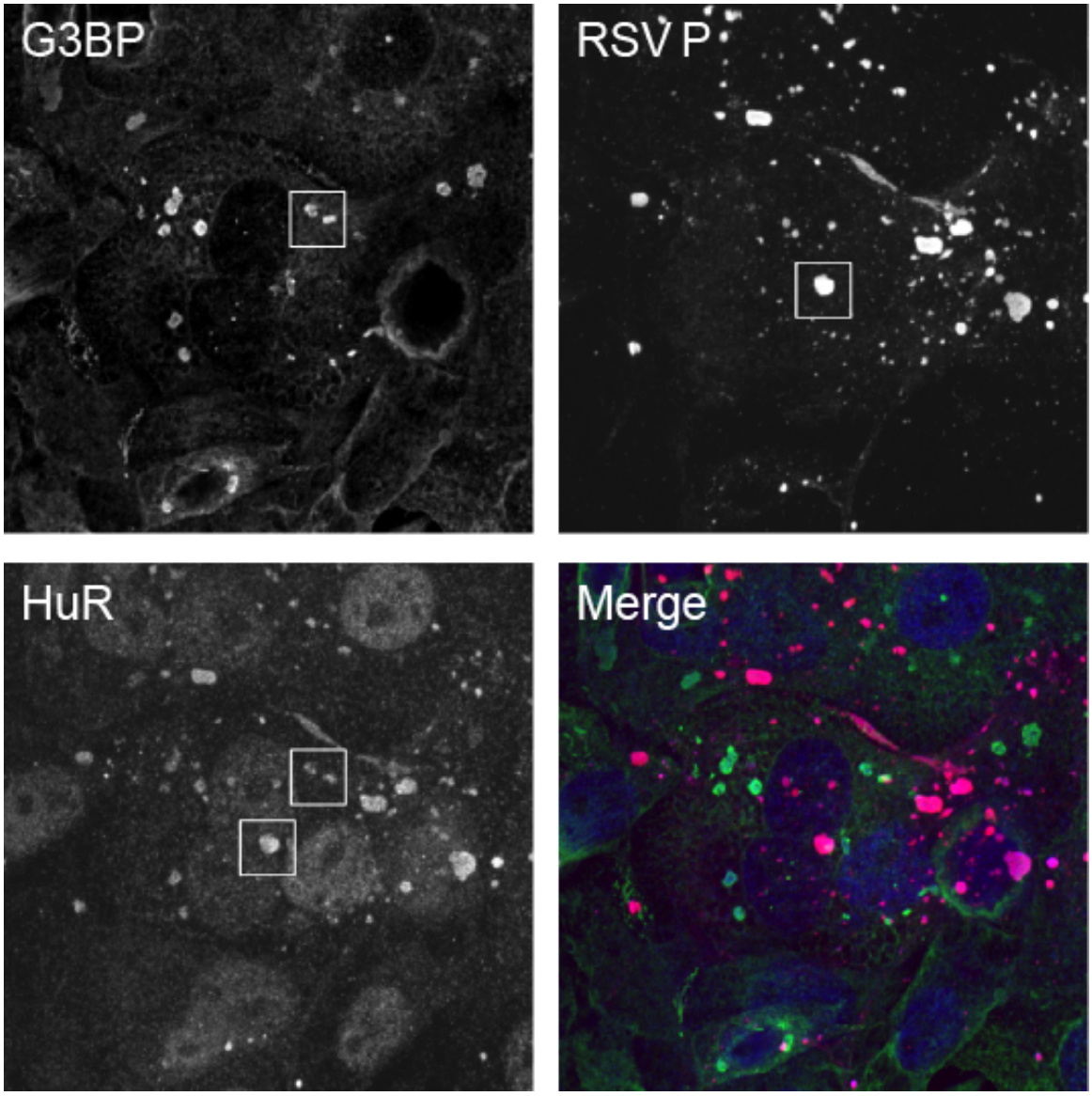

Figure 2-9. HuR protein colocalizes with RSV inclusion bodies. HEp-2 cells were infected with RSV (MOI=1.0) for 24 hours, fixed and prepared for immunofluorescence. Anti-G3BP was used to mark stress granules and appears green in the merge. Anti-RSV P was used to mark RSV inclusion bodies and appears red in the merge. HuR appears blue in the merge. White squares are used to mark areas in which HuR is contained in stress granules or inclusion bodies, respectively. The collapsed z-sections are shown for each image.

HuR expression when compared by western blot to wild-type cells or cells transduced with a non-targeting shRNA (Figure 2-10A). In contrast to G3BP knockdown, stress granule formation was not altered by HuR reduction when treated with sodium arsenite (data not shown). To test whether HuR plays a role in RSV infection, we inoculated wild-type HEp-2 or HuR-deficient cells with RSV (MOI=0.1) for 1, 2, 3, or 4 days. Viral supernatant and cell-associated virus was collected separately at each time point, and viral titer was determined by plaque assay. As shown in Figure 2-10C, we did not observe a significant change in viral titer for supernatant or cell-associated virus during infection in HuR-deficient cells. In addition, we monitored for any changes in RSV RNA levels. Wild-type or HuR-deficient cells were inoculated (MOI=0.1) for stated times and RNA was harvested. We again performed quantitative RNA studies. As shown in Figure 2-10B, we did not find a significant difference in RSV RNA levels when HuR expression was reduced. These data, combined with our viral titer results, indicate that wild-type level of HuR expression is not essential for viral replication even though a significant amount of HuR is recruited to inclusion bodies.

RSV genomic RNA is partially localized to stress granules. Previous reports using fluorescent molecular beacons specific for RSV genomic RNA suggested that RSV RNA could be found in RSV inclusion bodies during infection (Santangelo et al., 2006). In addition, more recent studies have shown that RSV RNA transiently interacts with arsenite-induced stress granules as well (Santangelo et al., 2009). Using a probe specific for RSV genomic RNA, we sought to determine whether RSV RNA could be found in

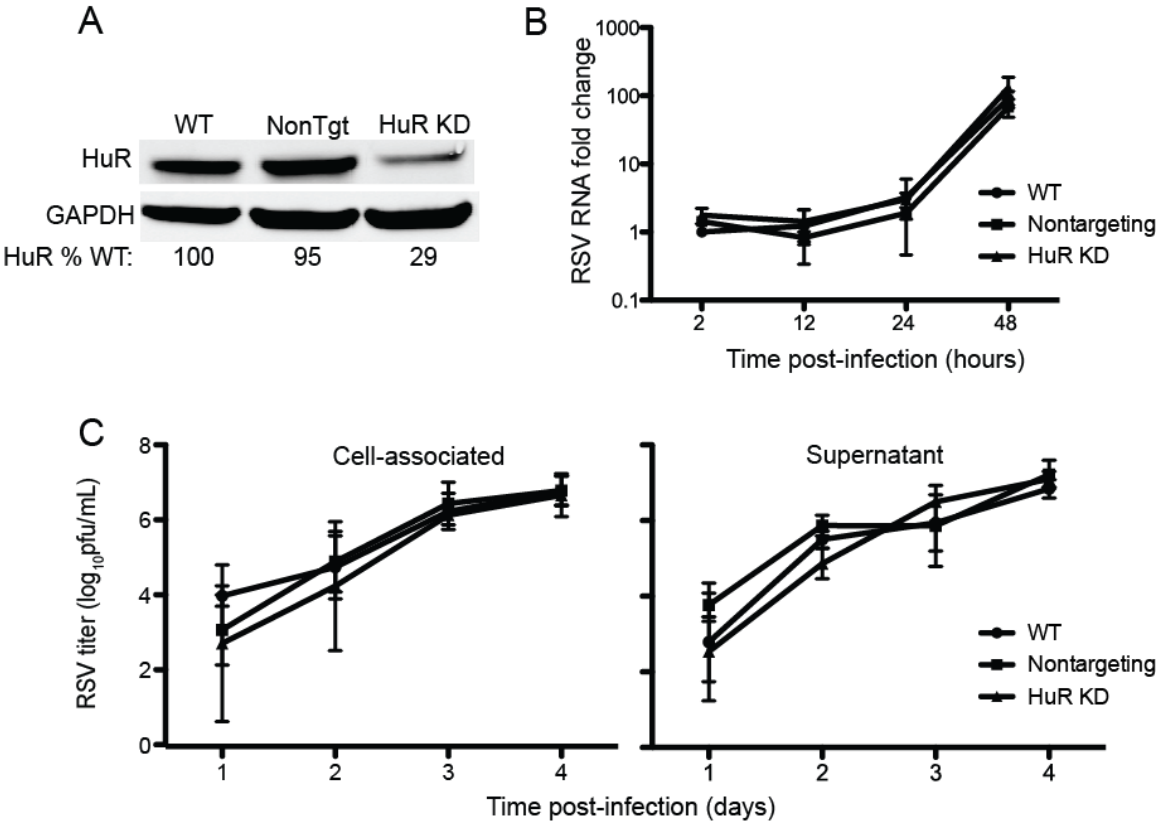

Figure 2-10. HuR protein is not required for RSV replication. (A) Cells transduced with non-targeting or HuR shRNA were compared with wild-type HEp-2 cells for expression levels of HuR. Total HuR levels were quantified for each cell type and compared to wild-type levels. (B) Wild-type HEp-2, nontargeting shRNA cells, or HuR-deficient cells were infected with RSV (MOI=0.1) for indicated times. Viral RNA was collected and assayed for fold change of RNA during infection. (C) Wild-type or HuR-deficient cells were infected with RSV (MOI=0.1) for indicated times. Cell-associated virus or supernatant virus was collected at each time point. Viral titer for each sample was determined by plaque assay.

RSV-induced stress granules as well as RSV inclusion bodies. HEp-2 cells were inoculated with RSV (MOI=1) for 1, 6, 12, and 24 hours. After infection, cells were reversibly permeabilized with streptolysin O and incubated with fluorescently labeled RNA probes. Cells then were fixed with paraformaldehyde and stained with a RSV N antibody to identify inclusion bodies and a monoclonal anti-G3BP antibody to identify stress granules (Figure 2-11). Using confocal microscopy, we then examined the localization of viral RNA at each time point. We observed colocalization between RSV inclusion bodies and viral RNA at all time points, quantifying 1, 12, and 24 hours after infection as shown in Figure 2-11. Using Volocity imaging software, we determined the average Manders overlap coefficients for the inclusion bodies with viral RNA, inclusion bodies with stress granules, and viral RNA with stress granules utilizing three fields of approximately 35 cells (Table 2-1). The images in Figures 2-11 and 2-12 and the data for Table 2-1 were kindly provided by Dr. Philip Santangelo and Aaron Lifland from the Georgia Institute of Technology. For viral RNA and inclusion bodies, the Manders overlap coefficient was 0.87, 0.96, and 0.91 (87, 96, and 91% overlap) for 1, 12 and 24 hours after infection, respectively. For the inclusion bodies with stress granules, the average Manders overlap coefficient was 0.0, 0.016, and 0.034 (0 – no stress granules, 1.6 and 3.4 % overlap), likely representing a transient interaction. For the viral RNA with stress granules, the average Manders overlap coefficient was 0.0, 0.022, and 0.045 (0 – no stress granules, 2.2, and 4.5% overlap), also likely representing a transient interaction. In addition, we show the overlapping intensity profiles of the viral RNA, inclusion bodies, and stress granules (as visualized in images in the first column of Figure 2-12) to demonstrate the amount of colocalization between each. Single plane confocal images

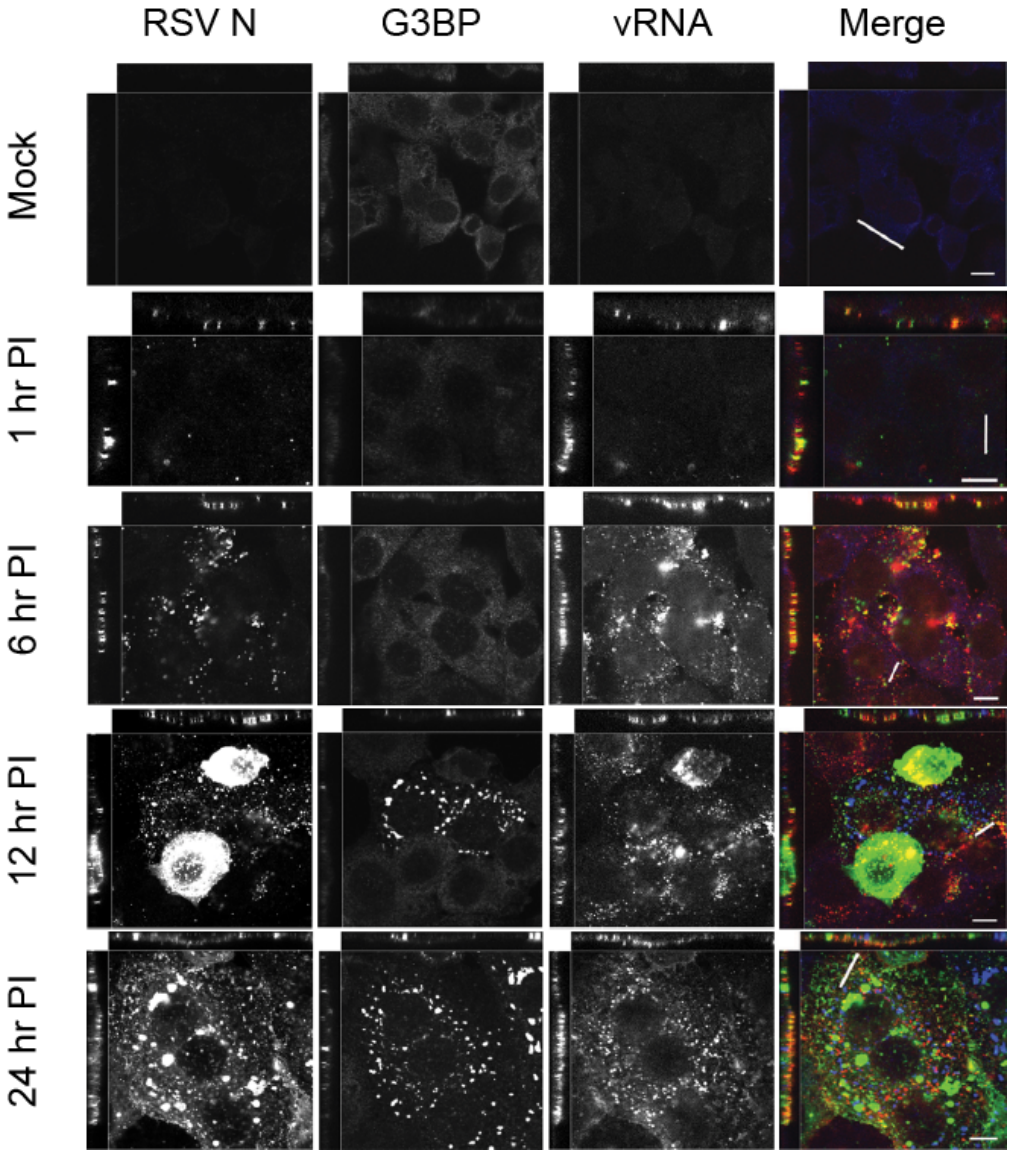

Figure 2-11. Viral genomic RNA predominantly colocalizes with RSV inclusion bodies. HEp-2 cells were mock-infected or infected with RSV (MOI=1) for indicated times. RSV RNA-specific probes were added as described in the Materials and Methods. Cells were fixed and processed for immunofluorescence. Anti-RSV N was used as an inclusion body marker and appears green in the merge panel. Anti-G3BP was used as a stress granule marker and appears blue in the merge panel. RSV RNA (vRNA) appears red in the merge panel (fourth column). The main images are XY, and the images above and below represent XZ and YZ cross-sections. The horizontal lines are scale bars, while the diagonal or vertical lines were used to calculate the intensity profiles.

Table 2-1. RSV RNA is predominantly associated with viral inclusion bodies.

	% Co-localization at time post infection		
	1 hour	12 hours	24 hours
Viral RNA + inclusion bodies	87	96	91
Viral RNA + stress granules	0.0	2.2	4.5
Inclusion bodies + stress granules	0.0	1.6	3.4

from the middle of cells that best reveal stress granules did not always also capture optimal representation of inclusion bodies and viral RNA in that cell (for ex 12 hr PI). Therefore, we also provided merge images for these structures at the surface of the same cells (Figure 2-12, second column).

Discussion

These experiments show that inoculation of human cells with RSV induces stress granules within 12 hours of inoculation, and the frequency of stress granules increases with time since inoculation. Although stress granule formation typically is associated with translation inhibition resulting in a potentially antiviral state, the findings here show that impairment of stress granule formation by G3BP-knockdown reduces RSV replication. In addition, the presence of stress granules was associated with more robust viral protein expression on a per-cell basis. Our data also suggest that even though RSV induces stress granules and these structures contain many RNA binding proteins, the site of viral RNA production is in viral inclusion bodies and not stress granules.

Following attachment and entry, RSV begins its life cycle with gene transcription using an RNA-dependent viral RNA polymerase. Following accumulation of viral mRNAs and proteins the viral polymerase switches from a predominant mode of transcription of mRNAs to replication of the viral genome. Interestingly, our results indicate that stress granule formation begins approximately when RSV initiates this switch.

G3BP was first described as an essential stress granule assembly protein through experiments that demonstrated that overexpression of G3BP results in spontaneous

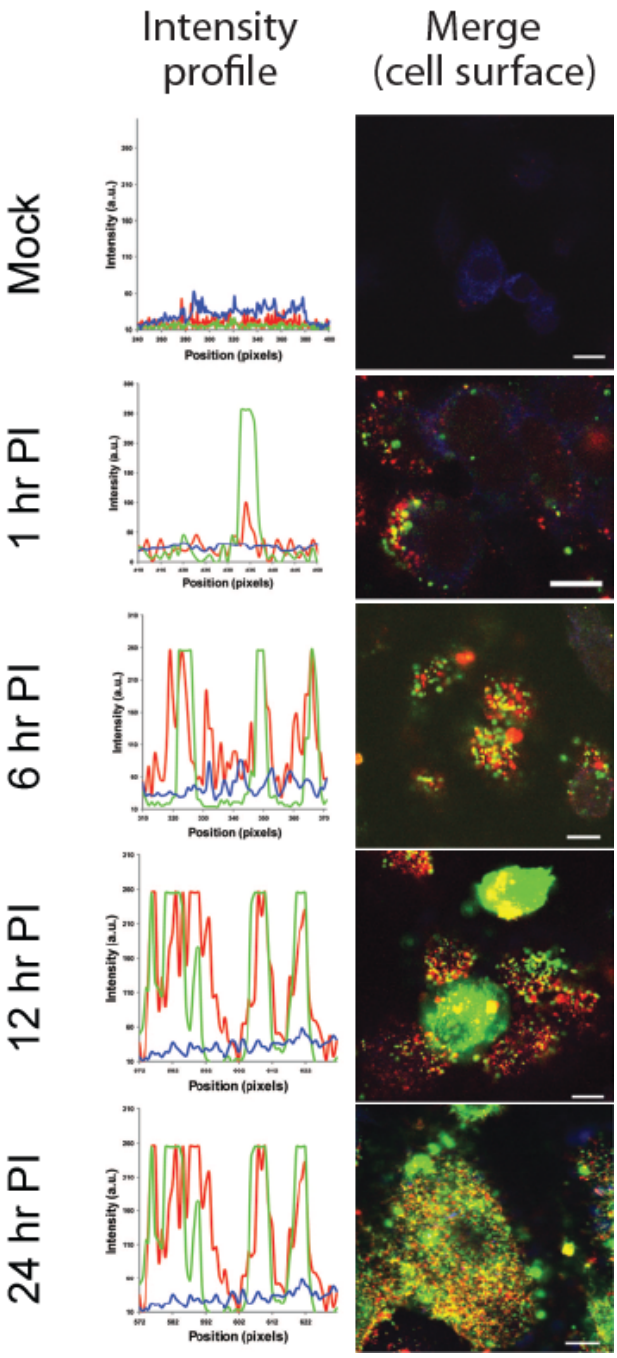

Figure 2-12. Viral genomic RNA predominantly colocalizes with RSV inclusion bodies. Intensity profiles at each time point from Figure 2-10 demonstrating the strong correlation between the N protein and viral genomic RNA (first column). Imaging of N (green), viral genomic RNA (red) and G3BP (blue) in mock, 1, 6, 12, and 24 hours post-infection at an image plane near the cell surface (second column).

formation of stress granules (Tourriere et al., 2003). Cells in which G3BP expression was modestly reduced by 30% using transient siRNA transfection were treated with arsenite. In these experiments large stress granules without G3BP could be observed in some cells while other cells contained smaller and fewer stress granules (White et al., 2007). TIA-1 also has been proposed to be an essential stress granule assembly protein. Previous reports demonstrated that TIA-1 knock-out mouse embryo fibroblasts treated with arsenite displayed a diminished capacity to form stress granules (Gilks et al., 2004). It has been proposed that these two proteins mediate stress granule formation in similar ways, because both proteins bind mRNA and both exhibit auto-aggregation properties. Other stress granule proteins such as TIAR (Gilks et al., 2004) and HuR (our studies) have been knocked down but appear to have little effect on stress granule formation. It should be noted that G3BP plays a role in other cellular functions besides stress granule formation. G3BP has been well characterized as a binding partner for Ras GTPase activating protein (RasGAP), a factor important in cellular proliferation pathways (Parker et al., 1996). In addition, G3BP is known to be a mRNA-binding protein with an endoribonuclease function (Gallouzi et al., 1998; Tourriere et al., 2001). Thus, knockdown of G3BP may have other unknown consequences on viral replication independent of stress granule formation.

In addition to RSV, parainfluenza virus 5 and Sendai virus are two other paramyxoviruses that are known to induce stress granules (Carlos et al., 2009; Iseni et al., 2002). In each case, stress granules were shown to be present at relatively late time points after infection (18-24 hours). This finding is in contrast to results with other viruses such as poliovirus and Semliki Forest virus that induce stress granules early after

infection but restrict stress granule assembly at later time points (McInerney et al., 2005; White et al., 2007). Thus, it is possible that stress granule formation enhances paramyxovirus replication during a portion of the viral life cycle. Further evidence of this enhancement comes from our results in G3BP-deficient cells. In these cells, stress granule formation was impaired and consequently viral replication was reduced. Other viruses such as West Nile virus and vaccinia virus recruit specific proteins involved in stress granule formation such as TIA-1 and G3BP respectively to viral replication factories (Emara and Brinton, 2007; Katsafanas and Moss, 2007). Our results show that neither TIA-1 nor G3BP associated with RSV RNA and neither protein was recruited to RSV inclusion bodies, which are the likely sites of viral replication.

HuR is a known mRNA binding protein thought to act as a translation enhancer. The protein typically binds AU-rich regions of the 3′ untranslated regions (UTR) of mRNAs and is a known component of stress granules (Kedersha et al., 2002). In addition, HuR has been shown to interact with elements of multiple viruses. HuR was shown to bind to the 3′ UTR of hepatitis C virus (HCV) (Spangberg et al., 2000). Knockdown of HuR resulted in reduction of HCV replicon RNA (Korf et al., 2005) indicating a potential role in HCV replication. Recently HuR was shown to interact with the HIV reverse transcriptase protein (Rivas-Aravena et al., 2009). When HuR was knocked down, HIV reverse transcription was impaired. Conversely, over-expression of HuR increased HIV reverse transcription. In our studies, although we observed HuR localization in viral inclusion bodies, knockdown of HuR by up to 70% did not affect viral replication. It is thus likely that HuR is not essential for RSV replication, or it is possible that modest levels of this protein can maintain such a role.

Interactions between viral RNA and stress granule proteins have been described. Previous studies have shown that Sendai virus RNA contains TIAR-binding sites, suggesting viral RNA interaction with stress granule proteins (Iseni et al., 2002). The West Nile virus 3′ terminal stem loop RNA binds TIA-1 and TIAR (Li et al., 2002). In addition, we recently showed that RSV RNA interacts transiently with stress granules when infected cells were treated with arsenite (Santangelo et al., 2009). In these studies, individual granules of RSV RNA were observed to move into juxtaposition with stress granules, dock, and then separate again. We observed similar transient interactions between RSV RNA and stress granules here, however our data suggest that viral genomic RNA is much more abundant in viral inclusion bodies.

Detailed understanding of the molecular mechanisms underlying stress granule effects during viral infection is lacking. In fact, evidence exists for both pro-viral and anti-viral roles. When TIA-1 knockout cells that exhibit impaired stress granule formation were infected with VSV or Sindbis virus, both viruses grew to higher titers, indicating that TIA-1 or possibly stress granules are restrictive to these viruses (Li et al., 2002). However infection of TIAR knockout cells with West Nile virus resulted in decreased viral titers, suggesting a pro-viral role for this protein. It is important to note however, that the functional role of stress granules in any sort of stress condition is still not completely understood. Stress granules have been proposed to be sites of mRNA sorting during periods of translation inhibition generated by a variety of stresses (Kedersha and Anderson, 2002). While multiple species of mRNA have been shown to be associated with stress granules, this association appears to be transient in nature (Kedersha et al., 2005; Kedersha et al., 1999; Mazroui et al., 2007). More recent studies

have suggested that mRNA cycles between the cytoplasm and stress granules, and that the vast majority of cellular mRNA remains cytoplasmic, suggesting that these structures are neither a holding nor modification site for mRNAs (Mollet et al., 2008).

Our studies suggest a functional role for stress granules during RSV infection that enhances replication. Further experiments will need to be carried out to determine the exact mechanism of induction and the true role of these structures. Identification of a specific function of stress granules during viral infection also could elucidate a general function for these structures in the normal cell life cycle.

CHAPTER III

RSV REPLICATION IS NOT DEPENDENT ON PKR-STIMULATED STRESS GRANULE FORMATION

Introduction

Following the observations I made in Chapter I, I designed a number of experiments to determine the upstream signaling pathways that lead to RSV-induced stress granule formation. As mentioned in the introduction, there are four known kinases that phosphorylate eIF2α, resulting in stress granule formation. I reasoned that the most likely of these kinases activated by RSV was PKR, given that many viruses are known to regulate expression and activation of this kinase. I attempted several methods to inhibit PKR, but here I present the two most reliable methods we found to block PKR activation.

In this chapter, I first determine that eIF2α and PKR are both phosphorylated during RSV infection. I then present data to show that the PKR inhibitor, 2-aminopurine (2-AP), also restricts RSV replication. However, knockdown of PKR by shRNA does not affect RSV replication. I then demonstrate that the reduction in RSV replication mediated by 2-AP treatment is independent of PKR expression or activation. Finally, I show that activation of PKR is the primary mechanism by which RSV induces stress granules.

Materials and Methods

Cells. HEp-2 cells (ATCC CCL-23) were maintained in OPTI-MEM I medium (Invitrogen) containing 5% (v/v) fetal calf serum (Sigma), 2 mM L-glutamine (Mediatech), 2.5 μg/mL amphotericin B (Mediatech), 10 μg/mL streptomycin (Mediatech), and 10 U/mL penicillin (Mediatech). L929 cells were grown in either suspension or monolayer cultures in Joklik's modified Eagles minimal essential medium (SMEM, Lonza) supplemented to contain 5% (v/v) fetal bovine serum (FBS, Invitrogen), 2 mM L-glutamine (Invitrogen), 100 U/mL of penicillin, 100 μg/mL of streptomycin (Invitrogen), and 250 μg/mL amphotericin B (Sigma).

Viruses. A suspension of RSV wild-type strain A2 prepared in HEp-2 cells (1×10^6 pfu/mL) was used to infect HEp-2 cell monolayer cultures. Infectious virus was adsorbed to the cells for one hour in a 37 °C incubator in 5% CO_2. Following adsorption, the inoculum was removed and fresh medium added. Cells then were incubated at 37 °C in 5% CO_2 for the duration of the infection period. Reovirus strain T1L was a kind gift from the laboratory of Dr. Terence Dermody.

Viral titration. For RSV plaque assays, cell-associated virus was harvested at indicated times by scraping infected HEp-2 cell culture monolayers into 1.0 mL of medium. Virus then was released from harvested cells as described previously (Utley et al., 2008). Viral titers were determined using plaque assays as described previously (Murphy et al., 1990). For reovirus, titers were determined by plaque assay using L929 cells. Reovirus-infected

HEp-2 cells were scraped into the medium, frozen at -80°C and thawed at room temperature twice prior to determination of viral titer in the suspension by plaque assay (Virgin et al., 1988). Reovirus yields were calculated according to the following formula: $\log_{10}$ yield$t$ = $\log_{10}$ (PFU/mL)t – $\log_{10}$ (PFU/mL)t0 where t is the time postinfection, t0 is the time at inoculation after absorption.

2-Aminopurine (2-AP) treatment. We generated a 150 mM stock solution of 2-AP (Sigma A3509) diluted in phosphate buffered saline (PBS) and glacial acetic acid (Fisher A-38-500). Glacial acetic acid was diluted at a ratio of 1:200 in PBS. For each use, the solution was heated to 60 °C for re-suspension. HEp-2 cells were pretreated with 10 mM 2-AP diluted in medium or mock-treated with vehicle (glacial acetic acid in PBS). Cells then were infected with RSV in the presence of 10 mM 2-AP or vehicle for one hour. Following infection, inoculum was removed and replaced with fresh medium containing 10 mM 2-AP or vehicle and incubated for the duration of infection.

Fixation and immunostaining. Cells were fixed with 3.7% (w/v) formaldehyde in PBS for 10 minutes at room temperature. Cells were permeabilized with 0.2% (w/v) Triton X-100 and 3.7% paraformaldehyde in PBS for 10 minutes at room temperature. Following fixation, cells were blocked in 5% (w/v) BSA in PBS for one hour followed by addition of primary antibody for one hour. Cells then were washed three times in PBS and species-specific IgG Alexa Fluor (Molecular Probes) was added at a dilution of 1:1,000 in block solution for detection of primary antibodies. Cells were washed 3 times in PBS and fixed on glass slides using Prolong Antifade kit (Molecular Probes). Images were

obtained on a Zeiss inverted LSM510 confocal microscope using a 40X Plan-Neofluar oil objective lens. A polyclonal anti-G3BP (ab37906) antibody was obtained from Abcam and used for immunostaining. Monoclonal anti-phosphorylated eIF2α (1090-1) and anti-PKR (1511-1) antibodies were from Epitomics. An anti-RSV F protein humanized mouse monoclonal antibody (palivizumab; MedImmune) was used to identify RSV F protein. Anti-RSV P protein (clone 3_5) monoclonal antibody was a kind gift of Earling Norrby and Ewa Bjorling.

shRNA reagents. Lentiviral shRNA particles were obtained from Dharmacon for human GAPDH (S-001000-01), a non-targeting control (S-005000-01), and a set of three PKR SMARTvector shRNA constructs (SK-003527-00-10). HEp-2 cells were plated in 96-well plates and transduced with individual lentiviral constructs according to the manufacturer's protocol. For selection of each target, cells containing integrated lentivirus sequences were selected using puromycin (5 μg/mL) diluted in medium. Medium containing puromycin was replaced every three days until resistant colonies were observed.

Western blots. HEp-2 cells were grown on 6-well plates and harvested for protein. Cell lysates were obtained using lysis buffer (50 mM Tris-HCl, 150 mM NaCl, 1% Triton X-100, pH 8.0) containing 0.5% (v/v) of protease inhibitor cocktail (Sigma) and 1.0% (v/v) of phosphatase inhibitors (Sigma). Lysates were separated on 4-12% NuPAGE Bis-Tris gels (Invitrogen) and transferred to nitrocellulose membranes using an iBlot dry blotting system (Invitrogen). Membranes were blocked for one hour using Odyssey blocking

buffer (Li-Cor) diluted 1:1 in PBS. Primary antibodies were diluted in blocking buffer and incubated overnight at 4 °C. Membranes then were washed four times in Tris buffered saline + 0.2% Tween (TBST) for five minutes each. Li-Cor IRDye 680CW or IRDye 800CW secondary antibodies were diluted 1:5,000 in blocking buffer and added to each membrane for one hour. Membranes were washed four times in TBST. Bands were imaged and quantitated using the Odyssey Infrared Imaging System. Total PKR or phosphorylated PKR were detected using monoclonal antibodies from Epitomics (1511-1 and 2283-1, respectively). GAPDH was detected using a monoclonal antibody from Millipore (MAB374).

Results

RSV induces the phosphorylation of eIF2α and PKR. We have shown previously that RSV infection of cells potently induces stress granule formation (Chapter II), (Lindquist et al., 2010). We sought here to determine the mechanism by which RSV initiates this process. Typcially, stress granules form following induction of one of many types of stress-related pathways that result in a common downstream event, phosphorylation of the translation initiation factor, eIF2α (Kedersha and Anderson, 2007). Therefore, we examined cells inoculated with RSV (MOI=1.0 pfu/cell) for the presence of phosphorylated eIF2α using indirect immunofluorescence. We observed a striking increase in eIF2α phosphorylation beginning 12 hours post-inoculation that was concomitant with the appearance of stress granules and continued throughout infection (Figure 3-1).

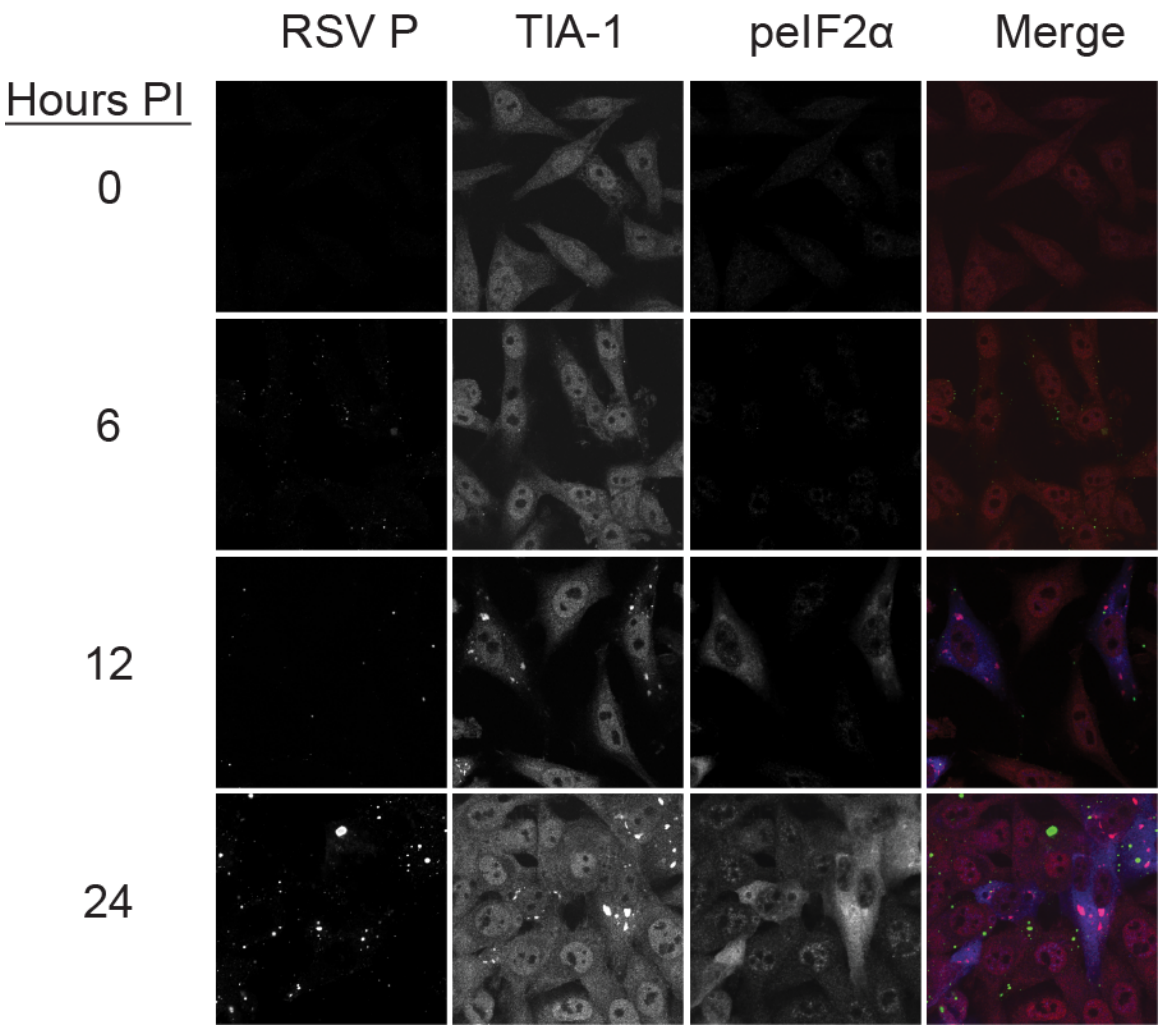

Figure 3-1. eIF2α is phosphorylated during RSV infection. HEp-2 cells were infected with RSV (MOI=1.0 pfu/cell) for the indicated times, fixed, and processed for immunofluorescence. Anti-RSV P monoclonal antibody was used to localize viral protein and appears green in the merge panel. Anti-TIA-1 antibody was used to detect stress granule formation and appears red in the merge panel. Phosphorylated eIF2α (peIF2α) appears blue in the merge panel.

We next sought to determine the mechanism by which RSV mediates the phosphorylation of eIF2α. There are four well-defined kinases capable of eIF2α phosphorylation: protein kinase RNA (PKR), a kinase activated by double-stranded RNA; PKR-like ER-localized eIF2α kinase (PERK); general control nonrepressed 2 (GCN2); and heme-regulated inhibitor kinase (HRI) (Proud). In cells inoculated with RSV (MOI=1.0 pfu/cell) for 24 hours, we observed phosphorylated PKR and higher expression of total PKR in comparison to mock-inoculated cells (Figure 3-2), consistent with previous reports.

The chemical inhibitor 2-AP prevents PKR signaling and reduces RSV infection. To confirm that PKR activation is dispensable for RSV replication, we sought another method to inhibit activation of the kinase. The nucleotide analog 2-AP prevents PKR activation (Hu and Conway, 1993). We first tested whether 2-AP treatment alters RSV-mediated PKR activation. HEp-2 epithelial cells were pretreated with 10 mM 2-AP or vehicle for two hours. We then inoculated cells with RSV (MOI=1.0 pfu/cell) in the presence of 2-AP or vehicle control for one hour. The inoculum was removed and replaced with medium containing 2-AP or vehicle, and the infection was allowed to proceed for 24 hours. Cell lysates were harvested for immunoblotting to assess the level of total or phosphorylated PKR. The phosphorylation of PKR in RSV-infected cells treated with 2-AP was greatly reduced in comparison to vehicle-treated cells (Figure 3-3). In addition, we did not observe an increase in total PKR levels in the presence of 2-AP that occurs during RSV infection following virus inoculation. As a control, we compared 2-AP-treated and vehicle-treated cells in the absence of infection and found no changes in

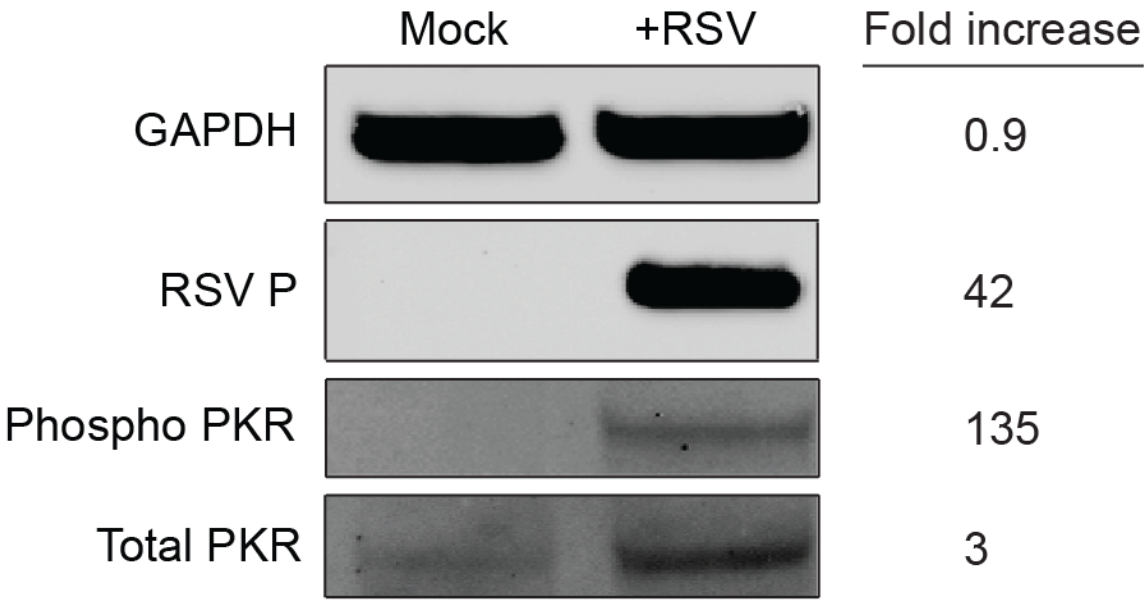

Figure 3-2. RSV infection results in PKR activation. HEp-2 cells were mock-inoculated or inoculated with RSV (MOI=1.0 pfu/cell) for 24 hours. Cell lysates were analyzed by immunoblots for GAPDH, RSV P, phosphorylated PKR, or total PKR. Relative protein densities comparing RSV-infected cells to mock-infected cells were quantified using Li-Cor Odyssey imaging software.

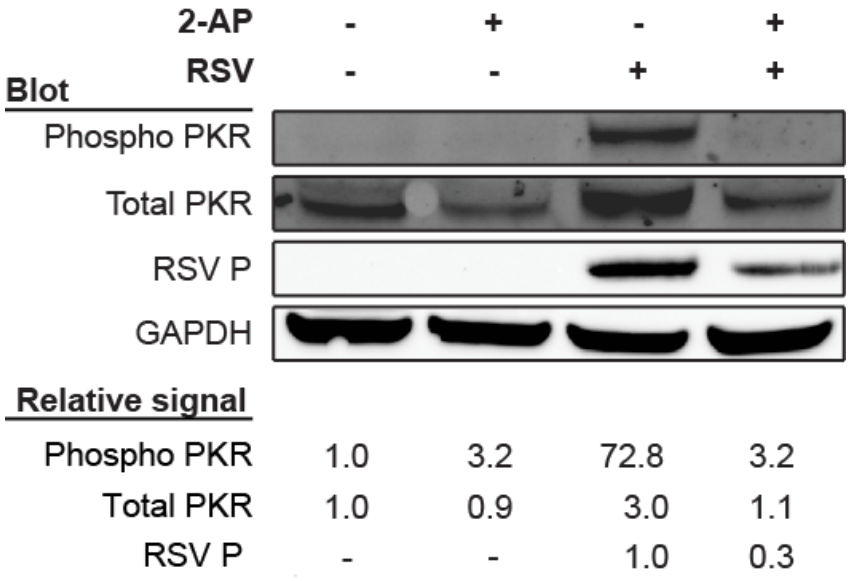

Figure 3-3. Treatment with 2-AP prevents PKR activation during RSV infection. HEp-2 cells were pretreated with 10 mM 2-AP or vehicle. Cells then were mock-inoculated or inoculated with RSV (MOI=1.0 pfu/cell) for 24 hours in the presence of 2-AP or vehicle. Cell lysates were analyzed by immunoblots for GAPDH, RSV P, phosphorylated PKR, or total PKR. Relative protein densities were quantified using Li-Cor Odyssey imaging software. The relative amount of RSV P protein expression was quantified for cells infected with RSV and treated with either vehicle or 2-AP. Protein levels were standardized to RSV-infected and vehicle-treated cells. The relative expression of PKR and phosphorylated PKR were quantified for each condition and compared to that of mock-infected cells treated with vehicle.

the levels of PKR or phosphorylated PKR. These results indicate that 2-AP inhibits PKR activation during RSV infection. We next assessed the effect of 2-AP treatment on viral protein expression using an immunobloting assay for RSV P protein as a surrogate marker. Relative amounts of total PKR, phosphorylated PKR, RSV P, and GAPDH were quantified using Odyssey imaging analysis software. Interestingly, we observed a 70% decrease in the amount of RSV P protein in 2-AP-treated cells in comparison to vehicle-treated cells. This result suggests that treatment with 2-AP inhibits viral protein synthesis.

To directly determine the effect of 2-AP treatment on RSV infection, we used indirect immunofluorescence to detect viral proteins in infected cells. Cells were pretreated with 2-AP or vehicle and inoculated with RSV (MOI=1.0 pfu/cell). After 24 hours, cells were fixed and stained for the RSV F protein as a marker for infection (Figure 3-4A). RSV-infected cells per high-powered field (HPF) were quantified for each treatment. We observed an approximately 80% decrease in the percent of cells that stained positively for RSV F protein following 2-AP treatment (Figure 3- 4B). Thus, 2-AP treatment diminishes RSV infectivity.

To determine the effects of 2-AP treatment on the capacity of RSV to complete an infectious cycle, cells were pretreated with vehicle or 2-AP and inoculated with RSV (MOI=0.1 pfu/cell). After a one-hour adsorption, the inoculum was replaced with medium containing vehicle or 2-AP. Titers of cell-associated virus were determined at 24-hour intervals for 0-4 days. The results show that 2-AP treatment mediated an approximately 1000-fold decrease in viral titer throughout the timecourse of infection (Figure 3-5A). To determine if 2-AP treatment affects viral entry, cells were pretreated with 2-AP and then inoculated with RSV (MOI=0.1 pfu/cell). The inoculum then was

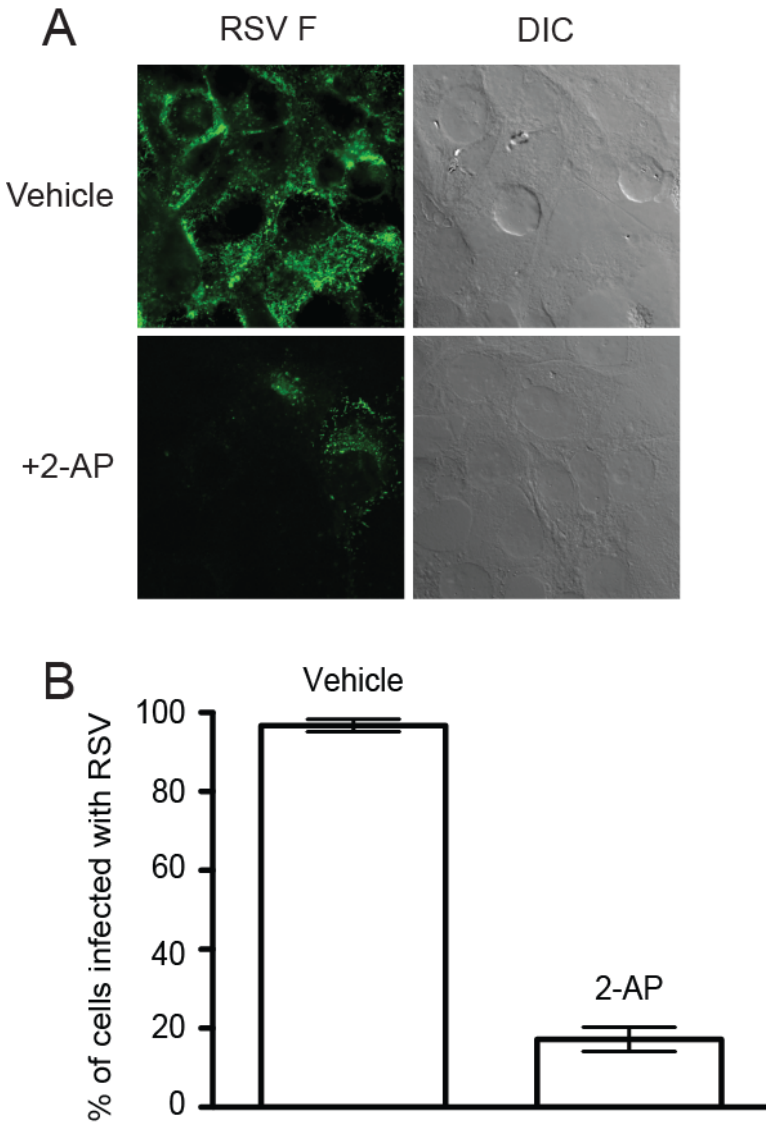

Figure 3-4. Treatment with 2-AP reduces RSV infectivity. (A) HEp-2 cells were pretreated with 2-AP or vehicle, inoculated with RSV (MOI=1.0 pfu/cell) for 24 hours in the presence of 2-AP or vehicle, and processed for immunofluorescence. Anti-RSV F antibody was used to detect virus-infected cells. Differential interference contrast (DIC) was used to define the periphery of each cell. (B) The percentage of cells per HPF that stained positively for RSV F protein in images from (A) was determined. Error bars indicate SEM.

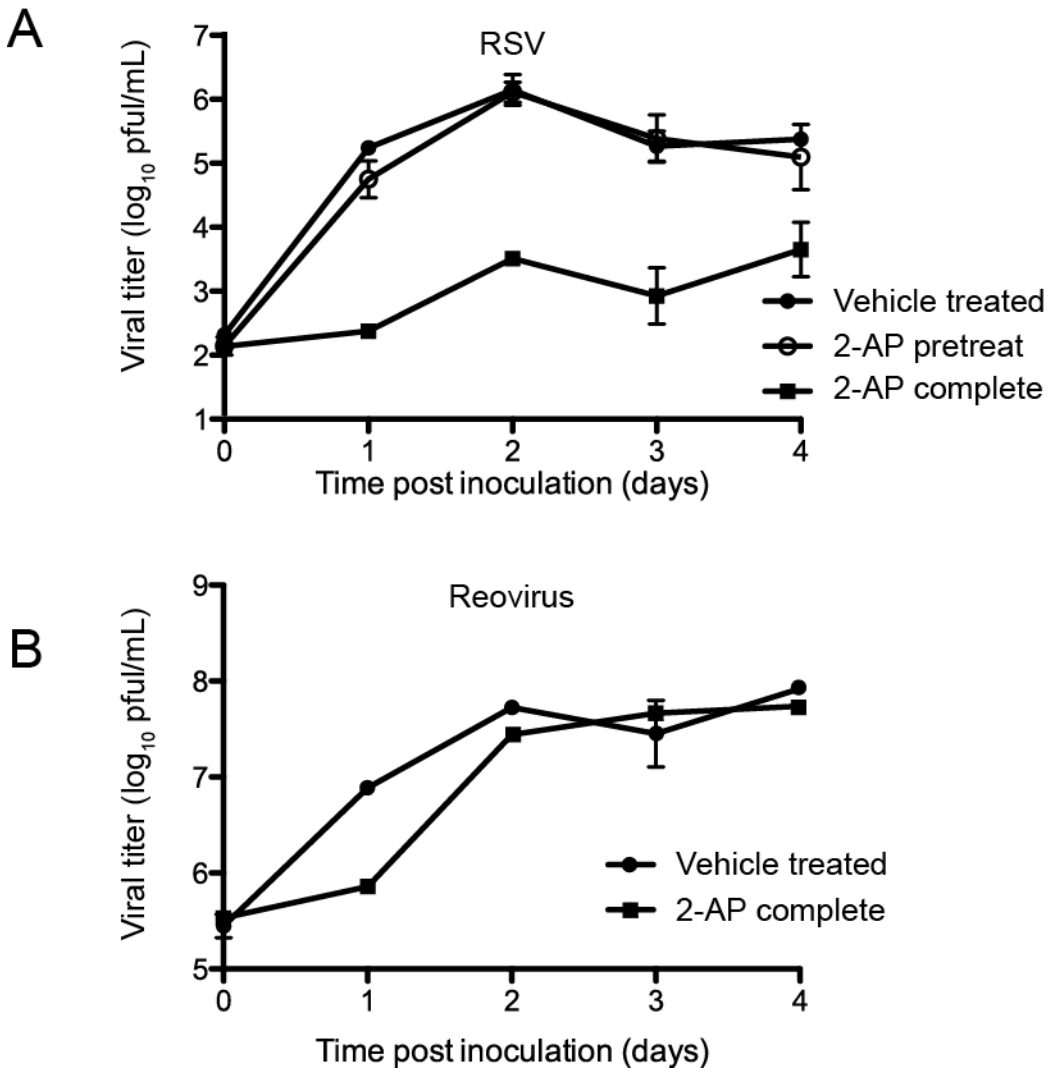

Figure 3-5. Treatment with 2-AP inhibits RSV replication. (A) HEp-2 cells were (i) pretreated with vehicle, inoculated with RSV (MOI=0.1 pfu/cell), and incubated in medium containing vehicle; (ii) pretreated with 2-AP, inoculated, and incubated in medium containing vehicle; or (iii) pretreated with 2-AP, inoculated, and incubated in medium containing 2-AP. (B) HEp-2 cells were incubated with vehicle or 2-AP and inoculated with reovirus (MOI=5.0 pfu/cell), in the presence of 2-AP or vehicle. Viral titers were determined at the intervals shown by plaque assay for (A) and (B). Error bars indicate standard deviations.

replaced with medium containing vehicle control only and incubated for 0-4 days. In contrast to cells incubated with 2-AP throughout infection, cells that had only been pretreated with 2-AP exhibited no change in viral titer when compared to vehicle-treated cells. These results suggest that 2-AP does not affect viral entry but rather a later step in the viral life cycle. To determine whether the effects of 2-AP treatment on RSV were virus-specific, we performed a similar experiment using reovirus. Reovirus replication is unaffected by PKR knockdown (Zhang and Samuel, 2007). In addition, the reovirus σ3 protein inhibits PKR activation by competitively binding dsRNA targets (Sherry, 2009). In contrast to our results with RSV, 2-AP treatment only affected reovirus replication during the first 24 hours after infection. After 24 hours, we did not observe a significant difference in viral titers between 2-AP treated or vehicle-treated cells, indicating that 2-AP treatment is much less inhibitory for reovirus replication in comparison to the effect on RSV (Figure 3-5B).

Knockdown of PKR expression does not affect RSV replication. We investigated what effects inhibition of PKR signaling might have on RSV replication. HEp-2 cells were transduced with shRNA lentiviral constructs specific for PKR or a non-targeting shRNA control. We selected for cells stably expressing the shRNA constructs and we compared PKR levels by immunoblotting in wild-type cells that were not transduced or cells transduced with PKR-targeting or non-targeting shRNA. Cells expressing the PKR shRNA construct exhibited an approximate 90% decrease in total PKR protein levels (Figure 3-6A) in comparison to wild-type cells or those expressing a non-targeting shRNA. Wild-type, non-targeting, or PKR-knockdown cells were inoculated with RSV

(MOI=1.0 pfu/cell) and incubated for 24 hours. Immunoblot analysis of cell lysates did not demonstrate an increase in PKR phosphorylation in the RSV-inoculated PKR-knockdown cells in comparison to wild-type or non-targeting shRNA cells. We next quantified the viral titers over a time course for each cell type. Cells were inoculated with RSV (MOI=0.1 pfu/cell) and incubated for 0-4 days. Cell-associated virus was harvested for each time point, and titers were determined by plaque assay. Viral titers in the PKR-knockdown cells did not differ significantly from those in either wild-type cells or non-targeting shRNA-expressing cells (Figure 3-6B). These results indicate that inhibition of PKR activation does not affect RSV replication.

2-AP inhibits RSV replication in the absence of PKR. We next tested whether the effect on viral replication observed following 2-AP treatment requires PKR. We quantified the effect on viral titers in RSV-inoculated wild-type, non-targeting shRNA, or PKR-knockdown cells treated with 2-AP or vehicle. Cells were inoculated with RSV (MOI=0.1 pfu/cell) and incubated for 0-4 days. Cells were collected for each time point, and titers of cell-associated virus were determined by plaque assay. Treatment of cells with 2-AP once again mediated a 1000-fold reduction in viral titers throughout the time course (Figure 3-7A). Remarkably, 2-AP inhibited RSV replication in each cell type regardless if whether PKR was expressed or induced.

We next treated wild-type, non-targeting shRNA, or PKR-knockdown cells with 2-AP or vehicle and inoculated the cells with RSV (MOI=1.0 pfu/cell). Following incubation for 24 hours, we harvested the cell lysates and used immunoblots to detect total PKR, phosphorylated PKR, or RSV P. The results show that 2-AP inhibited RSV P

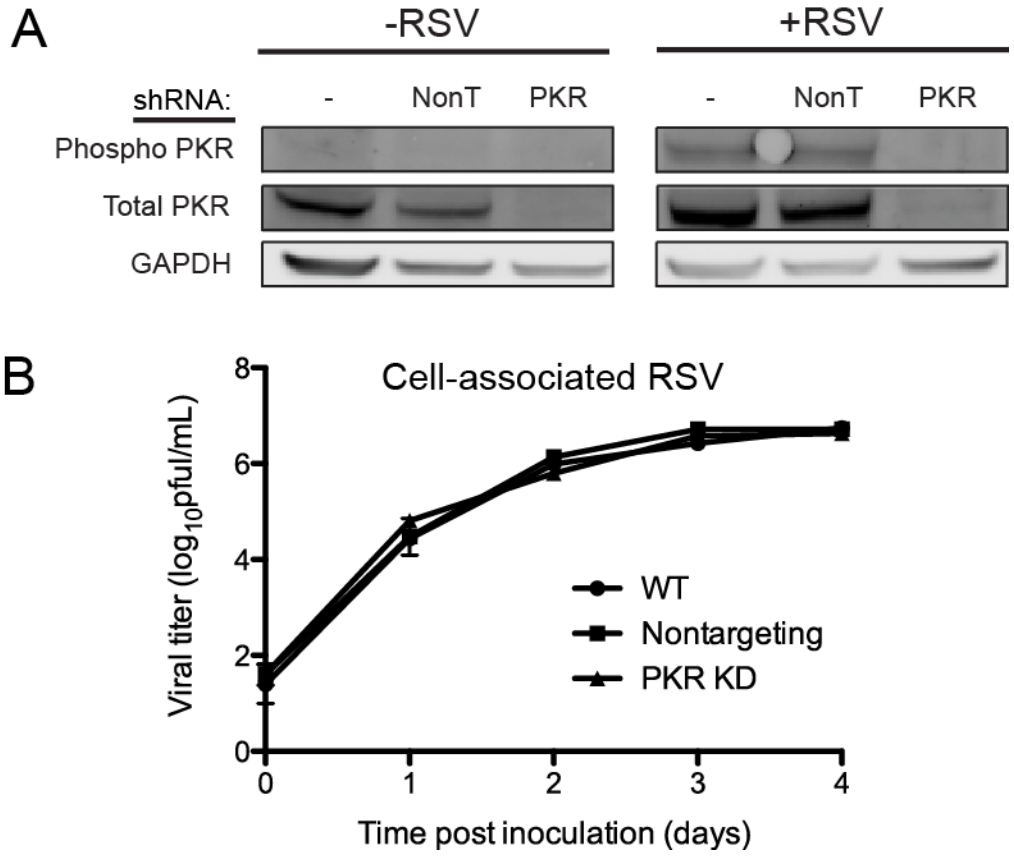

Figure 3-6. PKR knockdown does not affect RSV replication. (A) Wild-type HEp-2 cells or HEp-2 cells transduced with nontargeting shRNA (NonT) or PKR-specific shRNA were mock-inoculated or inoculated with RSV (MOI=1.0 pfu/cell) for 24 hours. Cell lysates were analyzed by immunoblotting for total PKR, phosphorylated PKR, or GAPDH. (B) Each cell type from (A) was inoculated with RSV (MOI=0.1 pfu/cell) for the indicated times. Titers of cell-associated virus were determined for each time point by plaque assay. Error bars indicate standard deviations.

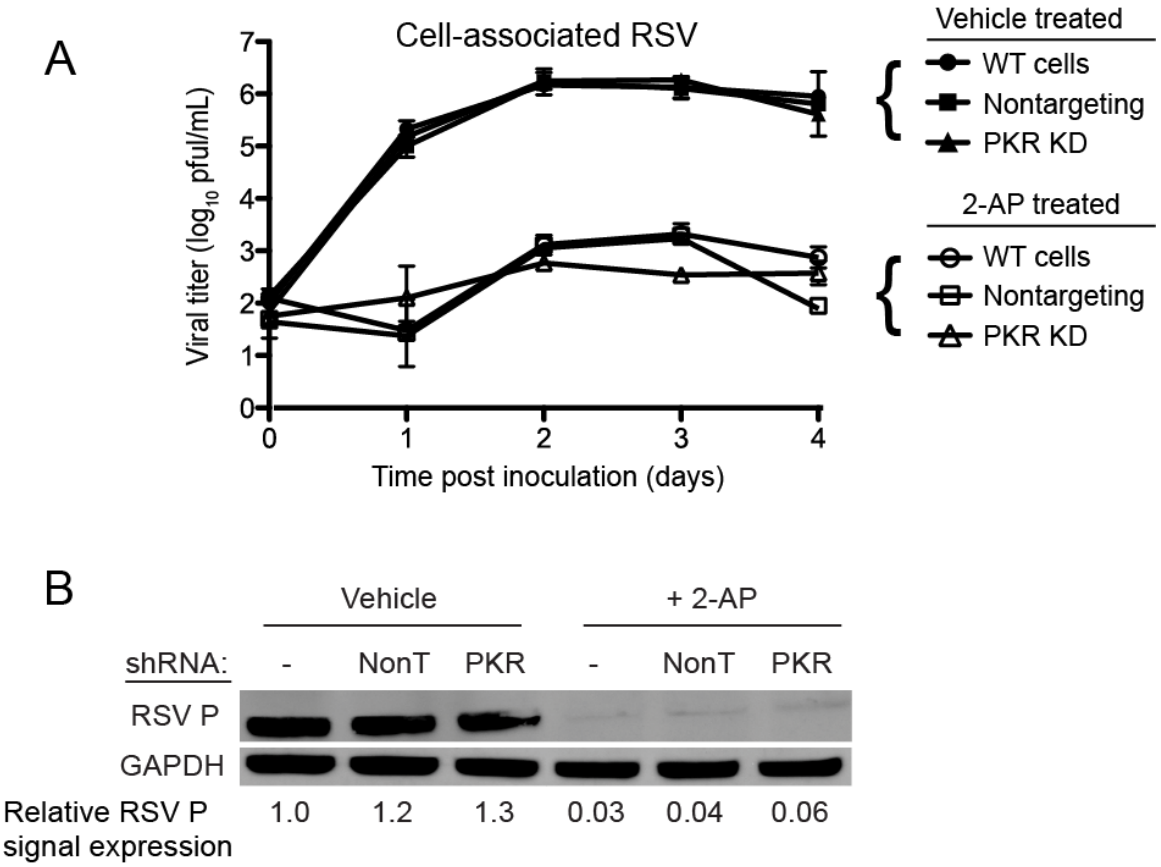

Figure 3-7. **Treatment with 2-AP inhibits RSV replication independent of PKR.** ((A) Wild-type HEp-2 cells or HEp-2 cells transduced with nontargeting shRNA (NonT) or PKR-specific shRNA were pretreated with 10 mM 2-AP or vehicle. Cells were inoculated with RSV (MOI=0.1 pfu/cell) in the presence of 2-AP or vehicle for the indicated intervals. Titers of cell-associated virus were determined for each time point by plaque assay. (B) Each cell type from (A) was pretreated with 10 mM 2-AP or vehicle and inoculated with RSV (MOI=1.0 pfu/cell) for 24 hours in the presence of 2-AP or vehicle. Cell lysates were subjected to immunoblotting for RSV P protein and GAPDH. The relative amount of RSV P protein was quantified for each cell type and compared to that in wild-type cells treated with vehicle. Error bars indicate standard deviations.

production in each cell type, independent of PKR levels (Figure 3-7B). Taken together, these data indicate that inhibition of PKR activation does not affect RSV replication. Furthermore, the decrease in RSV replication by 2-AP appears to be mediated via a PKR-independent mechanism.

PKR knockdown cells infected with RSV form fewer stress granules. We next determined whether PKR is the kinase responsible for stress granule formation during RSV infection. We infected wild-type, shRNA non-targeting, or PKR-knockdown cells with RSV for 48 hours (MOI=5.0 pfu/cell). We then examined cells for the presence of stress granules using indirect immunofluorescence (Figure 3-8). In wild-type and shRNA non-targeting cells, we observed robust stress granule formation in infected cells. However, in PKR-knockdown cells, stress granule formation was substantially diminished. These results confirm that PKR is required for stress granule formation following RSV infection.. As expected, the PKR knockdown cells displayed decreased staining for PKR, although this population was heterologous in PKR expression. We observed many fewer cells with stress granules in the PKR knockdown line, indicating that PKR is probably the primary mechanism by which RSV induces stress granules. Figure 3-9 shows that among those cells that formed stress granules in the PKR knockdown line, cells expressing the highest levels of PKR were more likely to form stress granules, although not all of the PKR-high cells formed stress granules.

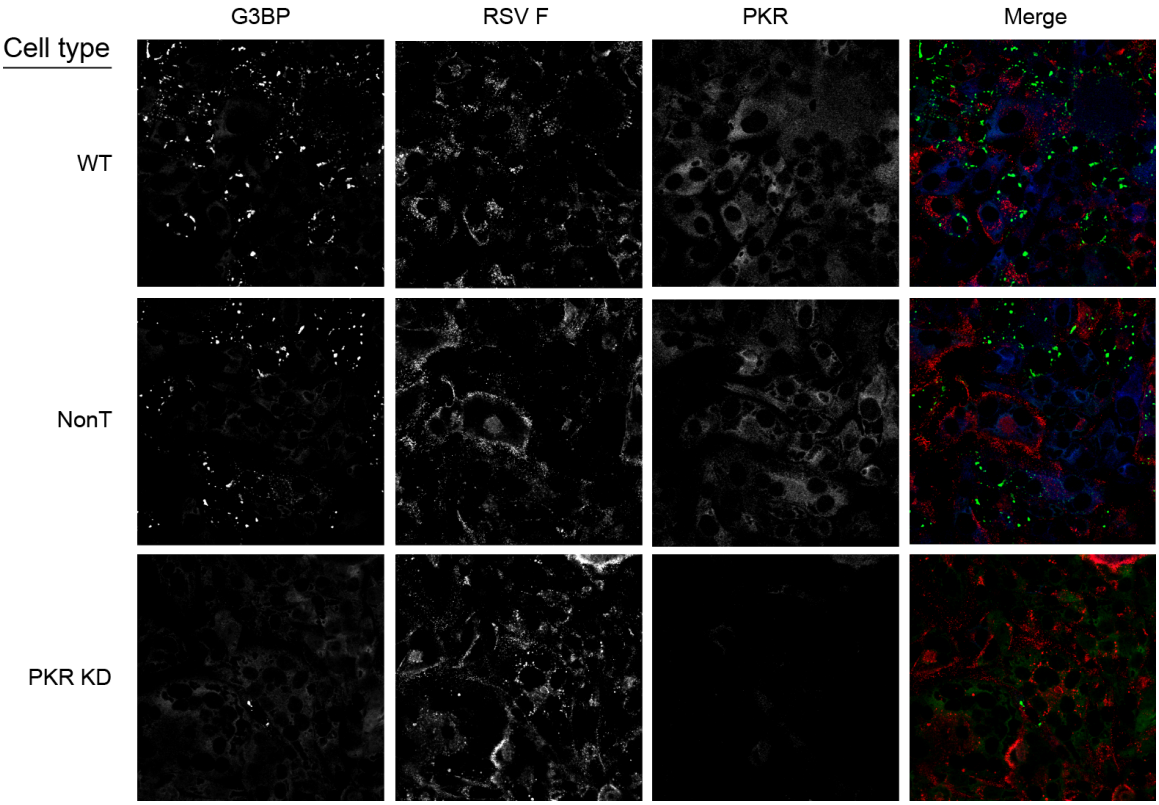

Figure 3-8. PKR knockdown reduces RSV-mediated stress granule formation. Wild-type cells or HEp-2 cells transduced with nontargeting shRNA (NonT) or PKR-specific shRNA were inoculated with RSV (MOI=5.0 pfu/cell) for 48 hours, fixed, and processesed for immunofluoresence. Anti-G3BP monoclonal antibody was used to detect stress granules and appears green in the merge panel. Anti-RSV F antibody was used to localize viral protein and appears red in the merge panel. PKR appears blue in the merge panel.

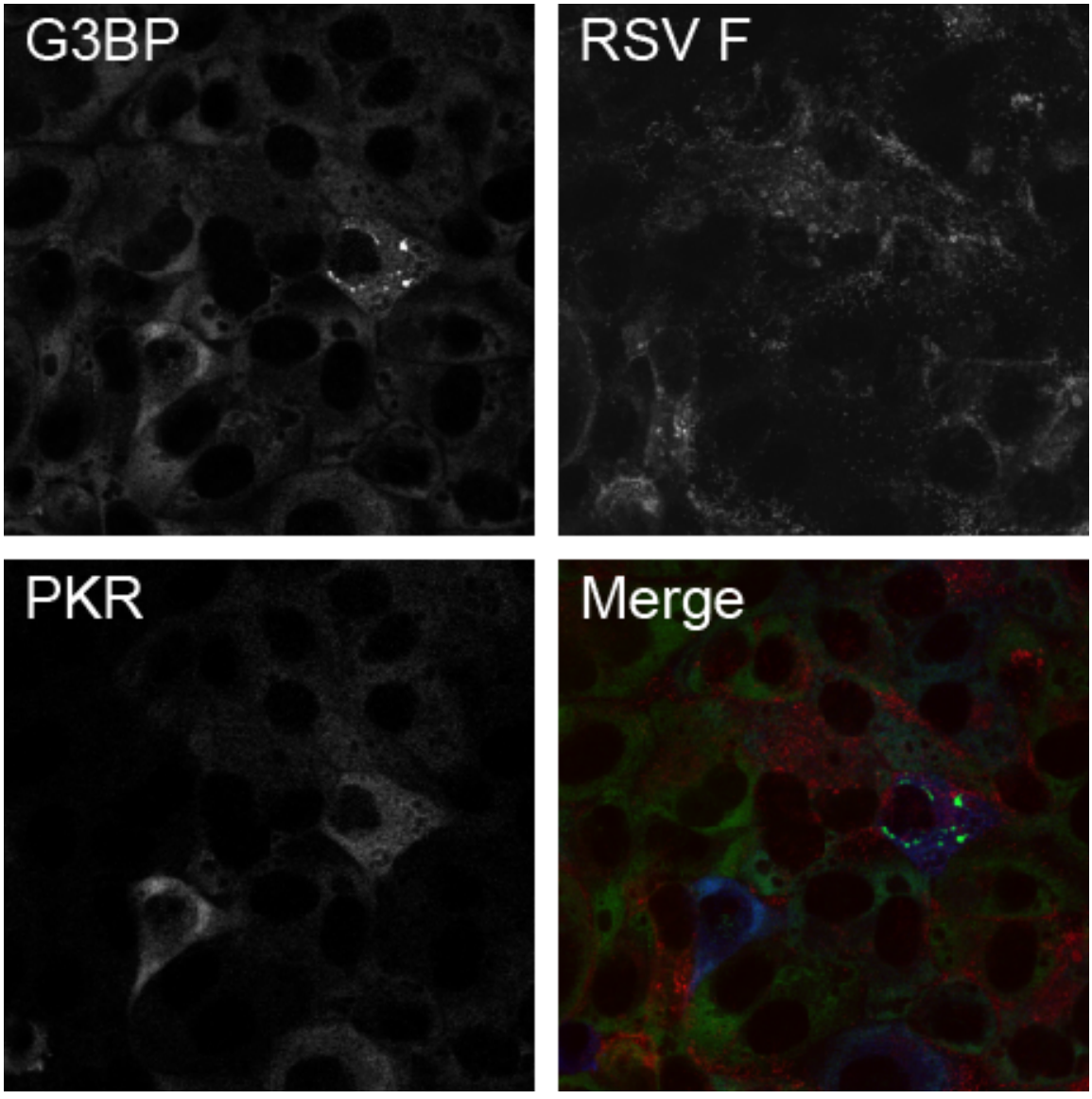

Figure 3-9. PKR-high cells are more likely to form stress granules during RSV infection. PKR knockdown cells were infected with RSV (MOI=5.0) for 48 hours and processed for immunofluorescence. G3BP was used to detect stress granules and appears green in the merge. RSV F was used to detect RSV infection and appears red in the merge. PKR appears blues in the merge panel.

Discussion

Since RSV induces the expression and activation of PKR, we hypothesized that activation of this dsRNA detector would mediate an antiviral effect during RSV infection. Surprisingly, we found that knockdown of PKR protein levels does not affect RSV replication. However, treatment with the kinase inhibitor 2-AP (which inhibits PKR) effectively blocks RSV replication regardless of PKR expression. This PKR-independent effect on RSV replication suggests that induction of other PKR-like kinases which are 2-AP sensitive, enhance RSV replication. The identity of such kinases is not known.

Our results are unexpected for two main reasons. First, PKR initiates a cascade of events resulting in phosphorylation of eIF2α and stress granule formation. These events are associated with stalled translation initiation complexes, which might be expected to diminish the capacity of host cells to support viral replication. Second, induction of PKR is often associated with an antiviral state. For example, both vesicular stomatitis virus and influenza virus replicate to higher titers in PKR-/- mice in comparison to wild-type mice (Balachandran et al., 2000). Similarly, PKR-/- mice succumb to infection at a higher frequency when infected with Bunyamwera virus in comparison to wild-type mice (Streitenfeld et al., 2003). However, there are cases, in which PKR has a minimal effect on viral replication. Severe acute respiratory syndrome coronavirus replication is unaffected in cells treated with phosphorodiamidate morpholino oligomers specific for PKR mRNA (Krahling et al., 2009). Similarly, treatment of cells with PKR siRNAs has little effect on adenovirus or reovirus replication (Zhang and Samuel, 2007) or rotavirus protein synthesis (Rojas et al., 2010). Rift Valley fever virus replication is not altered in

PKR -/- mouse embryo fibroblast cells (Habjan et al., 2009). However, PKR effects are not always antagonistic to viral infection. Knockdown of PKR by shRNA results in significantly decreased HCV RNA levels in cells treated with exogenous interferon and infected with HCV (Garaigorta and Chisari, 2009). Interestingly, levels of other proteins involved in the antiviral response are increased, suggesting that HCV induces PKR activation to inhibit host translation and prevent the expression of interferon-stimulated genes. We predicted a similar function for PKR during RSV infection since previous reports have demonstrated that 2-AP treatment leads to a dose-dependent increase in IFN-α production in RSV-infected cells (Hornung et al., 2004).

Although RSV is a single-stranded RNA virus, it produces multiple dsRNA intermediates during replication that are capable of activating PKR. PKR activation is likely required for eIF2α phosphorylation and subsequent stress granule formation during RSV infection (Lindquist et al., 2010) and (Hanley et al., 2010). Other studies have reported that RSV induces robust PKR activation during infection, but eIF2α phosphorylation is limited (Groskreutz et al., 2010). Phosphorylation of eIF2α may have been dampened by increased activity of protein phosphatase 2A (PP2A) during infection. In contrast, we observed extensive eIF2α phosphorylation during RSV infection, predominantly in cells that had been infected with RSV and in which stress granules had formed (Figure 1). Since phosphorylation of eIF2α frequently precedes stress granule formation (Kedersha and Anderson, 2007), our results are not surprising given the extensive stress granule formation induced by RSV (Lindquist et al., 2010). It is possible that PP2A activity is not sufficient to reverse eIF2α phosphorylation in RSV-infected

cells that form stress granules. Further experiments are required to assess PP2A activity in such cells.

Experiments using PKR-knockout mice show that RSV RNA levels increase during infection, suggesting a classic role for PKR as an antiviral molecule. In PKR-knockout mice, RSV infection induces lower levels of several cytokines, including TNF-α, IFN-β, and RANTES, among others, in comparison to wild-type mice. These results, when combined with histological analysis of mouse lung tissue, suggest that functional PKR leads to enhanced pathogenesis in RSV-infected animals (Minor et al., 2010).

Our previous data show that RSV replication is reduced in cells in which stress granule formation is inhibited by knockdown of the stress granule-related Ras-GAP SH3 domain-binding protein (G3BP) (Lindquist et al., 2010). In the current study, we found that RSV replication is unaffected in PKR-knockdown cells that similarly are deficient for stress granule formation. One possible explanation for this discrepancy is that knockdown of G3BP has effects in addition to inhibiting stress granule formation. Thus, viral replication might be inhibited by an alternative effect of the G3BP knockdown. Another possibility is that in PKR-knockdown cells, PKR signaling does not occur, preventing the activation of intrinsic antiviral responses to the virus. Thus, the potential pro-viral function for which stress granules may normally be required would not be necessary, allowing the virus to replicate efficiently.

The drug 2-AP has been cited as a specific inhibitor of PKR activation (Hu and Conway, 1993) (Loving et al., 2006) and (Silva et al., 2004) and used in a number of studies examining the role of PKR during viral infection. However, 2-AP also may inhibit activation of tumor suppressor p53 during genotoxic stress (Huang et al., 2003),

interfere with cell cycle progression (Andreassen and Margolis, 1994), and inhibit mitogen-activated protein kinase activation (Thorburn et al., 1994). Although PKR activation has been implicated in each of these processes (Garcia et al., 2006), it is possible that 2-AP inhibits multiple kinases. Our results demonstrate that while 2-AP is efficient at blocking PKR activation during RSV infection, its inhibitory effect on RSV replication is PKR-independent. Therefore, the reliability of 2-AP as a PKR-specific inhibitor is suspect, given that the drug mediates non-PKR-dependent effects. Defining the other targets of 2-AP might lend insight into the complex perturbations that occur in host gene function during RSV infection.

CHAPTER IV

SUMMARY AND FUTURE DIRECTIONS

Thesis Summary

The research I presented in this thesis examined the role of stress granules in RSV infection. I showed that RSV induces a robust stress response during infection and that inhibition of this response severely limits viral replication. I also showed that activation of PKR is the likely the mechanism by which RSV is able to induce stress granule formation.

In Chapter II, we showed that RSV infection results in stress granule formation. Using indirect immunofluorescence, we observed stress granules forming in RSV infected cells starting approximately 12 hours after inoculation. As infection progressed, we observed a higher percentage of infected cells forming stress granules. We also noted that these structures were separate and distinct from RSV inclusion bodies. An interesting correlation with this is that transcription of RSV genes generally ends approximately 12 hours after infection and a switch to viral replication occurs. It is possible that this switch is a factor in inducing the formation of stress granules; perhaps through the increased production of dsRNA intermediates. UV-inactivated virus does not induce stress granules, suggesting a requirement for active viral replication to induce these structures. We then showed that infected cells that have formed stress granules contain greater amounts of viral protein in comparison to cells that have not formed stress granules. This was our first evidence that stress granules may actually play a pro-viral role in infection.

Our next series of experiments sought to determine the effects of stress granule inhibition on viral replication. To accomplish this, we first had to generate a cell line with diminished capability of to form stress granules At the time, two proteins had been identified that were necessary for stress granule formation, TIA-1 and G3BP. We attempted to infect TIA-1 -/- MEFs, but RSV was not capable of replicating in these cells. We then generated a G3BP knockdown HEp-2 cell line. These cells displayed decreased capacity to form stress granules when treated with an exogenous stressor such as arsenite. When we infected these cells with RSV, we observed a significant decrease in viral titers throughout the time course in comparison to wild-type cells. Additionally, when we measured RSV RNA levels by RT-PCR, we observed a decrease in RSV RNA amounts in G3BP knockdown cells. These results also suggest a pro-viral role for stress granules in RSV replication.

When we determined that RSV inclusion bodies were separate from stress granules, we stained cells with a panel of stress granule specific markers. With the exception of HuR, none of these markers colocalized with viral inclusion bodies. We considered HuR colocalization with inclusion bodies an interesting phenomenon given the role of HuR in mRNA stabilization and our hypothesis that inclusion bodies contained viral RNA. To determine the relationship between inclusion bodies and HuR, we generated HuR knockdown cells. Stress granule and inclusion body formation were unaffected by this knockdown. In addition, we observed no significant difference in viral titers between HuR knockdown cells and control cells. Similarly, we observed no change in RSV RNA levels when detected by RT-PCR between control and HuR knockdown cells. Although these data indicate that HuR probably does not play an essential role in

inclusion body formation or viral replication, our knockdown levels may not have been sufficient to affect these aspects of infection.

Inclusion bodies have been theorized to be viral replication factories while numerous studies have shown that host RNAs are recruited to stress granules. Therefore, we attempted to determine a potential role for stress granules and inclusion bodies in viral RNA localization. To accomplish this, we introduced RSV genome-specific RNA probes into infected cells at multiple time-points. We then fixed and stained these cells for stress granules and inclusion bodies. Our results showed that although we could detect a small amount of RSV genomic RNA in stress granules, the majority of RNA was found in viral inclusion bodies. These findings suggest that RSV RNA only transiently associates with stress granules, which is in concordance with other RNA species that have been studied to date. This is also the strongest evidence to date that inclusion bodies serve as specific sites of RSV replication.

In Chapter II we established the characteristics of stress granule formation in RSV infection as well as a potential role in replication. In Chapter III we sought to determine the mechanisms by which RSV induces this process. We first confirmed that the translation initiation factor, eIF2α, was phosphorylated during RSV infection. This process is the most well-characterized method of stress granule formation. Through indirect immunofluorescence, we observed phosphorylated eIF2α in RSV-infected cells that had formed stress granules. We next attempted to determine the likely mechanism by which eIF2α is phosphorylated in RSV infected cells. PKR represented the most likely kinase responsible for this. We measured PKR phosphorylation in RSV infected cells and observed a significant increase over mock-infected cells.

After we determined that PKR is the likely kinase responsible for stress granule formation in RSV infection, we then attempted to inhibit activation of PKR and measure the effects on viral replication. We were able to use two reliable methods to accomplish this, treatment with the drug inhibitor, 2-AP, and knockdown of endogenous PKR expression. Treatment of infected cells with 2-AP effectively prevented the activation of PKR by RSV. Interestingly, we also observed a decrease in viral protein expression in cells that had been treated with 2-AP when compared to vehicle-treated cells. In addition, when we observed cells by indirect immunofluorescence, we noted a significant reduction in RSV infection in cells that had been treated with 2-AP when compared to vehicle-treated cells. We then measured the effect of drug treatment on viral titers. At each time-point measured, we detected a substantial decrease in cell-associated titer in 2-AP treated cells versus vehicle-treated cells

Our results demonstrating that 2-AP treatment inhibits PKR activation during RSV infection were quite exciting. However, given the possibility that 2-AP inhibits multiple targets, we sought to find another mechanism of PKR inhibition. To accomplish this, we generated a PKR knockdown cell line. These cells displayed an approximately 90% decrease in total PKR expression. When we infected PKR knockdown cells with RSV, we did not detect phosphorylated PKR. When we compared viral titers between PKR knockdown cells and control cells we observed no difference in titers among the cell types. This was in contrast to our 2-AP data that suggests PKR activation is essential for efficient viral replication.

To determine if the reduction in viral titers from 2-AP treatment was a result of an off-target effect, we repeated our 2-AP treatment experiments in the PKR knockdown

cell line. In these cells, we once again observed a significant decrease in RSV titers when compared to the control cell lines. Thus the inhibition of RSV replication by 2-AP was caused by an unknown, PKR-independent effect.

Finally, we determined the effect of PKR knockdown on stress granule formation during RSV infection. In PKR knockdown cells infected with RSV, we observed a significant reduction in infected cells that formed stress granules. We noted that the population of PKR knockdown cells was heterogenous for PKR expression. Taking this into account, we observed that most of the PKR knockdown cells that had formed stress granules generally had higher expression levels of PKR. These results confirm that PKR is the primary kinase activated by RSV that leads to the formation of stress granules.

While we showed that RSV replicates poorly in G3BP-knockdown cells deficient for stress granule formation, we also showed that RSV replication is unaffected in PKR-knockdown cells that similarly are deficient for stress granule formation. One possible explanation for this discrepancy is that knockdown of G3BP has unknown consequences besides inhibiting stress granule formation. Thus, viral replication could be inhibited by an alternate effect of this knockdown. Another possibility however, requires more thought. As I mentioned in Chapter I, stress granules appear to play a role in preventing or delaying apoptosis in stressed cells. A number of studies have shown that cells incapable of forming stress granules have poorer survival rates upon exposure to a stress (Buchan and Parker, 2009). Thus, perhaps in our G3BP-knockdown cells, increased rates of apoptosis could prevent efficient spreading of the virus. In PKR-knockdown cells however, PKR signaling does not occur, preventing the cell from activating cell-intrinsic antiviral responses. The signaling pathway that would normally induce stress granules

and promote apoptosis is not activated and the virus replicates unhindered. A diagram of this model is shown in Figure 4-1.

Future Directions

Our current understanding of stress granule function during viral infection is limited. The work I describe in this thesis utilizes basic and fundamental experiments that detail the formation and signaling involved in stress granule formation during RSV infection. However, I have not yet been able to determine the function of stress granules in this context. Therefore, I will outline a series of experiments to define a role for stress granules and the signaling pathway required for formation during RSV infection.

Some of the data in Chapters II and III have conflicting interpretations. In Chapter II, my experiments implicated a proviral role for stress granules during infection, since inhibition of stress granule formation resulted in decreased viral titers. However, in Chapter III, I showed that RSV replication was unchanged in cells deficient in PKR expression; stress granules also did not form in these cells. Thus, I propose an additional knockdown experiment to address this discrepancy. In Chapter II, I mentioned that I attempted in infect MEF TIA-1 knockout cells. This cell line, much like the G3BP knockdown line I generated, is deficient for stress granule formation. However, this cell line was not permissive for infection. To address whether the effect we observed on RSV replication is due to a lack of stress granule formation or a separate function of G3BP, I could perform a similar set of studies by knocking down TIA-1 expression. shRNAs exist that will inhibit the expression of TIA-1 in transduced cells. I could generate this cell line and then measure RSV titers as compared to wild-type cells. I would also

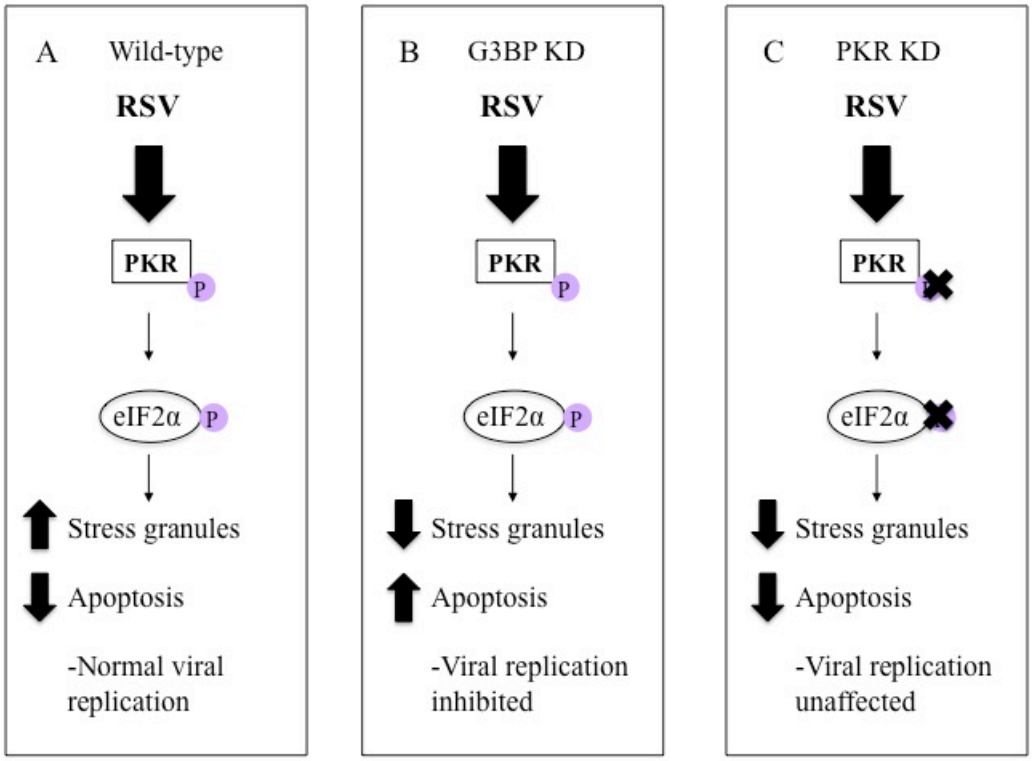

Figure 4-1. Proposed model for stress granule function in RSV infection. (A) RSV infects wild-type cells, resulting in the activation of PKR and the formation of stress granules following phosphorylation of eIF2α. Stress granules inhibit apoptosis in these cells, which allows for efficient viral replication to occur. (B) In G3BP knockdown cells, PKR activation occurs but stress granules do not form. This results in an increased rate of apoptosis and poor cell viability. RSV cannot efficiently replicate in these cells. (C) In PKR knockdown cells, PKR activation does not occur. Stress granules do not form and apoptosis is not induced due to the inability of the cell to react to the viral stress. RSV replication is unaffected by this change.

measure stress granule formation in these cells to verify that they are deficient for their formation. If a similar defect in viral replication in TIA-1 knockdown cells as compared to G3BP knockdown cells was observed, then the evidence would more convincingly implicate a role for stress granules in the RSV life cycle.

Others have shown that RSV mutants induce stress granules in a higher percentage of cells than wild-type virus (Hanley et al., 2010). In these studies, the authors used a viral construct in which the 5′ trailer region was replaced with a sequence complementary to the 3′ leader region. When cells were infected with this virus, a 50% increase was observed in infected cells containing stress granules as compared to wild-type virus. A mechanism for increased stress granule formation by this mutant virus was not determined. A likely possibility is that this mutant virus generates a greater abundance of dsRNA due to the mutations and structural changes in the genome. More dsRNA would likely result in greater activation of PKR, in turn causing a higher percentage of cells to form stress granules. To test this hypothesis, I would first compare PKR activation levels in cells infected by wild-type and mutant viruses. I would then infect wild-type and PKR knockdown cells with the mutant virus. I would expect to see stress granule formation reduced in mutant virus infected PKR knockdown cells to levels comparable to that of wild-type virus in wild-type cells.

In Chapter II, I attempted to define specific subcellular areas of viral replication. My experiments showed that RSV genomic RNA predominantly accumulates in viral inclusion bodies. While this was a very interesting observation, much work remains to be done to define the entire viral RNA life cycle. Although RNA accumulates in inclusion bodies, it is not known how the RNA traffics from the inclusion body to the apical

surface of infected cells so that it can be packaged into nascent virions. Our work examined static images of viral RNA at specific time points after infection. Live-cell imaging experiments would help track viral RNA as it is trafficked through the cell. Our laboratory currently has a number of GFP-tagged RSV proteins optimized for expression in human cells. One of these plasmids, such as RSV N, could be transfected into cells. These cells could then be infected with RSV followed by addition of the RSV-specific probe to living cells. This approach would allow visualization of inclusion bodies as well viral RNA in the living cells. We would be able to track the RNA as it moves through the cell. Based on the speed and direction of movement, these experiments might also reveal whether specific cellular machinery, such as the actin network or microtubules, is involved in viral RNA trafficking.

Another interesting set of experiments would be to track viral mRNA through cells. Our collaborators are currently attempting to provide specific probes to RSV mRNAs. Using experiments described in Chapter II and the approach above, we could track viral mRNA from sites of production to sites of translation.

My results in Chapter III show that the kinase inhibitor, 2-AP, greatly restricts RSV replication. Although I showed that the mechanism of viral inhibition was PKR independent, I did not identify the exact target of action of the drug. Experiments to identify other kinases that are inhibited by 2-AP could lead us to a critical mediator of the RSV replication. To address this possibility, a kinomic analysis could be performed. To perform this, I would vehicle-treat or 2-AP treat cells and inoculate with RSV, similar to the experiments performed in Chapter III. I would then prepare the cell lysates for each condition and use a kinase array to determine differences in kinase functionality (Bowick

et al., 2006) and (Johnson and Hunter, 2005). Ideally, I would be able to identify a few major changes in kinase function and then attempt to determine the role of each target in RSV infection. Alternatively, if I found many changes in kinase activity, I could group kinase activity according to specific pathways using Ingenuity Pathway Analysis. This would allow me to identify broad changes in cellular signaling induced by RSV.

PKR production and function is closely tied to type I interferon activation. Interferon α/β signaling is the primary method by which cells upregulate PKR expression during infection. RSV inhibits the host interferon response through expression of the NS1 and NS2 proteins, which block interferon signaling (See Chapter I). Therefore, although I observe PKR induction and activation in RSV-infected cells, perhaps the virus actively limits PKR function. NS1 and NS2 deletion viruses exist and are able to replicate; however, they are severely limited in this capacity compared to wild-type virus. I propose that NS1 and NS2 viruses are poorly infectious due to the fact that they more robustly activate PKR signaling, allowing cells to more effectively combat infection. To test this hypothesis, I would infect wild-type cells with NS1 deletion virus, NS2 deletion virus, or wild-type RSV. I would then measure and compare the levels of PKR expression and activation between each virus. Further, I would also measure titers for each virus in the PKR knockdown cell line I generated in Chapter III. I hypothesize that the NS1 and NS2 deletion viruses can grow to equal levels compared to that of wild-type virus in the PKR knockdown cells. These data would clarify whether increased activation of PKR is the limiting factor of NS1 and NS2 gene deletion viruses.

APPENDIX A

Respiratory syncytial virus uses a Vps4-independent budding mechanism controlled by Rab11-FIP2

Thomas J. Utley*, Nicole A. Ducharme†, Vasundhara Varthakavi‡, Bryan E. Shepherd§, Philip J. Santangelo¶, Michael E. Lindquist*, James R. Goldenring†‖, and James E. Crowe, Jr.*‡**††

*Departments of Microbiology and Immunology, †Surgery and Cell and Developmental Biology, ‡Pediatrics, and §Biostatistics and the **Program for Vaccine Sciences, Vanderbilt University Medical Center; Vanderbilt University, Nashville, TN 37232; ‖Nashville Veterans Affairs Medical Center, Nashville, TN 37232; and ¶Department of Biomedical Engineering, Georgia Institute of Technology and Emory University, Atlanta, GA 30332

Edited by Peter Palese, Mount Sinai School of Medicine, New York, NY, and approved May 8, 2008 (received for review December 28, 2007)

Respiratory syncytial virus (RSV) infects polarized epithelia, which have tightly regulated trafficking because of the separation and maintenance of the apical and basolateral membranes. Previously we established a link between the apical recycling endosome (ARE) and the assembly of RSV. The current studies tested the role of a major ARE-associated protein, Rab11 family interacting protein 2 (FIP2) in the virus life cycle. A dominant-negative form of FIP2 lacking its N-terminal C2 domain reduced the supernatant-associated RSV titer 1,000-fold and also caused the cell-associated virus titer to increase. These data suggested that the FIP2 C2 mutant caused a failure at the final budding step in the virus life cycle. Additionally, truncation of the Rab-binding domain from FIP2 caused its accumulation into mature filamentous virions. RSV budding was independent of the ESCRT machinery, the only well-defined budding mechanism for enveloped RNA viruses. Therefore, RSV uses a virus budding mechanism that is controlled by FIP2.

Pneumovirinae | Rab11 protein | virus replication | virus shedding

Respiratory syncytial virus (RSV) is the most common viral cause of serious lower respiratory tract illness in infants and children worldwide. RSV is a negative-sense, single-stranded RNA virus of the *Paramyxoviridae* family, which encodes 11 proteins. Infection is limited to the most superficial layer of polarized ciliated cells in the respiratory tract epithelium, entering through the apical surface (1, 2). Late steps of the RSV life cycle include assembly and budding of the virus, which also occur at the apical membrane in polarized cells (3).

RSV virions are pleomorphic, with a spherical form varying in size from 150 to 250 nm in diameter. The filamentous form of the virus has a smaller diameter of 50 nm and can have a length from 1 to 10 microns, depending on the cell line in which virus is grown (4). Filamentous RSV has been observed budding and fusing with cells during the spread of RSV infection (5). These long filaments destabilize into spherical forms that can be similar to the size of spherical particles collected during infection (4). Other related viruses also make filamentous virions such as influenza, Ebola, and parainfluenza viruses (6, 7, 8). In polarized cell culture monolayers, influenza virus is predominantly filamentous, and this filamentous form has a higher specific infectivity (9). A previous analysis of the RSV cell-surface filaments in live infected cells showed that these filaments are dynamic, demonstrating rotation, directed motion, and diffusion (10).

The minimal viral protein requirements for budding of RSV virus-like particles (VLPs) are fusion (F), matrix (M), nucleoprotein (N), and phosphoprotein (P) (11). The F protein follows the secretory pathway through the endoplasmic reticulum and Golgi and is directed to the apical membrane through a lipid raft-associated mechanism (12). The other viral structural proteins and the RNA genome must also traffic to the apical membrane from the cytoplasm and viral inclusion bodies through an undetermined mechanism. Lipid rafts have been associated with the assembly of RSV virions, possibly as sites of coordinated assembly, yet the mechanism by which membrane microdomains function during budding remains obscure (12, 13).

Polarized epithelial cells exhibit a complex distribution of proteins that is maintained by a polarized cytoskeleton and a series of discrete endosomal compartments. The apical recycling endosome (ARE) is located just below the apical membrane and is marked by the presence of Rab11a (14). The ARE serves as a slow recycling endosome as well as the final destination for basolateral to apical membrane transcytosing proteins (15). A number of Rab11-interacting proteins have been identified to date including myosin Vb (MVb) and the Rab11 family interacting proteins (Rab11-FIPs) (16, 17). Previously, we have shown that if a dominant-negative form of MVb is present, then RSV does not assemble properly at the apical membrane (18).

In the current study, we analyzed the role of another Rab11 interacting protein, Rab11-FIP2 (FIP2), in the RSV life cycle (Fig. 1*A*). FIP2 domains include an N-terminal C2 domain that binds preferentially to membrane lipids (19), a central MVb-binding domain (20), three NPF motifs (21), and a C-terminal Rab-binding domain (RBD) that is conserved among all FIPs (16, 22). We now demonstrate that expression of a dominant-negative form of the FIP2 protein lacking the C2 domain (FIP2-ΔC2) in polarized Madin–Darby canine kidney (MDCK) cells blocks RSV budding, causing retention of assembled virus on infected cells. Additionally, inhibition of the previously identified major mechanism of RNA virus budding, the ESCRT machinery, did not affect virus titers. These results suggest that RSV uses an RNA-enveloped virus budding mechanism controlled by FIP2.

Results

FIP2 Function Is Necessary for RSV Production. MDCK cell lines expressing FIP2 variants under doxycycline repression were tested to determine whether dominant-negative forms of FIP2 would alter RSV replication. Expression of the FIP2 variants had no observable effect on cell viability. Tight control of FIP2 variant expression and relative expression levels are shown in Fig. 1*C*. As expected, expression of FIP2-WT did not affect RSV supernatant titer measured at 5 days after infection (Fig. 1*B*). Expression of a mutant lacking the RBD (FIP2-ΔRBD) also did not inhibit the RSV supernatant titer. In contrast, a mutant that lacks the C2 domain (FIP2-ΔC2) reduced the RSV titer ≈1,000-fold. None of the three FIP2 variants affected vaccinia virus

Author contributions: T.J.U., J.R.G., and J.E.C. designed research; T.J.U. and V.V. performed research; T.J.U., N.A.D., P.J.S., and M.E.L. contributed new reagents/analytic tools; T.J.U., V.V., B.E.S., J.R.G., and J.E.C. analyzed data; and T.J.U. and J.E.C. wrote the paper.

The authors declare no conflict of interest.

This article is a PNAS Direct Submission.

††To whom correspondence should be addressed at: T-2220 Medical Center North, 1161 21st Avenue South, Nashville, TN 37232-2905. E-mail: james.crowe@vanderbilt.edu

This article contains supporting information online at www.pnas.org/cgi/content/full/0712144105/DCSupplemental.

© 2008 by The National Academy of Sciences of the USA

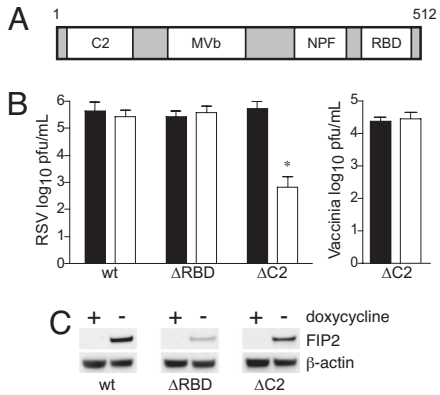

Fig. 1. FIP2 facilitates production of supernatant-associated virus. (*A*) FIP2 contains an N-terminal C2 domain, a MVb-binding domain, and three NPF motifs, followed by a C-terminal Rab11-binding domain. MDCK cells stably transfected with DNA encoding FIP2-GFP variants (FIP2-WT; C2 domain deletion, FIP2-ΔC2; or RBD deletion, FIP2-ΔRBD) under doxycycline repression, expressing (open square) or not expressing (filled square), were infected with RSV or *Vaccinia* virus. (*B*) Five days after infection, supernatants were collected, and the virus titer was measured by plaque assay. Representative data from three independent experiments are shown. (*C*) Relative expression levels for each FIP2 variant in either the presence or absence of doxycycline along with β-actin loading control. *, $P = 0.002$; Wilcoxon rank sum test. Data shown are mean ±SD.

replication (Fig. 1*B* and data not shown). There was no reduction in entry or viral RNA production in the FIP2-ΔC2 cells as measured by fluorescent focus or real-time RT-PCR assays (data not shown).

Production of RSV Was Delayed and Reduced. To determine whether the reduction of virus shedding observed at day 5 was an effect of delayed kinetics or reduced magnitude, we performed a 7-day growth curve. Supernatant and cell-associated fractions were collected daily and RSV titer measured by plaque assay. There was no alteration in RSV kinetics in the presence of FIP2-WT (Fig. 2*A*). In contrast, when FIP2-ΔC2 was expressed, the time

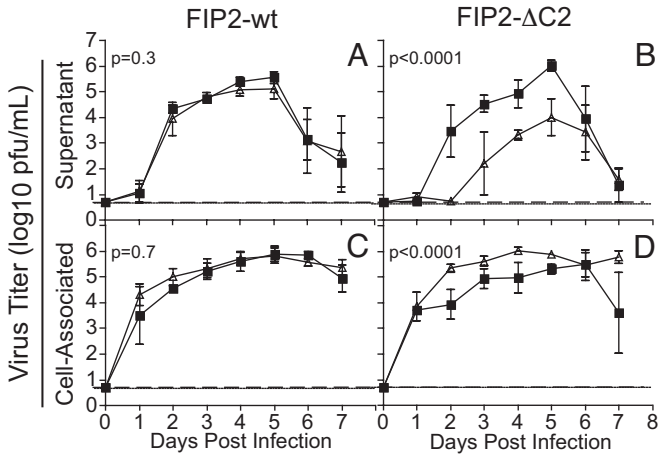

Fig. 2. FIP2-ΔC2 delays and reduces RSV budding. The MDCK FIP2-WT cell line (*A* and *C*) or FIP2-ΔC2 cell line (*B* and *D*) was infected with RSV. Viral titer was measured in both expressing (open triangle) and not expressing (filled square) cells over a 7-day period for both supernatant-associated virus (*A* and *B*) and cell-associated virus (*C* and *D*). Dotted lines indicate the limit of detection. Least-squares regression was used to estimate the best-fitting quadratic curves for viral titer over time, and *P* values were computed by using likelihood ratio tests comparing these curves between expressing and not expressing cells. Triplicate values were determined; error bars indicate ±SD.

to achieve 50% maximal peak titer of budded virus was delayed by 2 days, and the titer was reduced by 10- to >100-fold over the first 5 days (Fig. 2*B*). Although production of RSV was delayed and reduced, the peak titer still occurred on day 5, followed by a steep decline of RSV titer.

RSV Accumulates on the Cell in the Presence of FIP2-ΔC2. The titer of RSV in the cell-associated fraction was measured simultaneously with that in the supernatant fraction. There was no alteration in viral kinetics when FIP2-WT was expressed (Fig. 2*C*). Interestingly, when FIP2-ΔC2 was expressed, there was an increase in cell-associated, viral titer through day 6 (Fig. 2*D*). This statistically significant accumulation of RSV suggested that the FIP2-ΔC2 block occurs at a late budding step. This phenotype differs dramatically from that observed with the previous MVb-tail experiments in which the cell-associated fractions were decreased in titer ≈10,000-fold (18). Therefore, MVb acts earlier than FIP2 in the assembly and budding process of RSV.

Apical Filaments Are Fully Assembled Virus Structures. We determined the location of the structural proteins required for budding. The four necessary major structural proteins (F, M, N, and P) were localized to cell-surface filaments in both nonexpressing (data not shown) and FIP2-ΔC2-expressing, RSV-infected cells [supporting information (SI) Fig. S1]. Molecular beacon RNA probes specific for the RSV gene-start consensus sequence were used to identify the viral genomic RNA within the viral filaments. These data suggested that cell-surface filaments in RSV-infected FIP2-ΔC2-expressing cells are assembled, infectious, late-stage viral particles. Additionally, to determine whether these viral structures contained cytoskeletal elements, we stained infected cells for actin, microtubules, and ezrin (Fig. S2). None of these proteins were present in the viral filaments for either nonexpressing or expressing FIP2-ΔC2 cell lines. We repeated the actin localization studies by using visualization of a YFP-actin fusion construct or by using actin-specific antibodies, both of which confirmed the absence of actin from viral filaments (data not shown).

FIP2-ΔC2-Mediated Viral Inhibition Induced a Tethered Late-Domain-Like Phenotype. To determine how FIP2-ΔC2 affected the morphology of RSV budding from the apical membrane of polarized cells, we used scanning EM to visualize the viral filaments. Typically the filaments were 1–3 μm in length on the apical surface of infected MDCK cells (Fig. 3*A*). Microvilli, usually <0.5 μm in length, were observed in surrounding uninfected cells. When the MVb-tail mutant was expressed, we observed a loss of viral filaments from the apical plasma membrane, which was expected because of the known preassembly block (Fig. 3*B*). Finally, when FIP2-ΔC2 was expressed, we observed a significant elongation of viral filament length to ≈3–10 μm, suggesting that the filamentous virions were unable to undergo the fission process and continued to extend in length (Fig. 3 *D* and *E*). This cell morphology is markedly different from that of an uninfected monolayer expressing FIP2-ΔC2 (Fig. 3*C*).

The RSV Budding Mechanism Is Vps4-Independent. The primary mechanism for budding used by many enveloped RNA viruses is through hijacking the host ESCRT machinery, which is responsible for multivesicular body formation (23). Using WT Vps4a or each of the two dominant-negative Vps4a mutants K173Q or E228Q transfected into 293T cells, we tested whether RSV used this machinery for assembly and budding. No reduction of RSV titer was observed in the presence of either WT or dominant-negative Vps4a mutants (Fig. 4*A*). In contrast, a HIV pseudotyped with vesicular stomatitis virus (VSV) G protein (HIV_{NL4-3}), exhibited >90% reduced supernatant p24 levels in the presence of the dominant-negative Vps4a constructs, as

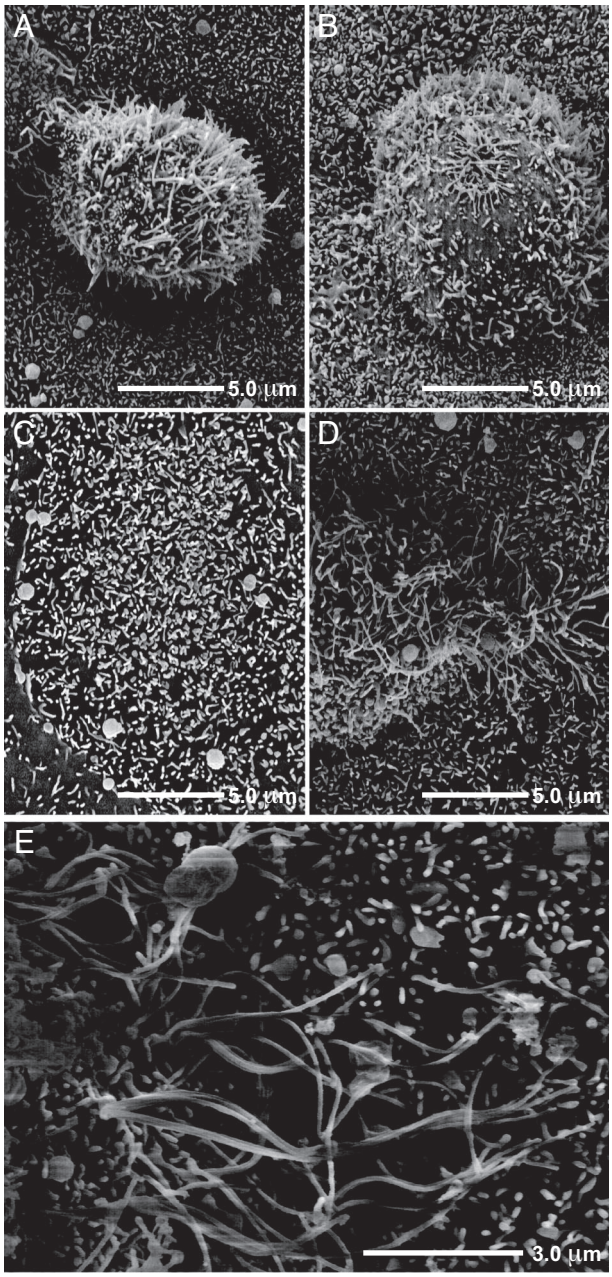

Fig. 3. FIP2 facilitates termination of RSV filament growth and virus budding. (*A*, *B*, *D*, and *E*) Scanning EM was performed to view the length of RSV filaments at the apical surface of MDCK cells expressing FIP2-WT, a dominant negative (*A*), an MVb-tail construct (*B*), or FIP2-ΔC2 (*D* or *E*) (images from separate cells at two resolutions). (*C*) Uninfected cells expressing FIP2-ΔC2.

expected (Fig. 4*A*). Experiments with similar Vps4b constructs also yielded the same results (Fig. 4*B*). The ubiquitination cycle is important for many viruses that use late domains (L-domains). However, three separate proteasome inhibitors did not affect budded RSV titers (Fig. S3*D*), again suggesting that RSV assembly and budding uses a mechanism independent of the ESCRT machinery.

Addition of Strong L-Domains to RSV M Did Not Render RSV Sensitive to Vps4a. To determine whether RSV possesses a cryptic or weak L-domain, we introduced the L-domain from the paramyxovirus PIV5 into the RSV M protein. A second mutant construct was made by adding the first 13 aa of the Ebola VP40 protein

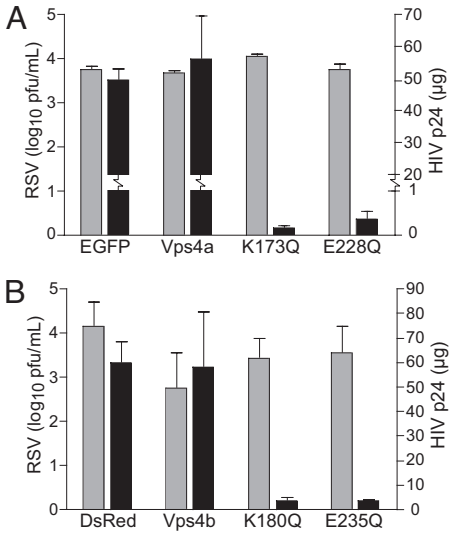

Fig. 4. RSV uses a Vps4-independent budding mechanism. Cells (293T) transfected with Vps4a constructs: pEGFP vector (EGFP) or Vps4a-EGFP (Vps4a), or dominant-negative mutants Vps4a-K173Q-EGFP (K173Q) or Vps4a-E228Q-EGFP (E228Q) (*A*), or Vps4b constructs: pDsRed vector (DsRed) or Vps4b-DsRed (Vps4b), or dominant-negative mutants Vps4b-K180Q-DsRed (K180Q) or Vps4a-E235Q-DsRed (E235Q) (*B*). Cells were infected 24 h after transfection at a moi of 1.0 with either WT RSV or HIV_{NL4-3}. Supernatant virus was collected 48 h after infection and assayed for either RSV by viral titer (gray bars) or HIV p24 by ELISA (black bars).

(containing a functional L-domain) to the N terminus of RSV M protein (Fig. S3*A*). These proteins were expressed in cells during RSV infection. Neither of the variant M proteins affected the magnitude of budded or cell-associated virus (Fig. S3*B*). Additionally, coexpression of the M protein variants in infected cells with WT Vps4a or either of the two dominant-negative Vps4a mutants did not affect RSV titer of supernatant or cell-associated virus (Fig. S3*C* and data not shown, respectively). These data further indicated that the FIP2-ΔC2 block of RSV budding is independent of the ESCRT machinery.

FIP2 Variants Localize with Viral Structures. Next we determined whether FIP2 localized with viral structures. Infected cell monolayers expressing FIP2-WT, FIP2-ΔC2, or FIP2-ΔRBD were stained for viral filaments (marked by RSV F protein) and viral inclusions (marked by RSV N protein). FIP2-WT showed 55% colocalization with viral inclusion bodies and little localization with viral filaments (Fig. 5). FIP2-ΔC2-containing tubulovesicular membranes appeared to be docked with viral inclusions, and colocalization was reduced to 13%. FIP2-ΔRBD also demonstrated colocalization with viral inclusion bodies (21% greater than FIP2-ΔC2, $P = 0.009$), but removal of the RBD caused a relocalization to the viral filaments (31%, $P < 0.0001$). Finally, when MDCK cells were infected with recombinant RSV, which expresses GFP in the cytoplasm, GFP was excluded from viral filaments (Fig. 5). These data suggest that truncation of the RBD blocks the cycling of FIP2 away from the apical membrane, causing it to assemble into RSV filaments.

Discussion

In this study we sought to define the role of the ARE in late steps of the RSV life cycle. Using a panel of FIP2 mutant-expressing MDCK cells, we determined that FIP2 is required at a late stage of RSV budding, most likely fission. Our studies show RSV does not use a Vps4-dependent virus budding mechanism, indicating that FIP2 acts in a previously uncharacterized pathway for enveloped virus budding.

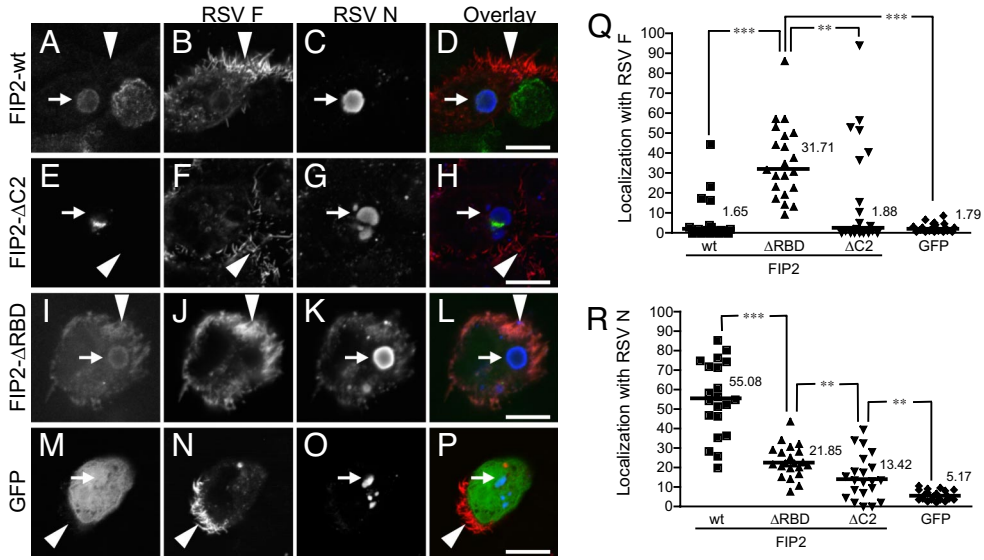

Fig. 5. FIP2 associates with both viral inclusions and viral filaments. (*A–P*) MDCK cells expressing FIP2-GFP variants [FIP2-WT (*A–D*), FIP2-ΔC2 (*E–H*), or FIP2-ΔRBD (*I–L*)] infected with RSV or MDCK cells infected with recombinant RSV expressing GFP (*M–P*) were stained by indirect immunofluorescence for both RSV F (*B*, *F*, *J*, and *N*) and RSV N (*C*, *G*, *K*, and *O*). In the overlays (*D*, *H*, *L*, and *P*), FIP2-GFP variants and GFP are pseudocolored green, RSV F is pseudocolored red, and RSV N is pseudocolored blue. The arrows with tails indicate viral inclusion body location, whereas the arrows without tails indicate an area of dense viral filament formation. (*Q* and *R*) Percentage of the total integrated pixel intensity indicating colocalization of FIP2-GFP variants or GFP with RSV F (*Q*) or RSV N (*R*) were calculated. The median value is shown. ***, $P < 0.0001$; **, $P \leq 0.009$; Wilcoxon rank sum test. No significant difference was measured among WT, ΔC2, and GFP groups in graph Q. Additional comparisons on graph R demonstrate that the WT differs significantly from ΔC2 and GFP (both $P < 0.0001$); ΔRBD differed significantly from GFP ($P < 0.0001$).

It has been shown that RSV is released from the apical surface in polarized cells, and the minimal requirements for virus-like particle formation are the RSV F, M, N, and P proteins (11). We observed all four proteins and the RSV genome in the viral filaments. In addition, when these viral proteins were cotransfected, we observed predominantly filamentous structures at the surface of cells (data not shown). Studies testing the effect of inhibitors of RSV have shown that loss of supernatant virus titer coincides with loss of surface filaments (24, 25). Not only does this study show that FIP2 controls fission of surface filaments, but the data also suggest that these filaments are virion particles.

It has been speculated that the filamentous structures at the surface of RSV-infected cells are actin-based structures (26, 27), yet our studies show that neither actin nor apical microvilli-associated proteins are present in the filaments. These findings do not eliminate the possibility that actin coordinates the assembly of virus at the base of filaments. In fact, some viral filaments appeared to be extensions of polymerized actin structures. High-resolution EM studies have recently suggested that the cortical actin network may be linked to the base of these viral filaments (28). Additionally, the lack of free diffusion of cytoplasmic GFP into filaments indicated that these viral filaments are specifically and tightly packaged, not passively filled tubular structures.

The only previously well delineated mechanism responsible for negative-sense RNA virus budding is the hijacking of the ESCRT machinery. The ESCRT mechanism of viral trafficking and virion formation is governed by viral proteins containing L-domains. RSV proteins do not contain any identifiable L-domains. Budding through the use of such L-domains depends on the AAA-ATPase Vps4. When dominant-negative forms of Vps4 are expressed in cells infected with viruses containing L-domains, virions appear to be tethered to the membrane through a thin stalk because of a loss of fission (23, 29). We studied RSV infection in cells expressing the Vps4a and Vps4b dominant-negative proteins and found there was no reduction in virus budding.

Unlike many viruses, infectious RSV virions are predominantly cell-associated in culture. This observation suggests that either RSV contains an inefficient L-domain or uses an undescribed budding mechanism that is less efficient. Therefore, we engineered recombinant forms of the RSV M protein that contained either the Ebola virus VP40 L-domain or the L-domain of the related paramyxovirus PIV5 (30, 31). Although L-domains are able to act in a location-independent manner, we inserted the sequences at positions similar to other viruses (32). Overexpression of these altered M proteins in cells during WT RSV infection did not increase budding or render RSV sensitive to the dominant-negative Vps4a proteins, suggesting that an inefficient or occult RSV L-domain is not a determining factor in the RSV budding pathway. A caveat of this interpretation is that WT M protein expressed by the virus was also present in cells. Although not entirely comparable, it has been shown that insertion of the Ebola virus L-domain into VSV M protein altered VLP budding (33).

Many viruses require ubiquitination for entry into the ESCRT pathway, although this correlation does not exist for all viruses. VSV is sensitive to proteasome inhibitors but does not appear to be sensitive to the dominant-negative Vps4a protein (33). Equine infectious anemia virus contains a Vps4a-dependent L-domain but is not sensitive to proteasome inhibitors (34). In our studies, RSV budding was not inhibited by proteasome inhibitors, suggesting that the FIP2-associated budding machinery belongs to a third category of budding mechanisms that is both Vps4-independent and ubiquitination-independent. Recent studies have demonstrated that both human cytomegalovirus and Semliki Forest virus budding also are independent of Vps4 and ubiquitination (35, 36). It will be interesting to determine whether the FIP2 mechanism, like ESCRT, is a common mechanism used by other enveloped viruses.

Analysis to determine whether FIP2 associated with viral structures demonstrated a significant localization with viral

inclusion bodies yet little apparent localization in viral filaments. This finding may be due to a low concentration required for function at the base of the filaments or a fast recycling rate. The dynamics of FIP2 recycling are demonstrated by the wide spread of values for localization of FIP2-WT with viral inclusion bodies. Further analysis of the FIP2 truncation mutants demonstrated that removal of the C2 domain blocked colocalization, yet viral inclusions appear to be docked to FIP2-ΔC2-containing vesicles. FIP2-ΔC2 expression blocks transcytosis from the basal to apical membrane at a transitional step between the common endosome and ARE (37). Together these findings indicate that the association of FIP2 with the viral inclusion body depends on endosomal transcytotic trafficking events through the ARE that occur after passage through the common endosome.

The other FIP2 truncation mutant, FIP2-ΔRBD, localized with both cytoplasmic viral inclusion bodies and apical viral filaments. These data suggest that the RBD is required for the recycling of FIP2 from the apical membrane back to the ARE and the viral inclusion body. Thus the dissociation of FIP2-ΔRBD from Rab11-dependent recycling allowed FIP2-ΔRBD to assemble into viral filaments. The RBD of FIP2 is required not only for binding Rab11 but also for homodimerization (21). The lack of FIP2-ΔRBD inhibition of RSV budding indicates that FIP2 may have functions independent of dimerization and Rab11 binding (38).

EM analysis of viral inclusion bodies suggest that they are not membrane-bound structures (39). Removal of the RBD also blocks the Rab-dependent association with membranes at the ARE through Rab myristoylation, which causes a cytoplasmic diffuse localization of FIP2-ΔRBD in the absence of infection (21). The localization of FIP2-ΔRBD and FIP2-WT to viral inclusion bodies suggests that FIP2 may also function in trafficking nonmembrane-bound cargo.

If this budding mechanism proves to be as complex as the ESCRT mechanism, FIP2 may be only one host protein from a large group of host proteins functioning together to facilitate virus budding. Current proteomic analysis of ARE vesicles is targeted at discovering this remaining host machinery involved in late steps of the RSV assembly and budding pathway. It is tempting to speculate that the mechanism hijacked by RSV may be an ARE-regulated mechanism for cellular deflagellation or shedding of microvilli because the N complex in filamentous virions mimics the periodicity of actin in microvilli or tubulin in cilia (4, 40).

Materials and Methods

Mammalian Cell Lines and Virus. MDCK T23 cell lines (Clontech) expressing tetracycline-repressible WT or mutant human EGFP-FIP2 were constructed as described (37). Suppression or induction of FIP2-GFP F protein expression was regulated by the presence or absence of 20 ng/ml doxycycline. MDCK and HEp-2 cell lines were maintained as described (18). The 293T cells were grown in DMEM and Ham's F-12 medium supplemented with 10% FBS, 320 μg/ml L-glutamine, 1% (vol/vol) nonessential amino acids, 2.7 μg/ml amphotericin B, and 45 μg/ml gentamicin. All cell lines were maintained at 37°C in 5% CO_2. The RSV WT strain A2 (41), recombinant RSV-GFP (42), VSV-G-pseudotyped HIV_{NL4-3} (43), and vaccinia virus strain Western Reserve have been described (18).

Viral Infection Assay. Cells were seeded in triplicate onto 48-well tissue culture plates (Costar) at 20% confluence and allowed to form fully-confluent cell monolayer cultures in the presence or absence of doxycycline to control expression of GFP-FIP2 variant proteins. Once confluent, the cell culture monolayers were inoculated with RSV at a multiplicity of infection (moi) of 0.25 plaque-forming units per cell. Virus was allowed to adsorb for 1 h at 37°C. After adsorption, virus infection medium was removed, tissue culture wells were washed three times with PBS, and 300 μl of growth medium (with or without doxycycline) was added. Infected cells were incubated at 37°C in 5% CO_2.

Virus Recovery and Titration. Tissue culture supernatant containing virus was collected and brought to a volume of 300 μl. After the collection of the supernatant fraction, tissue culture wells were washed three times with 250 μl of PBS. Cell-associated virus was harvested by scraping MDCK cell culture monolayers into 150 μl of medium, followed by an additional washing of the well with 150 μl of medium. Virus was released from harvested cells by using rapid freeze–thaw with movement between an ethanol dry-ice bath and a 37°C water bath, which was repeated three times. Recovered RSV was quantified by plaque assay as described (44). HIV p24 assay was performed as described (43). *Vaccinia* virus titer was quantified by plaque assay on BSC-40 cell monolayers, followed by staining with crystal violet (18).

Transfection. Forty micrograms of DNA was added to 2.5 μM calcium chloride, followed by dropwise addition of 2× BBS. This solution was incubated for 25 min and then added dropwise to 293T cells plated at 40% confluency in 10-cm dishes, followed by 24 h of incubation at 35°C in 3% CO_2. Transfected cells were washed with PBS and fresh DMEM and Hanks' F-12 medium was added. Transfection efficiency was assessed by visual inspection using microscopy with epifluorescence. Cells were inoculated with RSV at a moi of 5 on day 3 after transfection. RSV M protein variants were transfected into HEp-2 cells by using Effectene (Qiagen) with or without Vps4a constructs and then infected with RSV at an moi of 0.25 at 24 h after transfection.

Scanning EM. MDCK cells (with or without doxycycline) were seeded on 12-mm cover slips in 24-well plates. Cells were infected with RSV at a moi of 0.25 as described above. Samples were fixed 24 h after infection in 4% glutaraldehyde (Sigma) in 0.1 M cacodylate buffer (Sigma), treated with 1% osmium (Sigma), and dehydrated through a series of 70–100% ethanol washes. Dehydrated cells were critical-point dried, sputter-coated with gold, and visualized by using a Hitachi S4200 scanning electron microscope.

Fluorescence Assays. A molecular beacon molecule specific for the RSV genome at 1 mM was delivered by using transient permeablization with streptolysin O of live infected cells as described (10). Cells were fixed by using 3.7% formaldehyde (Sigma) in PBS, followed by 3.7% formaldehyde with 0.3% Triton X-100 (Sigma) in PBS. Cells were blocked by using 3% BSA (Sigma) and then stained with a primary antibody against F (palivizumab; MedImmune), M (clone B135), N (clone B130), P (clone 4.14.4), ezrin (Sigma), or α-tubulin (AbCam) in block. Cells were washed, and then antibodies were conjugated with Alexa Fluor 568 or 647 and/or phalloidin 647 (Invitrogen) in block were added. Slides were mounted by using ProLong Antifade (Invitrogen). Images were acquired on a Zeiss LSM 510 Meta confocal microscope. Analysis of colocalization was performed by using MetaMorph 7.1 software (Molecular Devices) on 21 fields from three separate assays. Western blot analyses were performed by using NuPAGE reagents (Invitrogen) following the manufacturer's instructions. Primary antibodies were against GFP (Clontech) or β-actin (AbCam). Secondary antibody was goat anti-mouse conjugated to HRP (KPL), followed by visualization with Chemiluminescent Substrate (Pierce).

Proteasome Inhibitor Assays. MG-132, lactacystin, and epoxomicin (EMD) were dissolved in DMSO (Sigma) and used within 2 weeks at a final concentration of 1.0 μM. HEp-2 cells were infected with either HIV_{NL4-3} or RSV at a moi of 2.0. Fresh media with inhibitor or DMSO vehicle were added 24 h after infection. Virus was collected 48 h after infection.

PCR Mutagenesis of RSV M Protein. A cDNA encoding the RSV strain A2 M protein was sequence-optimized for mammalian expression and synthesized by GENEART (designated M_{opt}). L-domain sequences from Ebola virus VP40 protein (amino acids PTAPPEY) or PIV5 M protein (amino acids FPIV) were designed for integration into, or as an addition to, the M sequence. PCR extension was performed to generate the chimeric RSV M proteins, designated RSV M_{opt}-EbV or M_{opt}-PIV5; primers are available upon request. All constructs were cloned into the Invitrogen plasmid vector pcDNA3.1(+) with restriction sites 5′-BamHI-EcoRI-3′.

ACKNOWLEDGMENTS. We thank Sarah Sewell for assistance with the SEM and Natalie Thornburg for assistance with *Vaccinia* experiments. Confocal microscopy and SEM experiments were performed in part through the use of the Vanderbilt University Medical Center Cell Imaging Shared Resource. We thank Wes Sundquist (Department of Biochemistry, University of Utah, Salt Lake City) for the Vps4 DNA constructs and Peter Collins (National Institute of Allergy and Infectious Disease, National Institutes of Health,

Bethesda, MD) and Mark Peeples (Center for Vaccines and Immunity, The Research Institute at Nationwide Children's Hospital, Columbus, OH) for RSV-GFP. J.E.C. holds a Clinical Scientist Award in Translation Research from the Burroughs Wellcome Fund. This work was supported by National Institutes of Health (NIH) Training Grant T32 GM08554 (to T.J.U.) and NIH Grant DK48370 (to J.R.G.).

1. Wright PF, *et al.* (2005) Growth of respiratory syncytial virus in primary epithelial cells from the human respiratory tract. *J Virol* 79:8651–8654.
2. Zhang L, Peeples ME, Boucher RC, Collins PL, Pickles RJ (2002) Respiratory syncytial virus infection of human airway epithelial cells is polarized, specific to ciliated cells, and without obvious cytopathology. *J Virol* 76:5654–5666.
3. Roberts SR, Compans RW, Wertz GW (1995) Respiratory syncytial virus matures at the apical surfaces of polarized epithelial cells. *J Virol* 69:2667–2673.
4. Bachi T, Howe C (1973) Morphogenesis and ultrastructure of respiratory syncytial virus. *J Virol* 12:1173–1180.
5. Bachi T (1988) Direct observation of the budding and fusion of an enveloped virus by video microscopy of viable cells. *J Cell Biol* 107:1689–1695.
6. Ellis DS, *et al.* (1978) Ultrastructure of Ebola virus particles in human liver. *J Clin Pathol* 31:201–208.
7. Mosley VM, Wyckoff RWG (1946) Electron micrography of the virus of influenza. *Nature* 157:263.
8. Yao Q, Compans RW (2000) Filamentous particle formation by human parainfluenza virus type 2. *J Gen Virol* 81:1305–1312.
9. Ada GL, Perry BT, Edney M (1957) Infectivity of influenza virus filaments. *Nature* 180:1134.
10. Santangelo PJ, Bao G (2007) Dynamics of filamentous viral RNPs prior to egress. *Nucleic Acids Res* 35:3602–3611.
11. Teng MN, Collins PL (1998) Identification of the respiratory syncytial virus proteins required for formation and passage of helper-dependent infectious particles. *J Virol* 72:5707–5716.
12. Brown G, *et al.* (2004) Analysis of the interaction between respiratory syncytial virus and lipid-rafts in HEp2 cells during infection. *Virology* 327:175–185.
13. McCurdy LH, Graham BS (2003) Role of plasma membrane lipid microdomains in respiratory syncytial virus filament formation. *J Virol* 77:1747–1756.
14. Casanova JE, *et al.* (1999) Association of Rab25 and Rab11a with the apical recycling system of polarized Madin–Darby canine kidney cells. *Mol Biol Cell* 10:47–61.
15. Apodaca G, Katz LA, Mostov KE (1994) Receptor-mediated transcytosis of IgA in MDCK cells is via apical recycling endosomes. *J Cell Biol* 125:67–86.
16. Hales CM, *et al.* (2001) Identification and characterization of a family of Rab11-interacting proteins. *J Biol Chem* 276:39067–39075.
17. Lapierre LA, *et al.* (2001) Myosin vb is associated with plasma membrane recycling systems. *Mol Biol Cell* 12:1843–1857.
18. Brock SC, Goldenring JR, Crowe JE, Jr (2003) Apical recycling systems regulate directional budding of respiratory syncytial virus from polarized epithelial cells. *Proc Natl Acad Sci USA* 100:15143–15148.
19. Lindsay AJ, McCaffrey MW (2004) The C2 domains of the class I Rab11 family of interacting proteins target recycling vesicles to the plasma membrane. *J Cell Sci* 117:4365–4375.
20. Hales CM, Vaerman JP, Goldenring JR (2002) Rab11 family interacting protein 2 associates with Myosin Vb and regulates plasma membrane recycling. *J Biol Chem* 277:50415–50421.
21. Cullis DN, Philip B, Baleja JD, Feig LA (2002) Rab11-FIP2, an adaptor protein connecting cellular components involved in internalization and recycling of epidermal growth factor receptors. *J Biol Chem* 277:49158–49166.
22. Meyers JM, Prekeris R (2002) Formation of mutually exclusive Rab11 complexes with members of the family of Rab11-interacting proteins regulates Rab11 endocytic targeting and function. *J Biol Chem* 277:49003–49010.
23. Garrus JE, *et al.* (2001) Tsg101 and the vacuolar protein sorting pathway are essential for HIV-1 budding. *Cell* 107:55–65.
24. Gower TL, *et al.* (2005) RhoA signaling is required for respiratory syncytial virus-induced syncytium formation and filamentous virion morphology. *J Virol* 79:5326–5336.
25. Oomens AG, Bevis KP, Wertz GW (2006) The cytoplasmic tail of the human respiratory syncytial virus F protein plays critical roles in cellular localization of the F protein and infectious progeny production. *J Virol* 80:10465–10477.
26. Fernie BF, Gerin JL (1982) Immunochemical identification of viral and nonviral proteins of the respiratory syncytial virus virion. *Infect Immun* 37:243–249.
27. Ulloa L, Serra R, Asenjo A, Villanueva N (1998) Interactions between cellular actin and human respiratory syncytial virus (HRSV). *Virus Res* 53:13–25.
28. Jeffree CE, *et al.* (2007) Ultrastructural analysis of the interaction between F-actin and respiratory syncytial virus during virus assembly. *Virology* 369:309–323.
29. Mebatsion T, Weiland F, Conzelmann KK (1999) Matrix protein of rabies virus is responsible for the assembly and budding of bullet-shaped particles and interacts with the transmembrane spike glycoprotein G. *J Virol* 73:242–250.
30. Licata JM, *et al.* (2003) Overlapping motifs (PTAP and PPEY) within the Ebola virus VP40 protein function independently as late budding domains: Involvement of host proteins TSG101 and VPS-4. *J Virol* 77:1812–1819.
31. Schmitt AP, Leser GP, Morita E, Sundquist WI, Lamb RA (2005) Evidence for a new viral late-domain core sequence, FPIV, necessary for budding of a paramyxovirus. *J Virol* 79:2988–2997.
32. Yuan B, Campbell S, Bacharach E, Rein A, Goff SP (2000) Infectivity of Moloney murine leukemia virus defective in late assembly events is restored by late assembly domains of other retroviruses. *J Virol* 74:7250–7260.
33. Irie T, Licata JM, McGettigan JP, Schnell MJ, Harty RN (2004) Budding of PPxY-containing rhabdoviruses is not dependent on host proteins TGS101 and VPS4A. *J Virol* 78:2657–2665.
34. Patnaik A, Chau V, Li F, Montelaro RC, Wills JW (2002) Budding of equine infectious anemia virus is insensitive to proteasome inhibitors. *J Virol* 76:2641–2647.
35. Fraile-Ramos A, *et al.* (2007) The ESCRT machinery is not required for human cytomegalovirus envelopment. *Cell Microbiol* 9:2955–2967.
36. Taylor GM, Hanson PI, Kielian M (2007) Ubiquitin depletion and dominant-negative VPS4 inhibit rhabdovirus budding without affecting alphavirus budding. *J Virol* 81:13631–13639.
37. Ducharme NA, *et al.* (2007) Rab11-FIP2 regulates differentiable steps in transcytosis. *Am J Physiol Cell Physiol* 293:C1059–C1072.
38. Ducharme NA, *et al.* (2006) MARK2/EMK1/Par-1B alpha phosphorylation of Rab11-family interacting protein 2 is necessary for the timely establishment of polarity in Madin–Darby canine kidney cells. *Mol Biol Cell* 17:3625–3637.
39. Garcia J, Garcia-Barreno B, Vivo A, Melero JA (1993) Cytoplasmic inclusions of respiratory syncytial virus-infected cells: Formation of inclusion bodies in transfected cells that coexpress the nucleoprotein, the phosphoprotein, and the 22K protein. *Virology* 195:243–247.
40. Norrby E, Marusyk H, Orvell C (1970) Morphogenesis of respiratory syncytial virus in a green monkey kidney cell line (Vero). *J Virol* 6:237–242.
41. Coates HV, Alling DW, Chanock RM (1966) An antigenic analysis of respiratory syncytial virus isolates by a plaque reduction neutralization test. *Am J Epidemiol* 83:299–313.
42. Hallak LK, Spillmann D, Collins PL, Peeples ME (2000) Glycosaminoglycan sulfation requirements for respiratory syncytial virus infection. *J Virol* 74:10508–10513.
43. Varthakavi V, *et al.* (2006) The pericentriolar recycling endosome plays a key role in Vpu-mediated enhancement of HIV-1 particle release. *Traffic* 7:298–307.
44. Murphy BR, Sotnikov AV, Lawrence LA, Banks SM, Prince GA (1990) Enhanced pulmonary histopathology is observed in cotton rats immunized with formalin-inactivated respiratory syncytial virus (RSV) or purified F glycoprotein and challenged with RSV 3–6 months after immunization. *Vaccine* 8:497–502.

APPENDIX B

Single molecule–sensitive probes for imaging RNA in live cells

Philip J Santangelo[1], Aaron W Lifland[1], Paul Curt[1], Yukio Sasaki[2], Gary J Bassell[2], Michael E Lindquist[3] & James E Crowe Jr[3,4]

To visualize native or non-engineered RNA in live cells with single-molecule sensitivity, we developed multiply labeled tetravalent RNA imaging probes (MTRIPs). When delivered with streptolysin O into living human epithelial cancer cells and primary chicken fibroblasts, MTRIPs allowed the accurate imaging of native mRNAs and a non-engineered viral RNA, of RNA co-localization with known RNA-binding proteins, and of RNA dynamics and interactions with stress granules.

Currently researchers use a vast excess of probes or plasmid-derived RNA to image RNA with single-molecule sensitivity. Either both the RNA and probe are expressed from a plasmid, requiring binding of up to 48 MS2-GFP[1,2] molecules, or just the RNA is expressed from a plasmid, requiring binding sites for 96 molecular beacon probes[3] to achieve single-molecule sensitivity. As plasmid-derived RNA restricts usage to cell types that can be efficiently transfected and is susceptible to artifacts caused by overexpression, imaging native RNA is preferred, but requires a more sensitive probe to achieve single-molecule sensitivity with a limited number of bound probes. We designed multiply labeled tetravalent RNA imaging probes (MTRIPs) composed of a 2′-*O*-methyl RNA-DNA chimera nucleic acid ligand with four or five amino-modified thymidines, 5′ biotin modification and a short (5–7-base) poly(T) sequence to extend the ligands from the surface of streptavidin. We used the amino-modified thymidines to conjugate *N*-hydroxy-succinimide (NHS) ester–modified fluorophores to the ligand. On average, each ligand was labeled with three fluorophores, limiting self-quenching. We chose fluorophores with quantum yields above 65% and they exhibited little triplet state excitation. The multiply labeled monovalent ligands were tetramerized via their binding to streptavidin, which increased probe brightness fourfold (**Fig. 1a**). MTRIPs, when delivered via reversible cell membrane permeabilization[4] with streptolysin O (**Fig. 1b**), allowed for single RNA molecule sensitivity using conventional fluorescence microscopy techniques. We identified the target RNA by the enhanced signal-to-background ratio achieved through the binding of multiple MTRIPs per RNA (two or three), via Watson-Crick base pairing[3,5], or if using a single MTRIP per RNA, through the natural localization of RNA (**Fig. 1c**). This is analogous to the MS2-GFP binding systems, but uses native target sequences and fewer binding sites.

To characterize probe sensitivity and delivery to the cytosol, we immobilized probes targeting the genomic RNA of the wild-type strain A2 of human respiratory syncytial virus (hRSV) on glass surfaces and delivered them into non-infected A549 cells using streptolysin O. After examining the images of the probe mixtures on glass, the histograms of mean probe intensity and

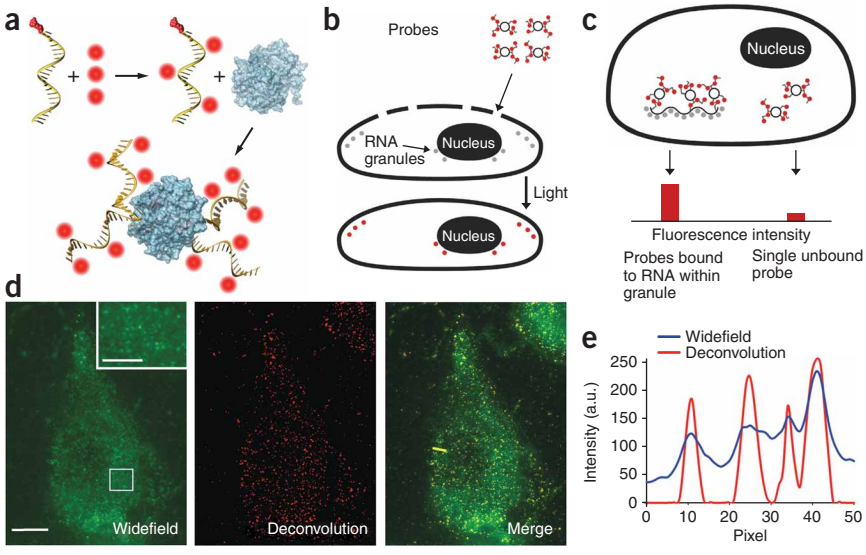

Figure 1 | Production and imaging of MTRIPs. (**a**) Fluorophores (red) were conjugated to amino-modified chimera oligonucleotides and bound to streptavidin (blue). (**b**) Cells, permeabilized with streptolysin O, allowed probe diffusion through pores; this was followed by rapid binding of the probes to targets, which was visualized after light stimulation. (**c**) Single RNAs bound to multiple probes were recognized by the enhanced signal-to-background ratio. (**d**) Live-cell widefield, deconvolved and merged images of a single optical plane of Cy3B-labeled hRSV-targeted probes in a noninfected A549 cell. Scale bars, 10 μm (2.5 μm in inset, which is a magnification of the boxed region). (**e**) Intensity profile of widefield and deconvolved images through yellow line in the merge image in **d**.

[1]Wallace H. Coulter Department of Biomedical Engineering, Georgia Institute of Technology and Emory University, Atlanta, Georgia, USA. [2]Department of Cell Biology, Emory University School of Medicine, Atlanta, Georgia, USA. [3]Department of Microbiology and Immunology, and [4]Department of Pediatrics, Vanderbilt University School of Medicine, Nashville, Tennessee, USA. Correspondence should be addressed to P.J.S. (philip.santangelo@bme.gatech.edu).

RECEIVED 15 DECEMBER 2008; ACCEPTED 20 FEBRUARY 2009; PUBLISHED ONLINE 6 APRIL 2009; DOI:10.1038/NMETH.1316

© 2009 Nature America, Inc. All rights reserved.

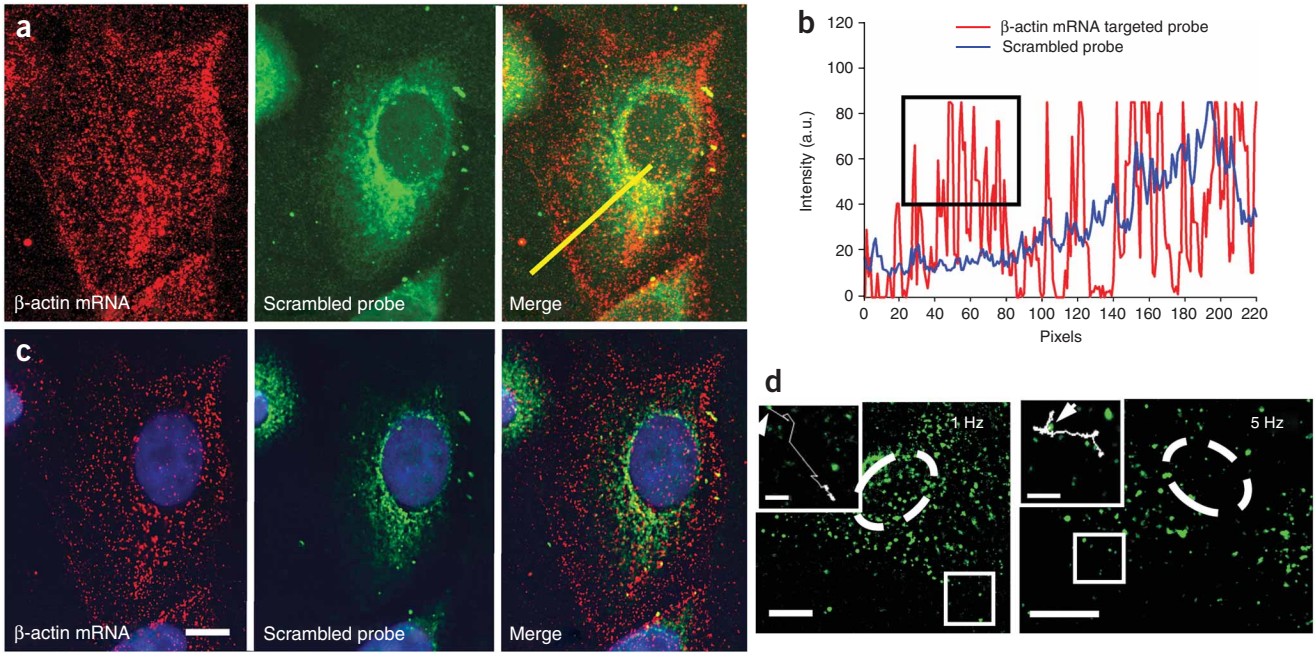

Figure 2 | Imaging of single molecules of β-actin mRNA in an A549 cell. (**a**) β-actin mRNA and 'scrambled' probe imaged with a laser scanning confocal microscope with all image planes represented. Merge images are also shown. (**b**) Intensity profiles along the yellow line in **a**. The black box highlights the large numbers of β-actin mRNA individual granules at the cell periphery detected by the targeted probe, but not by the scrambled probe. (**c**) Single optical plane of the same cell as in **a** resulting from widefield-deconvolution imaging. Scale bar, 5 μm. (**d**) Single optical plane of two living A549 cells (nucleus denoted with dashed line) imaged at 1 Hz for 3 min and 5 Hz for 30 s, respectively. Inset, images of boxed regions, including traces of β-actin mRNA granule trajectories for 70 s (1 Hz) and 30 s (5 Hz). Starting points are denoted by arrows. Scale bars, 10 μm (3 μm in insets).

three-dimensional plots of the intensity of individual probes on the glass surface, we concluded that the images detected single probes and not aggregates (**Supplementary Table 1** and **Supplementary Fig. 1** online). If the probes were aggregating, the histograms would show non-unimodal behavior and mixtures of different color probes would co-localize, which was not the case. In addition, we delivered hRSV targeting probes labeled with Cy3B (GE Healthcare) and Atto 647N (Atto-Tec GmbH) into non-infected A549 cells. From a single optical plane within the live cell, we observed individual probes to be homogenously distributed in the cytoplasm (**Fig. 1d,e**) and did not observe localization or accumulation of probes.

To test the ability to image single RNAs, we simultaneously delivered two Cy3B-labeled MTRIPs designed to target two regions of the human β-actin mRNA coding sequence (human β-actin mRNA probes 1 and 2; **Supplementary Table 1**) and an Atto 647N–labeled 'scrambled' probe (no target in human genome) (30 nM each) using streptolysin O into A549 cells. Twenty minutes after delivery, we fixed the cells in 4% paraformaldehyde and imaged them. We could image individual RNAs in both fixed and live cells, but we fixed the cells for quantification because of the dynamic nature of RNA granules. For β-actin, we observed individual 'unbound' probes as well as localized granules with twice the

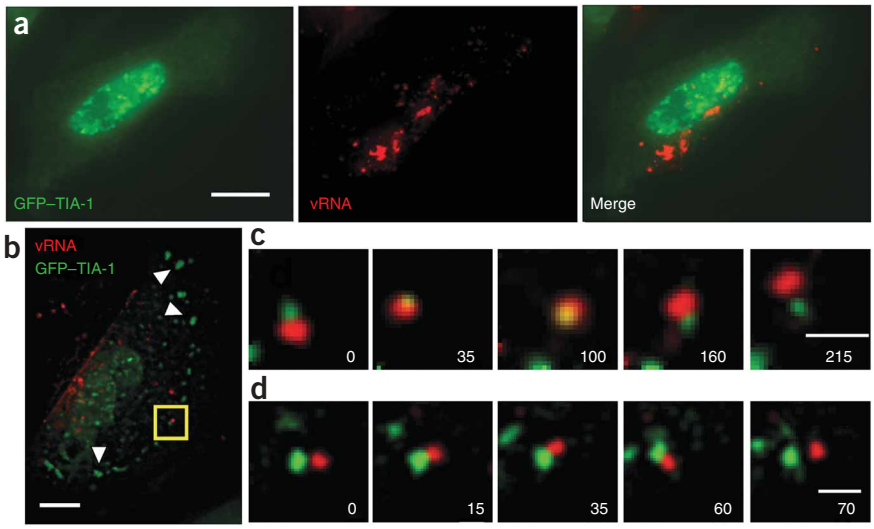

Figure 3 | Transient interactions between viral genomic RNA of hRSV and GFP–TIA-1. (**a**) Fluorescence images of a live A549 cell imaged 24 h after infection and 48 h after transfection, showing no stress granules. (**b**) Live-cell image of a single optical plane of GFP–TIA-1 and Cy3B-labeled hRSV-targeted MTRIPs (25 nM) in an A549 cell, 24 h after infection, 48 h after transfection and 20 min after exposure to 1 mM sodium arsenite. Arrowheads denote stress granules. (**c**) Time-lapse images of stress granule (green) collision, penetration and separation of a viral RNA granule (red). (**d**) Images of the docking of a stress and viral RNA granule, which occurred for only 45 s before separation. All granule interactions shown were imaged in the area denoted by the box in **b**. All times are given in seconds. Scale bars, 10 μm (**a**,**b**) and 1 μm (**c**,**d**).

© 2009 Nature America, Inc. All rights reserved.

intensity (**Fig. 2a–c**). β-actin mRNA was prevalent in the perinuclear region of the cell and also localized to the leading edges, whereas the 'scrambled' probe produced perinuclear signals and localized not at the cell periphery but in the cytoplasm, demonstrating β-actin probe specificity. We quantified localization in an intensity profile of the confocal image (**Fig. 2b**). From the lower-noise, widefield-deconvolved image (**Fig. 2c**) we removed via thresholding the average single-probe intensities, quantified from probes on the glass surface, and counted the remaining granules using Volocity (Improvision) software. Using this approach we observed single β-actin mRNAs, containing approximately twice the single probe intensity, in the cell (**Fig. 2c**) and detected a total of 1,455 granules. Granule mean fluorescence intensity (calculated from the three-dimensional reconstruction) had a measured s.d. of only 25% of the mean, reflecting the uniformity of the granules when measured in three dimensions. The granule count was consistent with previous quantifications ($\sim$1,500 in serum-stimulated cells), using a similar analysis for β-actin mRNA in epithelial cells[6]. In addition, we imaged β-actin mRNA granules in living cells by time-lapse widefield fluorescence microscopy (**Fig. 2d**). We collected images with 90-ms exposure times at both 1 Hz and 5 Hz for 3 min and 30 s, respectively (**Supplementary Videos 1–3** online). This demonstrated the capacity to use this method in low- and high-speed tracking experiments; similar particle trajectories have been demonstrated for plasmid-derived mRNAs[1]. As an additional control, we serum-starved A549 cells for 48 h and counted the β-actin mRNA granules in cells fixed after live-cell hybridization. A representative cell contained only 409 granules as compared with 1,455 granules detected in a cell grown with serum (data not shown), consistent with previous experiments[6,7]. We also performed single-probe imaging of clustered RNAs and co-localized them with β-actin mRNA binding protein, ZBP1 (ref. 8) in three dimensions (**Supplementary Figs. 2** and **3** online), and simultaneously imaged β-actin mRNA, actin-related protein 2 homolog mRNA and ZBP1 protein, in primary chicken embryonic fibroblasts (**Supplementary Fig. 4** online).

To test the utility of these probes for the study of RNA-protein colocalization in live cells, we used Cy3B-labeled MTRIPs targeted to the genomic RNA of hRSV in conjunction with a GFP–TIA-1 fusion protein in infected A549 cells, to evaluate the interaction between the stress granule protein TIA-1 and hRSV viral RNA when stress granules were induced by sodium arsenite treatment. Previous findings demonstrated that paramyxovirus RNA, which contains many possible TIA-1 or TIAR binding sites (uracil-rich regions), likely interacts with stress granules[9]; this interaction though, has not been characterized in living cells. In hRSV-infected cells transfected with GFP–TIA-1, stress granules had not formed 24 h after infection as identified by the lack of aggregation of GFP–TIA-1 in cells also containing viral RNA (**Fig. 3a**). MTRIPs were specific and did not aggregate RNA (**Supplementary Figs. 5–7** and **Supplementary Results** online).

To induce stress granules, we exposed the cells to 1.0 mM sodium arsenite[10] and observed substantial transient interactions between stress and viral RNA granules (**Fig. 3b–d**). We observed a stress granule moving into a viral RNA granule and residing within it for over a minute before it was released (**Fig. 3c** and **Supplementary Videos 4** and **5** online). Another stress granule then appeared to dock with a viral RNA granule (**Fig. 3d** and **Supplementary Video 6** online), and appeared to be in contact for approximately 45 s. Transient interactions between RNA granules on the same time scales had been reported, supporting our observations, but previously engineered RNAs or proteins were imaged, in contrast to the non-engineered RNAs imaged in this study[11–13]. We also observed more stable interactions between GFP–TIA-1 and the viral RNA (**Supplementary Figs. 8** and **9** and **Supplementary Videos 7** and **8** online). Notably, the time-lapse results we present here cannot be obtained using probes that require high (micromolar) probe concentrations and have lower sensitivity. The use of less-sensitive probes would result in large RNA-protein exposure time mismatches, resulting in the inability to track the interaction of individual granules accurately.

Here we demonstrated that MTRIPs have single-molecule sensitivity and can be used to target and follow native and non-engineered RNA granules in living cells, in both a cell line and a primary fibroblast using streptolysin O delivery; streptolysin O delivery induced only minimal cell death (**Supplementary Fig. 10** online) and did not change cellular morphology appreciably or induce stress granules. Owing to their brightness at multiple wavelengths, small size and ease of assembly, these probes should be broadly applicable for studying single-molecule RNA-related events in living cells.

METHODS

Methods and any associated references are available in the online version of the paper at http://www.nature.com/naturemethods/.

Note: Supplementary information is available on the Nature Methods website.

ACKNOWLEDGMENTS

This study was supported by the Georgia Institute of Technology administration (P.J.S.).

AUTHOR CONTRIBUTIONS

P.J.S. designed and performed experiments, analyzed data and wrote manuscript, A.W.L. performed experiments and analyzed data, P.C. performed experiments, Y.S. and G.J.B. provided novel antibody, M.E.L. and J.E.C. provided virus and antibody and edited manuscript.

Published online at http://www.nature.com/naturemethods/
Reprints and permissions information is available online at http://npg.nature.com/reprintsandpermissions/

1. Fusco, D. *et al. Curr. Biol.* **13**, 161–167 (2003).
2. Shav-Tal, Y. *et al. Science* **304**, 1797–1800 (2004).
3. Vargas, D.Y., Raj, A., Marras, S.A., Kramer, F.R. & Tyagi, S. *Proc. Natl. Acad. Sci. USA* **102**, 17008–17013 (2005).
4. Santangelo, P.J. & Bao, G. *Nucleic Acids Res.* **35**, 3602–3611 (2007).
5. Utley, T.J. *et al. Proc. Natl. Acad. Sci. USA* **105**, 10209–10214 (2008).
6. Femino, A.M., Fay, F.S., Fogarty, K. & Singer, R.H. *Science* **280**, 585–590 (1998).
7. Latham, V.M. Jr, Kislauskis, E.H., Singer, R.H. & Ross, A.F. *J. Cell Biol.* **126**, 1211–1219 (1994).
8. Ross, A.F., Oleynikov, Y., Kislauskis, E.H., Taneja, K.L. & Singer, R.H. *Mol. Cell. Biol.* **17**, 2158–2165 (1997).
9. Iseni, F. *et al. EMBO J.* **21**, 5141–5150 (2002).
10. Kedersha, N. *et al. Mol. Biol. Cell* **13**, 195–210 (2002).
11. Zeitelhofer, M. *et al. J. Neurosci.* **28**, 7555–7562 (2008).
12. Kedersha, N. *et al. J. Cell Biol.* **169**, 871–884 (2005).
13. Mollet, S. *et al. Mol. Biol. Cell* **19**, 4469–4479 (2008).

© 2009 Nature America, Inc. All rights reserved.

ONLINE METHODS

MTRIPs. The 2′ *O*-methyl RNA-DNA chimera nucleic acid ligands were synthesized by Biosearch Technologies, Inc. Each contains a 5′ biotin modification and multiple dT-C6-NH_2, modifications. The streptavidin used for the core was purchased from Pierce. Probes were assembled by first labeling the free amine groups on the ligands with either Cy3B–NHS ester (GE Healthcare) or Atto 647N–NHS ester (Atto-Tec GmbH) using manufacturers' protocols. Free dye was removed using both Nanosep spin columns (Pall Corp.) and illustra G-25 size-exclusion columns (GE Healthcare). The purified ligands were resuspended in 1× phosphate-buffered saline (PBS; pH 7.4) and mixed at a 10:1 molar ratio with streptavidin for 1 h at room temperature (18–22 °C). Free ligands were removed using 30 kDa Nanosep spin columns, and stored at 1 μM final concentration in 1× PBS at 4 °C. When multiple probes were used, each probe was completely assembled and filtered separately, and then mixed with equimolar concentrations in streptolysin O and medium just before delivery into cells We estimated the cost of MTRIPs, based on 30 nM delivery concentration, to be $0.15 per well, for a 24-well plate.

Cells and virus. A549 lung carcinoma cells (American Type Culture Collection CCL-185) were grown in DMEM (Sigma Aldrich) with 10% fetal bovine serum (FBS; Hyclone) with 100 U ml^{-1} of penicillin and 100 mg ml^{-1} of streptomycin. Virus used was the A2 strain of hRSV (American Type Culture Collection VR-1544) at a titer of 1×10^6 50% tissue culture infectious dose ($TCID_{50}$) ml^{-1}. The titer was evaluated by serial dilution and immunostaining, 4 d after infection. Infection data shown (**Fig. 3** and **Supplementary Figs. 5–7**) was at day 1 after infection and with a multiplicity of infection of 5. All cells were infected at greater than 80% confluence, by removing the media, washing with 1× PBS (without Ca^{2+} and Mg^{2+}) and then adding virus to the cells for 30 min at 37 °C. After the 30-min incubation, complete medium was added. For the motile epithelial cell experiments, A549 cells were seeded at 5% confluence such that there were a substantial number of cells without contacts with other cells. For the motile fibroblast experiments, primary chicken embryonic fibroblasts (Charles River Laboratories) were grown in CEF growth medium (Charles River Laboratories), containing 5% FBS and seeded at 5% confluence.

Probe delivery. MTRIPs were delivered into A549 and CEF cells using a reversible permeabilization method with streptolysin O (Sigma). Cells grown in complete medium were first washed with 1× PBS and then incubated with a mixture of 0.2 U ml^{-1} of streptolysin O and probe (concentrations were noted in the main text) in an appropriate amount of complete growth medium for 10 min at 37 °C. The mixture of streptolysin O, probe and medium was then removed and replaced with fresh, complete growth medium or Leibovitz's L15 medium supplemented with 10% FBS. Live cells were imaged typically 20 min immediately after delivery by epifluorescence microscopy. Using streptolysin O–based delivery, probes were delivered into A549 and CEF cells with 100% efficiency.

Counting granules and statistical analysis of RNA granule populations. For data shown in **Figure 2** and **Supplementary Figure 7**, granules were identified and counted using Improvision's Volocity software in three dimensions using either confocal images or from widefield fluorescence images, deconvolved using an iterative deconvolution algorithm in Volocity. For data shown in **Figure 2**, granules were counted using deconvolved data and identified based on the s.d. of intensities; 4 s.d. above the mean was used to locate the granules in all cases because it avoided the detection of noise or objects substantially smaller than the point spread function. Because of this, no limit on minimum granule size was necessary when counting granules. In general, the cells deconvolved using the three-dimensional interative algorithm in Volocity lacked considerable noise due to filtering in the algorithm. Notably, the s.d. in mean granule intensity for the granules in **Figure 2c** and in the serum-starved cell (data not shown) were only 25% and 21%, respectively, reflecting the uniformity of the granules when measured in three dimensions. For data shown in **Supplementary Figure 7**, the number of granules was detected using the same criteria using confocal data from tetravalent MTRIPs and a monovalent ligand (ligands not connected by streptavidin) in approximately 30 cells each. The results were compared using the Wilcoxon-Mann-Whitney (WMW) test to determine whether the two samples came from the same population. WMW is a nonparametric test is traditionally used to test equality of locations in two populations, but in its general form this test is about the equality of distributions[14]. The null hypothesis states that the distributions of the two samples coincide and the alternative is that the distributions differ. The *P* value for WMW test when comparing the number of granules detected by each probe was 0.8737, which means that the evidence for the null hypothesis is decisive; consequently, the distributions were assumed to be the same.

Plasmids and transfections. The pSRα-GFP-HA-TIA-1 plasmid[15] was used to image stress granules in living cells. A549 cells plated in penicillin- and streptomycin-free medium were transfected using Fugene HD (Roche) at a ratio of Fugene HD to DNA of 2.5 μl $μg^{-1}$.

Time-lapse fluorescence microscopy. Live-cell video microscopy was performed using cells grown in Bioptechs T4 plates with an objective heater. The cells were imaged in Leibovitz's L15 medium supplemented with 10% FBS. Images were taken with a Zeiss Axiovert 200M microscope, with an ×63, numerical aperture (NA) = 1.4 Plan-Apochromat objective and Hamamatsu ORCA-ER AG camera, using Chroma 49002 ET-GFP and 49004 ET-Cy3 filter sets, controlled by Volocity software. For β-actin mRNA granule dynamics, images were taken either at 1 or 5 Hz with 90-ms exposures for 3 min and 30 s, respectively. For the stress granule-RNA experiments, images of GFP–TIA-1 and the Cy3B-labeled MTRIPS were taken at 0.2 Hz (every 5 s), with exposure times of 71 and 41 ms, respectively, for up to 8 min.

Stress granule-RNA time-lapse microscopy. A549 cells, transfected with the above plasmid for 24 h were then infected with hRSV as above. Twenty-four hours after infection, the MTRIPs were delivered at 25 nM final concentration, and the cells exposed to 1.0 mM sodium arsenite for 30 min[15]. During the 30-min incubation, the cells were observed periodically using epifluorescence microscopy. After 15 min of exposure, stress granules (marked by GFP–TIA-1 aggregates) were observed; an imaging

© 2009 Nature America, Inc. All rights reserved.

doi:10.1038/nmeth.1316

plane containing both RNA granules and stress granules was chosen and time-lapse microscopy was initiated. Out-of-focus light was removed using Volocity's 2D deconvolution algorithm.

Starvation assay. A549 cells were serum-starved in DMEM with 100 U ml^{-1} of penicillin and 100 mg ml^{-1} of streptomycin for 48 h. MTRIPS (human β-actin mRNA probes 1 and 2) were delivered with streptolysin O. Twenty minutes after delivery, the cells were fixed in 4% paraformaldehyde and stained with DAPI. The granules in a particular cell were then counted using the method described above.

Immunostaining. Twenty to thirty minutes after probe delivery, cells were fixed in 4% paraformaldehyde in 1× PBS for 10 min at room temperature. After fixation, cells were permeabilized using 0.2% Triton-X 100 for 5 min at room temperature, washed in 1× PBS, blocked for 30 min in 5% BSA (ultrapure), washed in 1× PBS, incubated with primary antibody for 30 min at 37 °C, washed 3× with 1× PBS, incubated in secondary antibody labeled with Alexa 488 for 30 min at 37 °C, washed 3× with 1× PBS, labeled with DAPI for 5 min (in the RSV experiments) and then mounted in PVA with Dabco. The monoclonal antibody for the hRSV nucleocapsid protein was from Abcam, and the polyclonal Ab for ZBP1 from the Bassell laboratory. Polyclonal ZBP1 antibodies were produced by immunizing guinea pigs with a synthetic peptide corresponding to residues 162–175 (CGPENGRRGGFGSRG; the first Cys is for conjugation) within a hinge region between two RRM and four KH domains of human ZBP1. This region is conserved completely among mouse, rat and human ZBP1 proteins, but not Imp2 or Imp3. The ZBP1 antibody does not recognize mouse Imp2 or Imp3 by western blotting (data not shown). F-actin was stained using Alexa 488–labeled phalloidin (Invitrogen).

Fluorescence imaging. Immobilized Cy3B and Atto 647N probes on the glass surface were imaged using a Zeiss Axiovert 200M microscope with an ×63, NA = 1.4 Plan-Apochromat objective, using Chroma 49004 ET-Cy3 and 49006 ET-Cy5 filter sets, with 500-ms exposures. An EXFO excite 120 light source with a ND (neutral density) = 0.4 (40% transmission) was used for fluorescence excitation, and a Hamamatsu ORCA-ER AG for taking digital images. Live-cell images of single probes within A549 cells were taken with 350 ms exposures under the same illumination conditions. *Z*-dimension stacks were taken in both cases, in 200-nm steps, and deconvolved using Volocity iterative deconvolution algorithm. Cells used in the human β-actin mRNA-scrambled probe experiments were fixed after live-cell hybridization and imaged similarly to the immobilized probes, but with 200-ms exposures and deconvolved in Volocity. Time-lapse live cell images were taken as discussed above, and were processed with Volocity's 2D or fast deconvolution algorithm. In the stress granule control experiments, live cell images were taken similarly to the single probe images but with 50-ms exposures. hRSV after-delivery, fixed-cell control experiments were imaged with a ZeissLSM 510 Meta using an ×63, NA = 1.4, Plan-Apochromat objective. All images were taken using multi-track scanning for each fluorophore to prevent bleed-through. *Z*-dimension stacks were taken in 0.5-μm increments; the 543 nm laser (Cy3B probe) was set at 25% power, the 488 nm laser (for N protein immunostaining) was set at 37%, and the pinholes were set to an airy unit of 1 (equal to airy disk). β-actin mRNA, actin-related protein 2 homolog mRNA and ZBP1, in the chicken embryonic fibroblasts, were imaged under similar conditions to the human β-actin mRNA experiments.

Image analysis. Images were analyzed using Volocity software and NIH ImageJ. Volocity was used to deconvolve the widefield images (2D and full-iterative), reconstruct the images in three dimensions, identify individual probes based on intensity and measure the mean intensity within granules of all sizes. It was also used to perform the three-dimensional co-localization calculations of Manders coefficient. The Color Profiler tool in ImageJ was used to obtain profile data for the intensity plots from the merged images.

Live-dead assay. To asses the effects of streptolysin O, and the Invitrogen L-3224 Live/Dead Viability/Cytotoxicity kit for mammalian cells was used as per the manufacturers instructions. The images were taken on a Zeiss 200M widefield epi-fluorescence microscope with an LD Plan-Neofluar ×20, NA = 0.4 objective, Hamamatsu ORCA ER-AG camera, and appropriate filter sets described above.

14. Conover, W.J. *Practical Nonparametric Statistics* 3rd edn. (Wiley, New York, 1999).
15. Kedersha, N. *et al. J. Cell Biol.* **151**, 1257–1268 (2000).

© 2009 Nature America, Inc. All rights reserved.

APPENDIX C

JOURNAL OF VIROLOGY, Dec. 2010, p. 12274–12284 Vol. 84, No. 23
0022-538X/10/$12.00 doi:10.1128/JVI.00260-10
Copyright © 2010, American Society for Microbiology. All Rights Reserved.

Respiratory Syncytial Virus Induces Host RNA Stress Granules To Facilitate Viral Replication▽

Michael E. Lindquist,[1] Aaron W. Lifland,[4] Thomas J. Utley,[2] Philip J. Santangelo,[4] and James E. Crowe, Jr.[1,2,3]*

Departments of Microbiology and Immunology[1] and Pediatrics[2] and the Vanderbilt Vaccine Center,[3] Vanderbilt University Medical Center, Nashville, Tennessee 37232, and Department of Biomedical Engineering, Georgia Institute of Technology and Emory University, Atlanta, Georgia 30332[4]

Received 4 February 2010/Accepted 8 September 2010

Mammalian cell cytoplasmic RNA stress granules are induced during various conditions of stress and are strongly associated with regulation of host mRNA translation. Several viruses induce stress granules during the course of infection, but the exact function of these structures during virus replication is not well understood. In this study, we showed that respiratory syncytial virus (RSV) induced host stress granules in epithelial cells during the course of infection. We also showed that stress granules are distinct from cytoplasmic viral inclusion bodies and that the RNA binding protein HuR, normally found in stress granules, also localized to viral inclusion bodies during infection. Interestingly, we demonstrated that infected cells containing stress granules also contained more RSV protein than infected cells that did not form inclusion bodies. To address the role of stress granule formation in RSV infection, we generated a stable epithelial cell line with reduced expression of the Ras-GAP SH3 domain-binding protein (G3BP) that displayed an inhibited stress granule response. Surprisingly, RSV replication was impaired in these cells compared to its replication in cells with intact G3BP expression. In contrast, knockdown of HuR by RNA interference did not affect stress granule formation or RSV replication. Finally, using RNA probes specific for RSV genomic RNA, we found that viral RNA predominantly localized to viral inclusion bodies but a small percentage also interacted with stress granules during infection. These results suggest that RSV induces a host stress granule response and preferentially replicates in host cells that have committed to a stress response.

Respiratory syncytial virus (RSV) is a leading cause of serious viral lower respiratory tract illness in infants and the elderly worldwide. The virus is a member of the *Paramyxoviridae* family, and the genome consists of a single-stranded, negative-sense RNA molecule that encodes 11 proteins. The ribonucleoprotein complex necessary for transcription and replication includes the nucleoprotein (N), the phosphoprotein (P), and the large polymerase protein (L). M2-1 and M2-2 are accessory proteins that are involved in transcription and replication, respectively (7). The fusion (F) protein, attachment protein (G), and small hydrophobic (SH) protein are found on the surface of infectious virions, while the matrix (M) protein locates inside the virion particle. Two nonstructural proteins (NS1 and NS2) are expressed in the cytoplasm of infected cells and appear to act as interferon antagonists during infection (36). The mechanisms by which the virus replicates and assembles in infected epithelial cells are incompletely understood.

A hallmark feature of RSV infection in epithelial cells is the formation of discrete collections of viral replication proteins that have been termed viral inclusion bodies (28). These cytoplasmic structures increase in size during the course of infection and have been shown to contain the N, P, M2-1, L, and M proteins (3, 9, 21). It is thought that N and P are the minimal requirements for inclusion body formation, since the expression of both of these proteins in the absence of virus infection induces the formation of inclusion bodies similar to those observed during infection (10). The host proteins Hsp70 and actin associate with RSV inclusion bodies (1), but a functional role for either of these proteins in inclusion bodies is unknown. Although a function has not been defined experimentally for inclusion bodies, it has been proposed that these structures may represent sites of replication and/or transcription for the virus (32).

Stress granules are host RNA cytoplasmic granules formed in cells in response to multiple types of environmental stress (14). The best-studied pathway for stress granule formation involves phosphorylation of the translation initiation factor eIF2α, leading to the accumulation of stalled translation preinitiation complexes (19). RNA transcripts are bound by mRNA binding proteins, including TIA-1, Ras-GAP SH3 domain-binding protein (G3BP), and HuR. Several translation factors, such as eIF4E and eIF3, are recruited to stress granules, resulting in protein-RNA complexes that form the contents of the granules (14). Stress granules can also be induced by an alternate mechanism that is independent of eIF2α phosphorylation via inactivation of the translation factors eIF4A or eIF4G (5, 25).

Many viruses are known to modulate host translation in order to facilitate viral protein production. In recent years, several viruses have been studied to monitor their effect on the host stress response. Viruses that are known to induce host stress granules include the paramyxovirus Sendai virus, the coronavirus mouse hepatitis virus, the alphavirus Semliki Forest virus, reovirus, and poliovirus (12, 24, 30, 34, 39). Although

* Corresponding author. Mailing address: The Vanderbilt Vaccine Center, Vanderbilt University Medical Center, T-2220 MCN, Nashville, TN 37232-2905. Phone: (615) 343-8064. Fax: (615) 343-4456. E-mail: james.crowe@vanderbilt.edu.

▽ Published ahead of print on 15 September 2010.

both poliovirus and Semliki Forest virus induce stress granules early after infection, both viruses appear to functionally inhibit stress granule formation at later time points. In addition, West Nile virus prevents stress granule formation throughout infection (6). While it is reasonable to think that stress granules may play a role in infection for these viruses, the specific role or function of stress granules during infection has not been well defined.

Stress granule proteins also have been shown to interact directly with viral processes. Sindbis virus and vaccinia virus recruit the stress granule protein G3BP to viral structures (4, 13), while West Nile virus interacts with the host stress granule proteins TIA-1 and TIAR (6). Sendai virus trailer RNAs have been shown to bind TIAR (12), and the poliovirus 3C proteinase has been shown to cleave G3BP (39). HuR has been shown to associate with regions of hepatitis C virus (HCV) RNA and the reverse transcriptase protein of human immunodeficiency virus (31, 35).

In the present study, we sought to determine whether the pneumovirus RSV initiates a stress response. Our results demonstrate that RSV induces a robust stress response that continues throughout the course of infection, indicating that RSV may specifically initiate and maintain the stress response. Interestingly, we show that cells that have formed stress granules contain more RSV protein than cells without stress granules. Our data show that, while RSV inclusion bodies are distinct from stress granules, the stress granule marker HuR appears to be a shared component between both structures. In addition, we created a stable cell line deficient for the stress granule assembly protein G3BP. RSV replication in these cells was diminished, offering further evidence that stress granule formation enhances RSV replication. Finally, we show that RSV genomic RNA is strongly associated with RSV inclusion bodies while only a transient interaction occurs with stress granules. This evidence suggests that RSV inclusion bodies and not host stress granules are the active sites of viral replication.

MATERIALS AND METHODS

Cells. HEp-2 cells (ATCC CCL-23) were maintained in Opti-MEM I medium (Invitrogen) containing 5% (vol/vol) fetal calf serum, 1% (vol/vol) L-glutamine, 2.5 μg/ml amphotericin B, and 50 μg/ml gentamicin. MA104 cells (ATCC CRL 2738.1), which were used to prepare rotavirus, and RGD3 and U2OS cells (kindly provided by Paul Anderson, Brigham and Women's Hospital) were maintained in Dulbecco's modified Eagle's medium (DMEM) containing 5% (vol/vol) fetal calf serum, 1% (vol/vol) sodium pyruvate, 1% (vol/vol) L-glutamine, 1% (vol/vol) nonessential amino acids, 2.5 μg/ml amphotericin B, and 50 μg/ml gentamicin.

Viruses. A suspension of RSV wild-type strain A2 prepared in HEp-2 cells (1×10^6 PFU/ml) was used to infect HEp-2 cell monolayer cultures. Infectious virus was adsorbed to the cells for 1 h in a 37°C incubator in 5% CO_2. Following adsorption, the inoculum was removed and fresh medium added. The cells were then incubated at 37°C in 5% CO_2 for the duration of the infection period. UV-inactivated virus was prepared from the same virus stock by irradiation in a UV cross-linker for 15 min. Rhesus rotavirus was a kind gift from Susana Lopez.

Fixation and immunostaining. Cells were fixed with 3.7% (wt/vol) paraformaldehyde in phosphate-buffered saline (PBS) for 10 min at room temperature. Cells were permeabilized with 0.2% (wt/vol) Triton X-100 and 3.7% paraformaldehyde in PBS for 10 min at room temperature. Following fixation, cells were blocked in 5% (wt/vol) bovine serum albumin (BSA) in PBS for 1 h, followed by the addition of the primary antibody for 1 h. Cells were then washed three times in PBS, and species-specific IgG Alexa Fluor (Molecular Probes) was added at a dilution of 1:1,000 in blocking solution to detect primary antibodies. Cells were washed 3 times in PBS and fixed on glass slides using a Prolong antifade kit (Molecular Probes). Images were obtained on a Zeiss inverted LSM510 confocal microscope using a 40× Plan-Neofluar oil objective lens. Polyclonal anti-G3BP (ab37906) antibody was obtained from Abcam and used for immunostaining. The following antibodies were obtained from Santa Cruz for immunostaining: polyclonal anti-TIA-1 (sc-1751), polyclonal anti-HuR (sc-20694), and polyclonal anti-eIF3η (sc-16377). Anti-RSV P protein (clone 3_5) and anti-RSV N protein (clone B130) monoclonal antibodies were a kind gift of Earling Norrby and Ewa Bjorling. An anti-RSV F protein humanized mouse monoclonal antibody (palivizumab; MedImmune) was obtained from the Vanderbilt Pharmacy. Imaging of the RNA with G3BP and RSV N protein was performed using a 63×/1.4 numerical aperture Plan-Apochromat objective using a Zeiss LSM 510 confocal microscope. For images where three-dimensional z-stacks were obtained, we collapsed the series of fields into an extended view using Volocity imaging software.

RT-PCR. HEp-2 cells were grown on 48-well plates and infected with RSV for the times indicated below. RNA was extracted using an RNeasy mini kit (Qiagen). Reverse transcriptase PCR (RT-PCR) was performed using a OneStep RT-PCR kit (Qiagen) and primer-probe combinations for RSV F, rotavirus VP3, or human glyceraldehyde-3-phosphate dehydrogenase (GAPDH). The normalized cycle threshold (ΔC_T) was calculated for each time point using the following formula: ΔC_T = RSV F C_T − GAPDH C_T. The change in normalized C_T over time ($\Delta\Delta C_T$) was calculated for each condition using the ΔC_T of wild-type cells 2 h postinfection (p.i.) as the initial point of reference for the relative amount of viral RNA: $\Delta\Delta C_T$ = [ΔC_T at x h p.i. ± shRNA] − [ΔC_T in wild-type cells 2 h p.i.], where x equals each specific time point.

shRNA reagents. A stable cell line exhibiting knockdown of HuR expression was generated using a set of three SMARTvector lentiviral small hairpin RNA (shRNA) particles (Dharmacon), along with cells treated with nontargeting shRNA particles. HEp-2 cells were plated into 48-well plates at approximately 50% confluence and transduced with the lentiviral particles according to the manufacturer's protocol. A panel of stable cell lines exhibiting knockdown of G3BP expression was generated using Mission shRNA lentiviral transduction particles (Sigma). HEp-2 cells were plated onto 6-well plates and transduced with lentiviral particles according to the manufacturer's protocol. For selection of each target, cells containing integrated lentivirus sequences were selected using puromycin (5 μg/ml) diluted in medium. Medium containing puromycin was replaced every 3 days until resistant colonies were observed. Puromycin-resistant colonies were isolated using cloning cylinders (Sigma) and tested for target protein expression.

Western blotting. HEp-2 cells were grown on 6-well plates and harvested for protein. Cell lysates were obtained using lysis buffer (50 mM Tris-HCl, 150 mM NaCl, 1% Triton X-100, pH 8.0) containing 0.5% (vol/vol) protease inhibitor cocktail (Sigma) and 1.0% (vol/vol) phosphatase inhibitors (Sigma). The lysates were separated on 4-to-12% NuPAGE bis-Tris gels (Invitrogen) and transferred to nitrocellulose membranes using an iBlot dry blotting system (Invitrogen). The membranes were blocked for 1 h using Odyssey blocking buffer (Li-Cor) diluted 1:1 in PBS. Primary antibodies were diluted in blocking buffer and incubated overnight at 4°C. The membranes were then washed four times in Tris-buffered saline plus 0.2% Tween (TBST) for 5 min each. Li-Cor IRDye 680CW or IRDye 800CW secondary antibodies were diluted 1:5,000 in blocking buffer and added to each membrane for 1 h. The membranes were washed four times in TBST. Bands were imaged and quantitated using an Odyssey infrared imaging system. G3BP protein was detected using a monoclonal antibody from BD Biosciences (611127). GAPDH was detected using a monoclonal antibody from Millipore (MAB374). HuR was detected using a monoclonal antibody from Santa Cruz Biotechnology (sc-5261).

RNA probe and live cell delivery. Single-RNA-sensitive probes (33) designed to target the gene start-intergenic region of the genomic RNA of human RSV were delivered at 30 nM via reversible permeabilization with streptolysin O into separate sets of infected or mock-infected HEp-2 cells at 1, 6, 12, 18, and 24 h p.i. Delivery took approximately 10 min, and 15 min after delivery, the cells were fixed with 3.7% (wt/vol) paraformaldehyde in PBS for 10 min at room temperature. The cells could then be immunostained for G3BP and the RSV N protein as discussed above.

Quantification of imaging. To determine quantitative features of stress granule induction by RSV, HEp-2 cells were plated onto coverslips placed in wells of a 24-well plate. Cells were grown to approximately 75% confluence and were infected with RSV for 0, 6, 12, 16, 20, or 24 h (multiplicity of infection [MOI] of 1). Cells were fixed as described above. Cells were stained with anti-G3BP antibody (BD Transduction Laboratories) diluted 1:1,000 in blocking solution, the anti-RSV F protein antibody palivizumab (MedImmune) diluted 1:10,000 in blocking solution, and the nuclear stain To-Pro-3 iodide (Invitrogen) diluted 1:1,000 in blocking solution for 1 h. Twenty high-powered fields (HPFs) were obtained for each time point. Images were examined using Volocity imaging

software (version 5.1; Improvision). The total number of cells in each HPF was quantified by counting the number of nuclei. We also quantified the number of infected cells by staining for the presence of RSV F protein, the number of cells containing stress granules by staining for the presence of G3BP protein, and the number of infected cells that also contained stress granules per HPF. To calculate the stress granule size in wild-type or G3BP-deficient cells, cells were plated onto coverslips placed in wells of a 24-well plate. The cells were then treated with 0.5 mM arsenite for 15 min. The cells were fixed and stained for G3BP (1:500) and TIA-1 (1:250). Images for 10 HPFs were obtained for each cell line. We then used Volocity imaging software to determine the percentage of cells with stress granules per HPF and the size of each stress granule for those cells containing stress granules. To determine inclusion body number and volume, HEp-2 cells were placed on coverslips in 24-well plates. Cells were infected with RSV for 24 h (MOI = 1.0) and fixed. Cells were stained for inclusion bodies using anti-RSV P protein antibody and for stress granules using anti-G3BP antibody. At least 10 cells containing or not containing stress granules were analyzed for inclusion bodies. Volocity imaging software was used to determine the number and volume of individual inclusion bodies per cell. Volocity was also used to quantify the colocalization of the viral genomic RNA with inclusion bodies (marked by the RSV N protein) or with stress granules, in addition to the colocalization of inclusion bodies with stress granules. Manders overlap coefficients were calculated using voxels generated from three-dimensional reconstructions.

RESULTS

RSV infection induces stress granule formation. We first tested whether RSV infection of epithelial cells induced stress granules. HEp-2 cell monolayer cultures were inoculated with RSV wild-type strain A2 at an MOI of 1 and incubated in liquid medium for 24 h. We then fixed the cells and immunostained them for the stress granule proteins G3BP, eIF3η, or TIA-1. The results in Fig. 1A (first column) show that each of these markers frequently relocalized into dense cytoplasmic foci that are characteristic of stress granules. We noted that the host stress granules appeared similar in size, shape, and location to previously described viral inclusion bodies that form during RSV infection. To investigate whether the granules containing stress granule-associated proteins were viral inclusion bodies, we costained infected cells with antibodies to stress granule markers and one of the viral proteins found in inclusion bodies (RSV P protein) (Fig. 1A, middle column). The results indicate that viral inclusion bodies are spatially separated from stress granules and represent distinct structures in the cytoplasm.

We next performed a time course of infection to determine the kinetics of stress granule formation in RSV-infected cells. We inoculated cells with RSV (MOI = 1) and then incubated them for various times (0 to 24 h). We fixed and immunostained cells for RSV F protein and the stress granule protein marker G3BP. After 12 h, stress granules formed, and the number of infected cells containing stress granules increased incrementally throughout the 24-h period of observation (Fig. 1B). We did not observe stress granules in mock-infected cells over the time course. In addition, in the cultures in which RSV was added, we did not observe stress granules in cells that did not stain for RSV protein (data not shown). These results demonstrated that RSV induces a potent stress granule response beginning at about 12 h after inoculation and continuing throughout the viral life cycle. In order to verify that RSV replication is necessary for stress granule formation, we mock inoculated cells, inoculated cells with replication-competent RSV (MOI = 1.0), or inoculated cells with an equivalent volume of UV-inactivated RSV for 48 h and then fixed and immunostained them for RSV F and G3BP. RSV infection once again induced robust stress granule formation (Fig. 2, bottom row), while we did not observe stress granules in mock-inoculated or UV-inactivated RSV-inoculated samples (Fig. 2, top and middle rows). These results confirmed that RSV replication and not simply the presence of RSV protein is required for stress granule formation.

We next compared RSV protein levels between cells with and without stress granules. HEp-2 cells were inoculated with RSV (MOI = 1.0) for 24 h and then fixed and immunostained for RSV P and G3BP. We used RSV inclusion body size and number as a measure to compare the amounts of viral protein present in cells. Interestingly, the results indicated that infected cells that have formed stress granules contain more inclusion bodies than cells that have not formed stress granules (Fig. 3A). In addition, individual inclusion bodies were larger in cells that had formed stress granules (Fig. 3B) and the total amount of protein contained in inclusion bodies was greater (Fig. 3C). Although quantification of the size and number of inclusion bodies in infected cells in the cultures clearly showed larger and more inclusion bodies in cells with stress granules, we also did observe some individual cells without stress granules that contained large amounts of RSV protein (for example, two cells with high N expression in Fig. 7, at 12 h postinfection). These data suggested that stress granules enhance viral protein production and inclusion body formation but are not absolutely required for these viral processes.

Inhibition of host stress granule formation reduces RSV replication. To investigate whether stress granule formation is beneficial to the virus or the host, we inoculated mouse embryo fibroblast (MEF) lines derived from TIA-1- or TIAR-deficient mice (kindly provided by Paul Anderson); however, RSV did not establish a productive infection in these cells (data not shown). It is well established that human RSV strains do not infect murine cells efficiently. Next, we created human cell lines deficient for stress granule formation by transducing HEp-2 cells with lentiviral shRNA transduction particles to induce stable knockdown of G3BP expression. When analyzed by Western blotting, G3BP was not detected in the knockdown cells (Fig. 4A). However, when these cells were compared with wild-type cells by immunofluorescence, we could still observe a small amount of G3BP in fixed and permeabilized knockdown cells. The G3BP-deficient cells expressed normal amounts of other stress granule proteins, such as TIA-1 (Fig. 4B). G3BP-deficient cells were treated with 0.5 mM arsenite for 15 min to determine if they were capable of forming stress granules. Stress granules were detected using anti-TIA-1 antibodies (Fig. 4C). We compared the percentages of cells with stress granules per high-powered field. In G3BP-deficient cells, approximately 75% fewer cells per HPF formed stress granules. We also examined individual G3BP knockdown cells that did form stress granules and noted that there was also a slight decrease in stress granule size compared to those in wild-type HEp-2 cells. These results indicated that G3BP-deficient cells are impaired for stress granule formation.

We next determined whether RSV replication was altered in the G3BP-deficient cell line. Wild-type or G3BP-deficient cells were infected with RSV (MOI = 1) for 1, 2, or 4 days. Cell-associated and supernatant virus were collected separately, and viral titers were determined using plaque assays. The G3BP-deficient cells consistently demonstrated a 10-fold reduction in

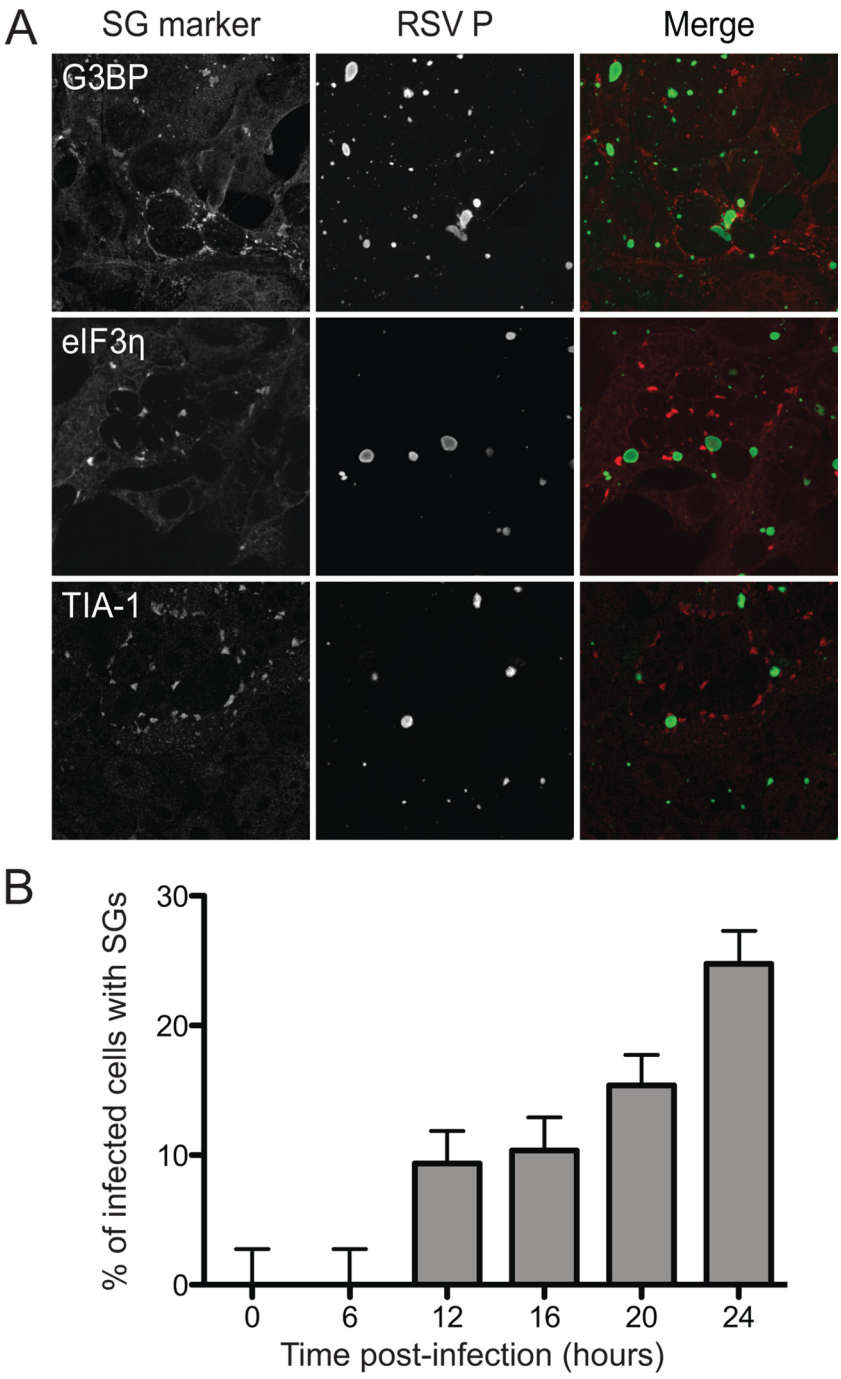

FIG. 1. Stress granules (SGs) are induced during RSV infection. (A) HEp-2 cells were infected with RSV (MOI = 1.0) for 24 h, fixed, and processed for immunofluorescence. Anti-G3BP, anti-eIF3η, and anti-TIA-1 were used as stress granule markers and appear red in the merged image. Anti-RSV P was used as the viral inclusion body marker and appears green in the merged image. The collapsed z-sections are shown for each image. (B) HEp-2 cells were infected with RSV (MOI = 1.0) for the indicated times. The percentages of infected cells and cells containing stress granules per HPF were quantified as described in Materials and Methods. Error bars show standard deviations.

viral titer when comparing supernatant or cell-associated virus with the titers collected from wild-type cells (Fig. 5A). In addition, RSV infection was associated with the death of most wild-type HEp-2 cells after 2 days, while in contrast, the G3BP-deficient cells consistently remained viable for 4 days after infection. We next sought to determine if the reduction of G3BP expression and stress granule formation affected the efficiency of replication of viral RNA. We infected wild-type or G3BP-deficient cells for 0, 2, 12, 24, or 48 h and then harvested total RNA from cell lysates. We performed reverse transcriptase PCR and normalized the RNA levels to that of host GAPDH and compared them with the levels found at 2 h

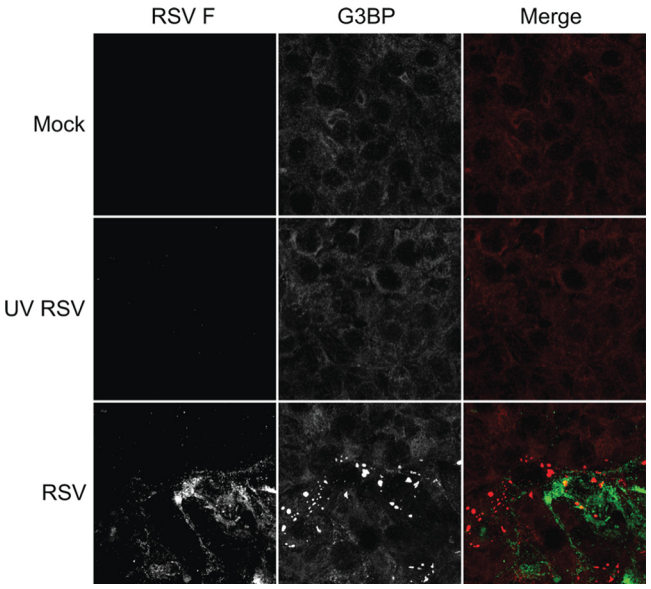

FIG. 2. RSV-induced stress granule formation is dependent on virus replication. HEp-2 cells mock infected (top row), inoculated with replication-competent RSV (MOI = 1.0), or inoculated with UV-inactivated RSV for 48 h were fixed and processed for immunofluorescence. Anti-G3BP was used as a marker for stress granules and appears red in the merged image. Anti-RSV F was used as a marker for viral infection and appears green in the merged image. The collapsed z-sections are shown for each image.

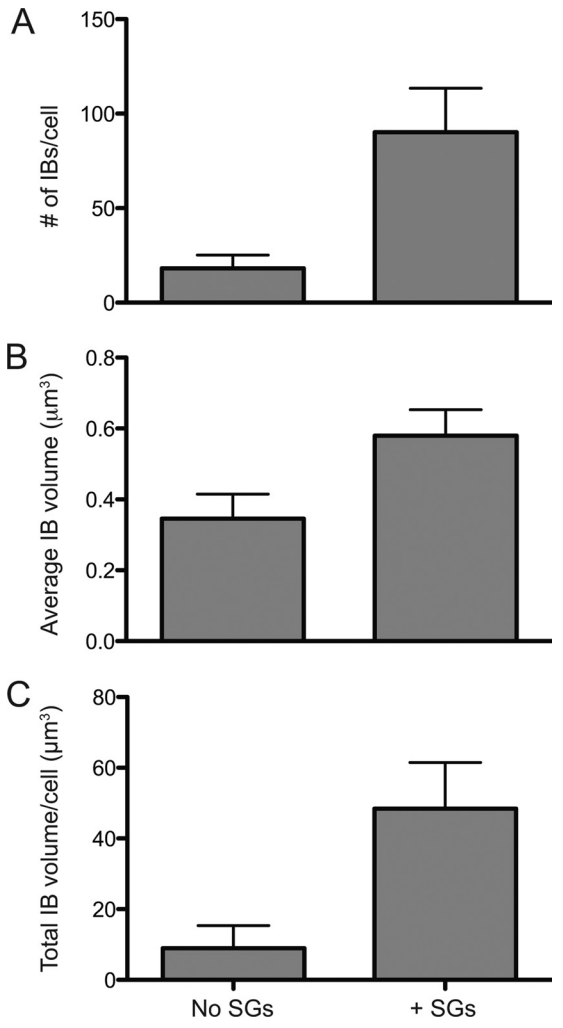

FIG. 3. RSV protein levels are higher in cells with stress granules. HEp-2 cells were infected with RSV (MOI = 1.0) for 24 h. At least 10 infected cells containing or not containing stress granules were analyzed. (A) The total average number of inclusion bodies (IBs) per cell was determined as described in Materials and Methods for cells containing stress granules (+SGs) or not containing stress granules (No SGs). (B) The average volumes (μm^3) of individual inclusion bodies were determined for cells containing or not containing stress granules. (C) The volumes of all individual inclusion bodies in single cells containing or not containing stress granules were totaled on a per cell basis to determine average total inclusion body volume per cell. Error bars show standard deviations.

postinfection in the wild-type HEp-2 cells. We observed a decrease in RSV RNA in the G3BP-deficient cell line at each time point tested after infection (Fig. 5B). Interestingly, when these cells were infected with rhesus rotavirus, a virus that does not induce stress granule formation (27), the replication of rotavirus was unaffected. These data indicate that stress granule formation may play an important role in the RSV life cycle even at very early time points after infection.

We also determined the effects of G3BP overexpression on RSV replication using RGD3 cells, a U2OS osteosarcoma cell line selected to express green fluorescent protein-G3BP. We inoculated RGD3 or parental U2OS cells with RSV (MOI = 1.0) and harvested cell-associated virus for plaque assays at time points spanning 0 to 4 days after inoculation. RSV replication remained largely unaltered in cells overexpressing G3BP (Fig. 5C). Interestingly, although G3BP levels are higher in RGD3 cells, stress granule formation is largely unaltered (18). These data indicated that the presence of artificially elevated levels of G3BP do not enhance replication.

The stress granule marker HuR is recruited to RSV inclusion bodies. We examined other markers of stress granules and found a nonclassical feature involving the mRNA binding stress granule protein HuR. In cells infected with RSV, HuR was recruited to stress granules during infection but the protein was also largely associated with structures that were not marked by other stress granule proteins. When cells were infected (MOI = 1) and costained for G3BP and viral proteins in RSV inclusion bodies, we noted that HuR was present both in host stress granules and in RSV inclusion bodies (Fig. 6A). Thus, HuR protein is a shared component of the two structures. Using RNA interference, we sought to determine the effect of decreased HuR expression on RSV replication. shRNA knockdown of HuR resulted in an approximately 70% reduction of HuR expression when compared by Western blotting to its expression in wild-type cells or cells transduced with a nontargeting shRNA (Fig. 6B). In contrast to G3BP knockdown, stress granule formation was not altered by HuR reduction when cells were treated with sodium arsenite (data not shown). To test whether HuR plays a role in RSV infection, we infected wild-type HEp-2- or HuR-deficient cells with RSV (MOI = 0.1) for 1, 2, 3, or 4 days. Supernatant and cell-associated virus were collected separately at each time point, and viral titers were determined by plaque assay. As shown by the results in Fig. 6D, we did not observe a significant change

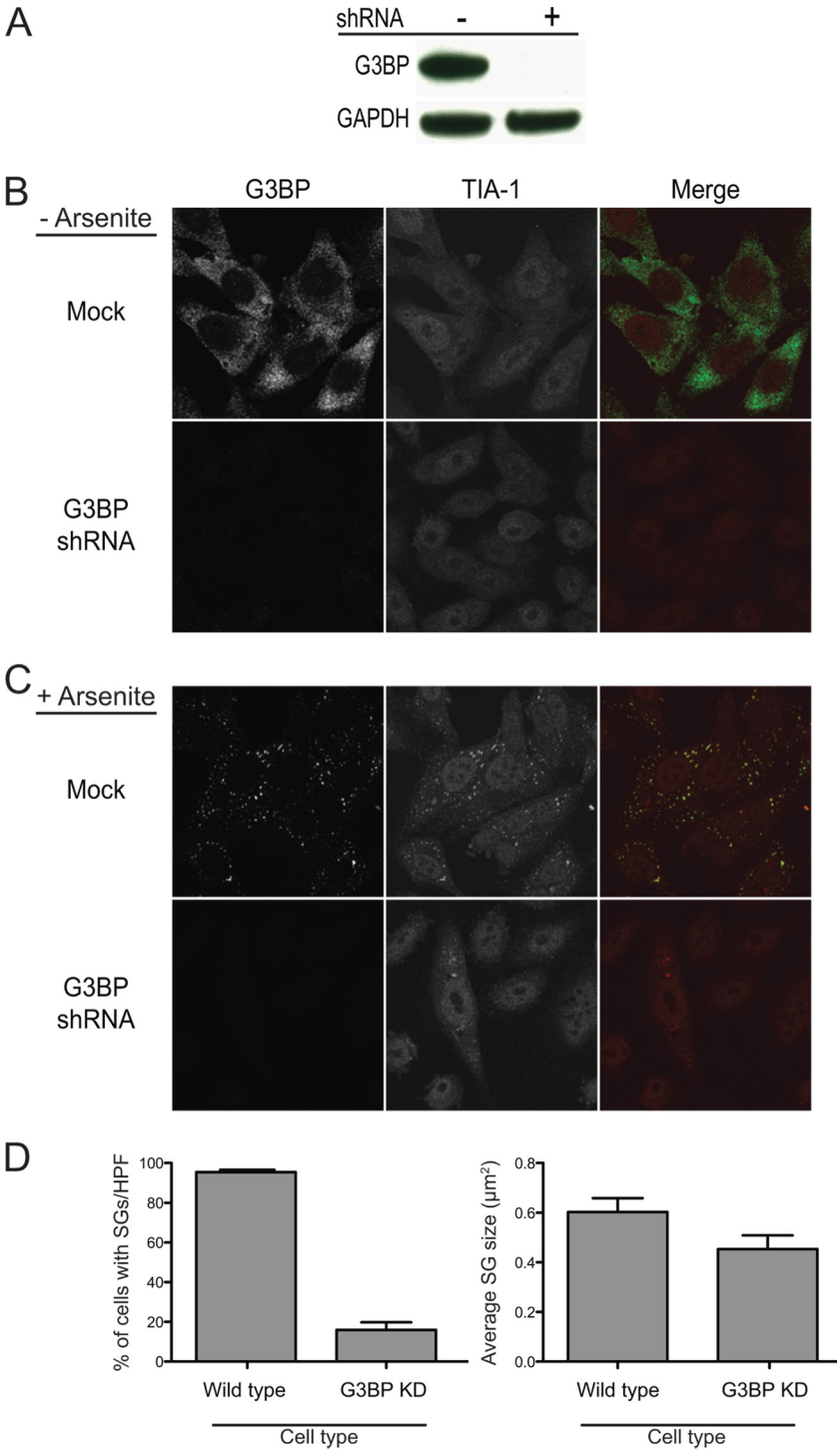

FIG. 4. Decreased levels of G3BP inhibit stress granule formation. (A) Wild-type or representative G3BP-deficient HEp-2 cells were analyzed for G3BP expression via Western blotting. (B) Wild-type or G3BP-deficient HEp-2 cells not treated with arsenite were analyzed for G3BP (green in merged image) and TIA-1 (red in merged image) expression using indirect immunofluorescence. (C) Wild-type or G3BP-deficient HEp-2 cells were treated with arsenite, fixed, and processed for immunofluorescence. Stress granule proteins were stained using anti-G3BP (green in merged image) and TIA-1 (red in merged image) antibodies. (D) Each cell type was examined for the percentage of cells containing stress granules per HPF and the size of stress granules per cell using TIA-1 as a marker for stress granules, as described in Materials and Methods. Error bars show standard deviations. KD, knockdown.

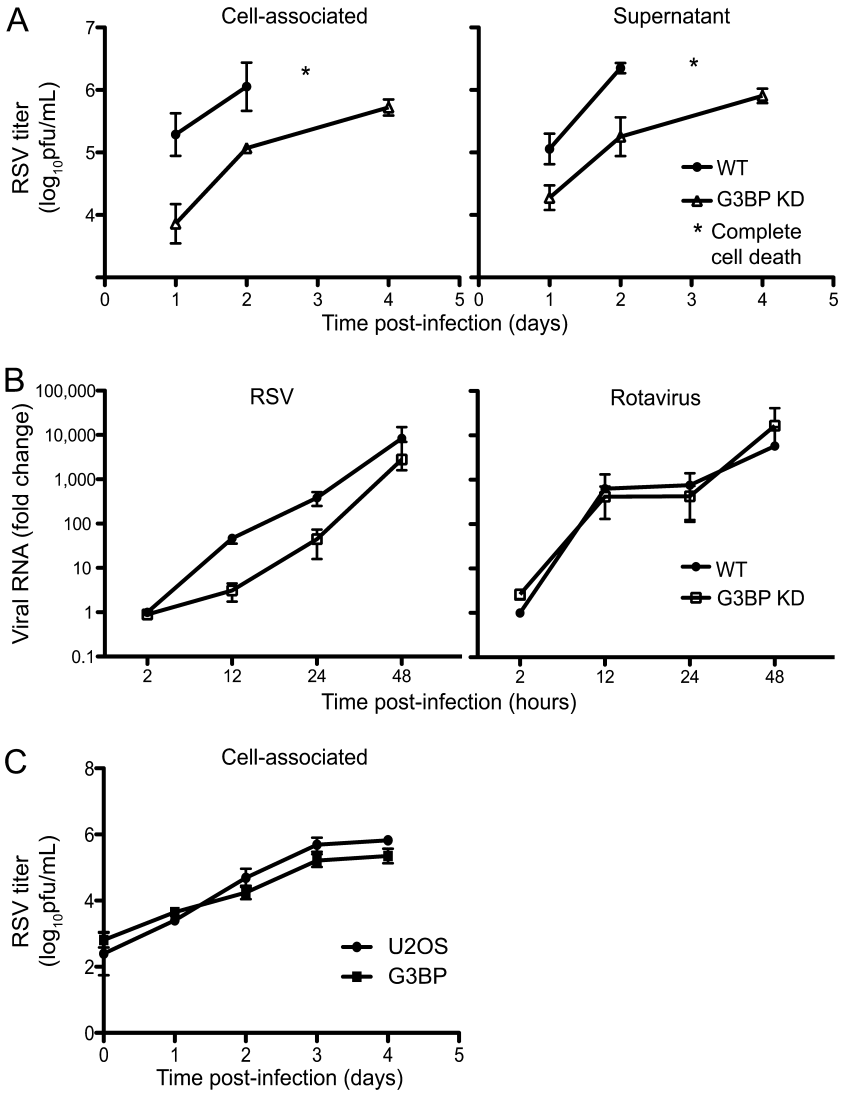

FIG. 5. RSV replication is inhibited in G3BP-deficient cells. (A) Wild-type (WT) or representative G3BP-deficient cells were infected with RSV (MOI = 1.0) for indicated times. Cell-associated or supernatant virus was collected at each time point. Viral titer for each sample was determined by plaque assay. (B) Wild-type or G3BP-deficient cells were infected with RSV or rotavirus for indicated times. Viral RNA was collected and assayed for fold change of RNA during infection. (C) Wild-type or G3BP-overexpressing cells derived from U2OS cells (RGD3) were infected with RSV (MOI = 1.0) for indicated times. Cell-associated virus was collected at each time point, and viral titer for each sample was determined by plaque assay. Error bars show standard deviations.

in viral titer for supernatant or cell-associated virus during infection in HuR-deficient cells. In addition, we monitored for any changes in RSV RNA levels. Wild-type or HuR-deficient cells were infected (MOI = 0.1) for the times stated above, and RNA was harvested. We again performed quantitative RNA studies. As shown by the results in Fig. 6C, we did not find significant differences in RSV RNA levels when HuR expression was reduced. These data, combined with our viral titer results, indicate that the wild-type level of HuR expression is not essential for viral replication even though a significant amount of HuR is recruited to inclusion bodies.

RSV genomic RNA is partially localized to stress granules. Previous reports using fluorescent molecular beacons specific for RSV genomic RNA suggested that RSV RNA could be found in RSV inclusion bodies during infection (32). In addition, more recent studies have shown that RSV RNA transiently interacts with arsenite-induced stress granules as well (33). Using a probe specific for RSV genomic RNA, we sought to determine whether RSV RNA could be found in RSV-induced stress granules, as well as RSV inclusion bodies. HEp-2 cells were infected with RSV (MOI = 1) for 1, 6, 12, and 24 h. After infection, cells were reversibly permeabilized with streptolysin O and incubated with fluorescently labeled RNA probes. Cells were then fixed with paraformaldehyde and stained with a monoclonal RSV N antibody to identify inclusion bodies and a monoclonal anti-G3BP antibody to identify stress granules (Fig. 7). Using confocal microscopy, we then examined the localization of viral RNA at each time point. We observed colocalization between RSV inclusion bodies and viral RNA at all time points, 1, 12, and 24 h after infection, as

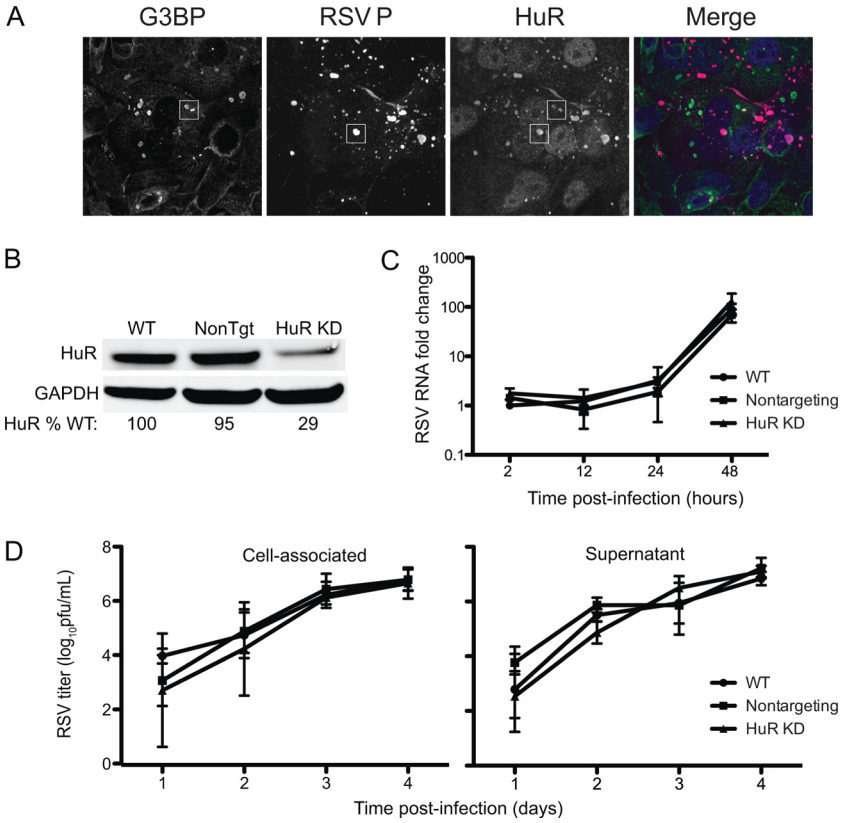

FIG. 6. HuR protein colocalizes with RSV inclusion bodies but is not necessary for replication. (A) HEp-2 cells were infected with RSV (MOI = 1.0) for 24 h, fixed, and prepared for immunofluorescence. Anti-G3BP was used to mark stress granules and appears green in the merged image. Anti-RSV P was used to mark RSV inclusion bodies and appears red in the merged image. HuR appears blue in the merged image. White squares are used to mark areas in which HuR is contained in stress granules or inclusion bodies, respectively. The collapsed z-sections are shown for each image. (B) Cells transduced with nontargeting (NonTgt) or HuR shRNA were compared with wild-type HEp-2 cells for expression levels of HuR. Total HuR levels were quantified for each cell type and compared to wild-type levels. (C) Wild-type HEp-2 cells, cells treated with nontargeting shRNA, or HuR-deficient cells were infected with RSV (MOI = 0.1) for the indicated times. Viral RNA was collected and assayed for the fold change in RNA levels during infection. (D) Wild-type or HuR-deficient cells were infected with RSV (MOI = 0.1) for the indicated times. Cell-associated virus and supernatant virus were collected at each time point. The viral titer for each sample was determined by plaque assay. Error bars show standard deviations.

shown in Fig. 7. Using Volocity imaging software, we determined the average Manders overlap coefficients for inclusion bodies with viral RNA, inclusion bodies with stress granules, and viral RNA with stress granules, utilizing three fields of approximately 35 cells (Table 1). For viral RNA and inclusion bodies, the Manders overlap coefficients were 0.87, 0.96, and 0.91 (87, 96, and 91% overlap) for 1, 12, and 24 h after infection, respectively. For the inclusion bodies with stress granules, the average Manders overlap coefficients were 0.0, 0.016, and 0.034 (0 [no stress granules], 1.6, and 3.4% overlap), likely representing a transient interaction. For the viral RNA with stress granules, the average Manders overlap coefficients were 0.0, 0.022, and 0.045 (0 [no stress granules], 2.2, and 4.5% overlap), also likely representing a transient interaction. In addition, we show the overlapping intensity profiles of the viral RNA, inclusion bodies, and stress granules (as visualized in intensity profiles in the fifth column of Fig. 7) to demonstrate the amount of colocalization between each. Single-plane confocal images from the middle of cells that best reveal stress granules did not always also capture optimal representation of inclusion bodies and viral RNA in that cell (for example, at 12 h p.i.). Therefore, we also provided merge images for these structures at the surface of the same cells (Fig. 7, sixth column).

DISCUSSION

These experiments show that inoculation of human cells with RSV induces stress granules within 12 h of inoculation, and the frequency of stress granules increases with the time since inoculation. Although stress granule formation typically is associated with translation inhibition, resulting in a potentially antiviral state, the findings here show that impairment of stress granule formation by G3BP knockdown reduces RSV replication. In addition, the presence of stress granules was associated with more robust viral protein expression on a per-cell basis. Our data also suggest that even though RSV induces stress granules and these structures contain many RNA binding proteins, the site of viral RNA production is in viral inclusion bodies and not stress granules.

Following attachment and entry, RSV begins its life cycle with gene transcription using an RNA-dependent viral RNA

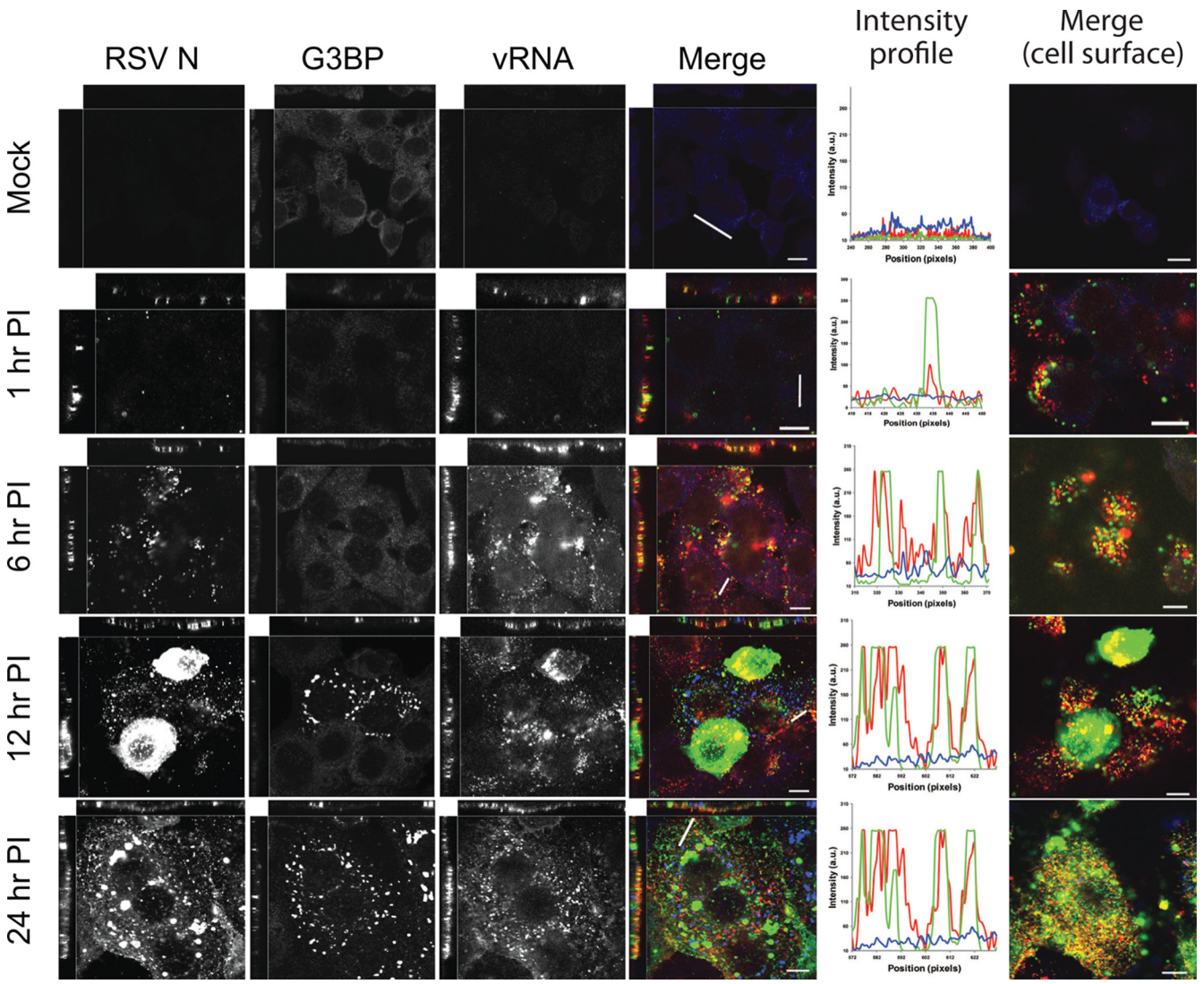

FIG. 7. Viral genomic RNA predominantly colocalizes with RSV inclusion bodies. HEp-2 cells were mock-infected or infected with RSV (MOI = 1) for the indicated times. RSV RNA-specific probes were added as described in Materials and Methods. Cells were fixed and processed for immunofluorescence. Anti-RSV N was used as an inclusion body marker and appears green in the merged image. Anti-G3BP was used as a stress granule marker and appears blue in the merged image. RSV RNA (vRNA) appears red in the merged image (fourth column). The main images are *xy* cross sections, and the images above and to the left represent *xz* and *yz* cross sections, respectively. The horizontal lines are scale bars, while the diagonal or vertical lines were used to calculate the intensity profiles. Intensity profiles at each time point demonstrate the strong correlation between the N protein and viral genomic RNA (fifth column). Images of N (green), viral genomic RNA (red), and G3BP (blue) in mock infection and at 1, 6, 12, and 24 h postinfection at an image plane near the cell surface are in the sixth column. PI, postinfection; a.u., absorbance units.

polymerase. Following the accumulation of viral mRNAs and proteins, the viral polymerase switches from a predominant mode of transcription of mRNAs to replication of the viral genome. Interestingly, our results indicate that stress granule formation begins approximately when RSV initiates this switch.

TABLE 1. RSV RNA is predominantly associated with viral inclusion bodies

Pair of structures analyzed	% Colocalization at time (h) postinfection		
	1	12	24
Viral RNA + inclusion bodies	87	96	91
Viral RNA + stress granules	0.0	2.2	4.5
Inclusion bodies + stress granules	0.0	1.6	3.4

G3BP was first described as an essential stress granule assembly protein through experiments that demonstrated that the overexpression of G3BP results in the spontaneous formation of stress granules (37). In more recent studies, cells in which G3BP expression was modestly reduced, by 30%, using transient small interfering RNA, transfected cells were treated with arsenite. In these experiments, large stress granules without G3BP could be observed in some cells, while other cells contained smaller and fewer stress granules (39). TIA-1 also has been proposed to be an essential stress granule assembly protein. Previous reports demonstrated that TIA-1 knockout mouse embryo fibroblasts treated with arsenite displayed a

diminished capacity to form stress granules (11). It has been proposed that these two proteins mediate stress granule formation in similar ways, because both proteins bind mRNA and both exhibit autoaggregation properties. Other stress granule proteins, such as TIAR (11) and HuR (our studies), have been knocked down but appear to have little effect on stress granule formation. It should be noted that G3BP plays a role in other cellular functions besides stress granule formation. G3BP has been well characterized as a binding partner for Ras GTPase-activating protein (RasGAP), a factor important in cellular proliferation pathways (29). In addition, G3BP is known to be an mRNA binding protein with an endoribonuclease function (8, 38). Thus, knockdown of G3BP may have other unknown consequences for viral replication independent of stress granule formation.

In addition to RSV, parainfluenza virus 5 and Sendai virus are two other paramyxoviruses that are known to induce stress granules (2, 12). In each case, stress granules were shown to be present at relatively late time points after infection (18 to 24 h). This finding is in contrast to results with other viruses, such as poliovirus and Semliki Forest virus, that induce stress granules early after infection but restrict stress granule assembly at later time points (24, 39). Thus, it is possible that stress granule formation enhances paramyxovirus replication during a portion of the viral life cycle. Further evidence of this enhancement comes from our results with G3BP-deficient cells. In these cells, stress granule formation was impaired and, consequently, viral replication was reduced. Other viruses, such as West Nile virus and vaccinia virus, recruit specific proteins involved in stress granule formation, such as TIA-1 and G3BP, respectively, to viral replication factories (6, 13). Our results show that neither TIA-1 nor G3BP associated with RSV RNA and neither protein was recruited to RSV inclusion bodies, which are the likely sites of viral replication.

HuR is a known mRNA binding protein thought to act as a translation enhancer. The protein typically binds AU-rich regions of the 3′ untranslated regions (UTR) of mRNAs and is a known component of stress granules (16). In addition, HuR has been shown to interact with elements of multiple viruses. HuR was shown to bind to the 3′ UTR of HCV (35). Knockdown of HuR resulted in a reduction of HCV replicon RNA (20), indicating a potential role in HCV replication. Recently, HuR was shown to interact with the HIV reverse transcriptase protein (31). When HuR was knocked down, HIV reverse transcription was impaired. Conversely, overexpression of HuR increased HIV reverse transcription. In our studies, although we observed HuR localization in viral inclusion bodies, knockdown of HuR by up to 70% did not affect viral replication. It is thus likely that HuR is not essential for RSV replication, or it is possible that modest levels of this protein can maintain such a role.

Interactions between viral RNA and stress granule proteins have been described. Previous studies have shown that Sendai virus RNA contains TIAR-binding sites, suggesting viral RNA interaction with stress granule proteins (12). The West Nile virus 3′-terminal stem-loop RNA binds TIA-1 and TIAR (22). In addition, we recently showed that RSV RNA interacts transiently with stress granules when infected cells are treated with arsenite (33). In these studies, individual granules of RSV RNA were observed to move into juxtaposition with stress granules, dock, and then separate again. We observed similar transient interactions between RSV RNA and stress granules here; however, our data suggest that viral genomic RNA is much more abundant in viral inclusion bodies.

A detailed understanding of the molecular mechanisms underlying stress granule effects during viral infection is lacking. In fact, evidence exists for both proviral and antiviral roles. When TIA-1 knockout cells that exhibit impaired stress granule formation were infected with vesicular stomatitis virus or Sindbis virus, both viruses grew to higher titers, indicating that TIA-1 or, possibly, stress granules are restrictive to these viruses (22). However, infection of TIAR knockout cells with West Nile virus resulted in decreased viral titers, suggesting a proviral role for this protein. It is important to note, however, that the functional role of stress granules in any sort of stress condition is still not completely understood. Stress granules have been proposed to be sites of mRNA sorting during periods of translation inhibition generated by a variety of stresses (15). While multiple species of mRNA have been shown to be associated with stress granules, this association appears to be transient in nature (17, 19, 23). More recent studies have suggested that mRNA cycles between the cytoplasm and stress granules and that the vast majority of cellular mRNA remains cytoplasmic, suggesting that these structures are neither a holding nor a modification site for mRNAs (26).

Our studies suggest a functional role for stress granules during RSV infection that enhances replication. Further experiments will need to be carried out to determine the exact mechanism of induction and the true role of these structures. The identification of a specific function of stress granules during viral infection could also elucidate a general function for these structures in the normal cell life cycle.

ACKNOWLEDGMENTS

Confocal microscopy imaging experiments were performed in the Vanderbilt Cell Imaging Shared Resources. We thank Paul Anderson for supplying U2OS and RGD3 cells.

This work was supported by a Burroughs Wellcome Fund Clinical Scientist Award in Translation Research (J.E.C.) and the March of Dimes.

REFERENCES

1. **Brown, G., H. W. Rixon, J. Steel, T. P. McDonald, A. R. Pitt, S. Graham, and R. J. Sugrue.** 2005. Evidence for an association between heat shock protein 70 and the respiratory syncytial virus polymerase complex within lipid-raft membranes during virus infection. Virology **338:**69–80.
2. **Carlos, T. S., D. F. Young, M. Schneider, J. P. Simas, and R. E. Randall.** 2009. Parainfluenza virus 5 genomes are located in viral cytoplasmic bodies whilst the virus dismantles the interferon-induced antiviral state of cells. J. Gen. Virol. **90:**2147–2156.
3. **Carromeu, C., F. M. Simabuco, R. E. Tamura, L. E. Farinha Arcieri, and A. M. Ventura.** 2007. Intracellular localization of human respiratory syncytial virus L protein. Arch. Virol. **152:**2259–2263.
4. **Cristea, I. M., J. W. Carroll, M. P. Rout, C. M. Rice, B. T. Chait, and M. R. MacDonald.** 2006. Tracking and elucidating alphavirus-host protein interactions. J. Biol. Chem. **281:**30269–30278.
5. **Dang, Y., N. Kedersha, W. K. Low, D. Romo, M. Gorospe, R. Kaufman, P. Anderson, and J. O. Liu.** 2006. Eukaryotic initiation factor 2alpha-independent pathway of stress granule induction by the natural product pateamine A. J. Biol. Chem. **281:**32870–32878.
6. **Emara, M. M., and M. A. Brinton.** 2007. Interaction of TIA-1/TIAR with West Nile and dengue virus products in infected cells interferes with stress granule formation and processing body assembly. Proc. Natl. Acad. Sci. U. S. A. **104:**9041–9046.
7. **Fields, B. N., D. M. Knipe, and P. M. Howley.** 2007. Fields virology, 5th ed. Lippincott Williams & Wilkins, Philadelphia, PA.
8. **Gallouzi, I. E., F. Parker, K. Chebli, F. Maurier, E. Labourier, I. Barlat, J. P. Capony, B. Tocque, and J. Tazi.** 1998. A novel phosphorylation-dependent

RNase activity of GAP-SH3 binding protein: a potential link between signal transduction and RNA stability. Mol. Cell. Biol. **18:**3956–3965.
9. **Garcia, J., B. Garcia-Barreno, A. Vivo, and J. A. Melero.** 1993. Cytoplasmic inclusions of respiratory syncytial virus-infected cells: formation of inclusion bodies in transfected cells that coexpress the nucleoprotein, the phosphoprotein, and the 22K protein. Virology **195:**243–247.
10. **Garcia-Barreno, B., T. Delgado, and J. A. Melero.** 1996. Identification of protein regions involved in the interaction of human respiratory syncytial virus phosphoprotein and nucleoprotein: significance for nucleocapsid assembly and formation of cytoplasmic inclusions. J. Virol. **70:**801–808.
11. **Gilks, N., N. Kedersha, M. Ayodele, L. Shen, G. Stoecklin, L. M. Dember, and P. Anderson.** 2004. Stress granule assembly is mediated by prion-like aggregation of TIA-1. Mol. Biol. Cell **15:**5383–5398.
12. **Iseni, F., D. Garcin, M. Nishio, N. Kedersha, P. Anderson, and D. Kolakofsky.** 2002. Sendai virus trailer RNA binds TIAR, a cellular protein involved in virus-induced apoptosis. EMBO J. **21:**5141–5150.
13. **Katsafanas, G. C., and B. Moss.** 2007. Colocalization of transcription and translation within cytoplasmic poxvirus factories coordinates viral expression and subjugates host functions. Cell Host Microbe **2:**221–228.
14. **Kedersha, N., and P. Anderson.** 2007. Mammalian stress granules and processing bodies. Methods Enzymol. **431:**61–81.
15. **Kedersha, N., and P. Anderson.** 2002. Stress granules: sites of mRNA triage that regulate mRNA stability and translatability. Biochem. Soc. Trans. **30:**963–969.
16. **Kedersha, N., S. Chen, N. Gilks, W. Li, I. J. Miller, J. Stahl, and P. Anderson.** 2002. Evidence that ternary complex (eIF2-GTP-tRNA(iMet))-deficient preinitiation complexes are core constituents of mammalian stress granules. Mol. Biol. Cell **13:**195–210.
17. **Kedersha, N., G. Stoecklin, M. Ayodele, P. Yacono, J. Lykke-Andersen, M. J. Fritzler, D. Scheuner, R. J. Kaufman, D. E. Golan, and P. Anderson.** 2005. Stress granules and processing bodies are dynamically linked sites of mRNP remodeling. J. Cell Biol. **169:**871–884.
18. **Kedersha, N., S. Tisdale, T. Hickman, and P. Anderson.** 2008. Real-time and quantitative imaging of mammalian stress granules and processing bodies. Methods Enzymol. **448:**521–552.
19. **Kedersha, N. L., M. Gupta, W. Li, I. Miller, and P. Anderson.** 1999. RNA-binding proteins TIA-1 and TIAR link the phosphorylation of eIF-2 alpha to the assembly of mammalian stress granules. J. Cell Biol. **147:**1431–1442.
20. **Korf, M., D. Jarczak, C. Beger, M. P. Manns, and M. Kruger.** 2005. Inhibition of hepatitis C virus translation and subgenomic replication by siRNAs directed against highly conserved HCV sequence and cellular HCV cofactors. J. Hepatol. **43:**225–234.
21. **Li, D., D. A. Jans, P. G. Bardin, J. Meanger, J. Mills, and R. Ghildyal.** 2008. Association of respiratory syncytial virus M protein with viral nucleocapsids is mediated by the M2-1 protein. J. Virol. **82:**8863–8870.
22. **Li, W., Y. Li, N. Kedersha, P. Anderson, M. Emara, K. M. Swiderek, G. T. Moreno, and M. A. Brinton.** 2002. Cell proteins TIA-1 and TIAR interact with the 3′ stem-loop of the West Nile virus complementary minus-strand RNA and facilitate virus replication. J. Virol. **76:**11989–12000.
23. **Mazroui, R., S. Di Marco, R. J. Kaufman, and I. E. Gallouzi.** 2007. Inhibition of the ubiquitin-proteasome system induces stress granule formation. Mol. Biol. Cell **18:**2603–2618.
24. **McInerney, G. M., N. L. Kedersha, R. J. Kaufman, P. Anderson, and P. Liljestrom.** 2005. Importance of eIF2alpha phosphorylation and stress granule assembly in alphavirus translation regulation. Mol. Biol. Cell **16:**3753–3763.
25. **Mokas, S., J. R. Mills, C. Garreau, M. J. Fournier, F. Robert, P. Arya, R. J. Kaufman, J. Pelletier, and R. Mazroui.** 2009. Uncoupling stress granule assembly and translation initiation inhibition. Mol. Biol. Cell **20:**2673–2683.
26. **Mollet, S., N. Cougot, A. Wilczynska, F. Dautry, M. Kress, E. Bertrand, and D. Weil.** 2008. Translationally repressed mRNA transiently cycles through stress granules during stress. Mol. Biol. Cell **19:**4469–4479.
27. **Montero, H., M. Rojas, C. F. Arias, and S. Lopez.** 2008. Rotavirus infection induces the phosphorylation of eIF2alpha but prevents the formation of stress granules. J. Virol. **82:**1496–1504.
28. **Norrby, E., H. Marusyk, and C. Orvell.** 1970. Morphogenesis of respiratory syncytial virus in a green monkey kidney cell line (Vero). J. Virol. **6:**237–242.
29. **Parker, F., F. Maurier, I. Delumeau, M. Duchesne, D. Faucher, L. Debussche, A. Dugue, F. Schweighoffer, and B. Tocque.** 1996. A Ras-GTPase-activating protein SH3-domain-binding protein. Mol. Cell. Biol. **16:**2561–2569.
30. **Raaben, M., M. J. Groot Koerkamp, P. J. Rottier, and C. A. de Haan.** 2007. Mouse hepatitis coronavirus replication induces host translational shutoff and mRNA decay, with concomitant formation of stress granules and processing bodies. Cell Microbiol. **9:**2218–2229.
31. **Rivas-Aravena, A., P. Ramdohr, M. Vallejos, F. Valiente-Echeverria, V. Dormoy-Raclet, F. Rodriguez, K. Pino, C. Holzmann, J. P. Huidobro-Toro, I. E. Gallouzi, and M. Lopez-Lastra.** 2009. The Elav-like protein HuR exerts translational control of viral internal ribosome entry sites. Virology **392:**178–185.
32. **Santangelo, P., N. Nitin, L. LaConte, A. Woolums, and G. Bao.** 2006. Live-cell characterization and analysis of a clinical isolate of bovine respiratory syncytial virus, using molecular beacons. J. Virol. **80:**682–688.
33. **Santangelo, P. J., A. W. Lifland, P. Curt, Y. Sasaki, G. J. Bassell, M. E. Lindquist, and J. E. Crowe, Jr.** 2009. Single molecule-sensitive probes for imaging RNA in live cells. Nat. Methods **6:**347–349.
34. **Smith, J. A., S. C. Schmechel, A. Raghavan, M. Abelson, C. Reilly, M. G. Katze, R. J. Kaufman, P. R. Bohjanen, and L. A. Schiff.** 2006. Reovirus induces and benefits from an integrated cellular stress response. J. Virol. **80:**2019–2033.
35. **Spangberg, K., L. Wiklund, and S. Schwartz.** 2000. HuR, a protein implicated in oncogene and growth factor mRNA decay, binds to the 3′ ends of hepatitis C virus RNA of both polarities. Virology **274:**378–390.
36. **Spann, K. M., K. C. Tran, B. Chi, R. L. Rabin, and P. L. Collins.** 2004. Suppression of the induction of alpha, beta, and lambda interferons by the NS1 and NS2 proteins of human respiratory syncytial virus in human epithelial cells and macrophages [corrected]. J. Virol. **78:**4363–4369.
37. **Tourriere, H., K. Chebli, L. Zekri, B. Courselaud, J. M. Blanchard, E. Bertrand, and J. Tazi.** 2003. The RasGAP-associated endoribonuclease G3BP assembles stress granules. J. Cell Biol. **160:**823–831.
38. **Tourriere, H., I. E. Gallouzi, K. Chebli, J. P. Capony, J. Mouaikel, P. van der Geer, and J. Tazi.** 2001. RasGAP-associated endoribonuclease G3Bp: selective RNA degradation and phosphorylation-dependent localization. Mol. Cell. Biol. **21:**7747–7760.
39. **White, J. P., A. M. Cardenas, W. E. Marissen, and R. E. Lloyd.** 2007. Inhibition of cytoplasmic mRNA stress granule formation by a viral proteinase. Cell Host Microbe **2:**295–305.

REFERENCES

Anderson, P., Kedersha, N., 2002. Visibly stressed: the role of eIF2, TIA-1, and stress granules in protein translation. Cell Stress Chaperones 7, 213-221.

Andreassen, P.R., Margolis, R.L., 1994. Microtubule dependency of p34cdc2 inactivation and mitotic exit in mammalian cells. J Cell Biol 127, 789-802.

Arimoto, K., Fukuda, H., Imajoh-Ohmi, S., Saito, H., Takekawa, M., 2008. Formation of stress granules inhibits apoptosis by suppressing stress-responsive MAPK pathways. Nat Cell Biol 10, 1324-1332.

Atreya, P.L., Kulkarni, S., 1999. Respiratory syncytial virus strain A2 is resistant to the antiviral effects of type I interferons and human MxA. Virology 261, 227-241.

Awomoyi, A.A., Rallabhandi, P., Pollin, T.I., Lorenz, E., Sztein, M.B., Boukhvalova, M.S., Hemming, V.G., Blanco, J.C., Vogel, S.N., 2007. Association of TLR4 polymorphisms with symptomatic respiratory syncytial virus infection in high-risk infants and young children. J Immunol 179, 3171-3177.

Balachandran, S., Roberts, P.C., Brown, L.E., Truong, H., Pattnaik, A.K., Archer, D.R., Barber, G.N., 2000. Essential role for the dsRNA-dependent protein kinase PKR in innate immunity to viral infection. Immunity 13, 129-141.

Bermingham, A., Collins, P.L., 1999. The M2-2 protein of human respiratory syncytial virus is a regulatory factor involved in the balance between RNA replication and transcription. Proc Natl Acad Sci U S A 96, 11259-11264.

Boo, K.H., Yang, J.S., 2010. Intrinsic cellular defenses against virus infection by antiviral type I interferon. Yonsei Med J 51, 9-17.

Bowick, G.C., Fennewald, S.M., Elsom, B.L., Aronson, J.F., Luxon, B.A., Gorenstein, D.G., Herzog, N.K., 2006. Differential signaling networks induced by mild and lethal hemorrhagic fever virus infections. J Virol 80, 10248-10252.

Brown, G., Aitken, J., Rixon, H.W., Sugrue, R.J., 2002. Caveolin-1 is incorporated into mature respiratory syncytial virus particles during virus assembly on the surface of virus-infected cells. J Gen Virol 83, 611-621.

Brown, G., Rixon, H.W., Steel, J., McDonald, T.P., Pitt, A.R., Graham, S., Sugrue, R.J., 2005. Evidence for an association between heat shock protein 70 and the respiratory syncytial virus polymerase complex within lipid-raft membranes during virus infection. Virology 338, 69-80.

Buchan, J.R., Parker, R., 2009. Eukaryotic stress granules: the ins and outs of translation. Mol Cell 36, 932-941.

Burke, E., Dupuy, L., Wall, C., Barik, S., 1998. Role of cellular actin in the gene expression and morphogenesis of human respiratory syncytial virus. Virology 252, 137-148.

Burke, E., Mahoney, N.M., Almo, S.C., Barik, S., 2000. Profilin is required for optimal actin-dependent transcription of respiratory syncytial virus genome RNA. J Virol 74, 669-675.

Carlos, T.S., Young, D.F., Schneider, M., Simas, J.P., Randall, R.E., 2009. Parainfluenza virus 5 genomes are located in viral cytoplasmic bodies whilst the virus dismantles the interferon-induced antiviral state of cells. J Gen Virol 90, 2147-2156.

Carter, S.D., Dent, K.C., Atkins, E., Foster, T.L., Verow, M., Gorny, P., Harris, M., Hiscox, J.A., Ranson, N.A., Griffin, S., Barr, J.N., 2010. Direct visualization of the small hydrophobic protein of human respiratory syncytial virus reveals the structural basis for membrane permeability. FEBS Lett 584, 2786-2790.

Cristea, I.M., Carroll, J.W., Rout, M.P., Rice, C.M., Chait, B.T., MacDonald, M.R., 2006. Tracking and elucidating alphavirus-host protein interactions. J Biol Chem 281, 30269-30278.

Cuddihy, A.R., Wong, A.H., Tam, N.W., Li, S., Koromilas, A.E., 1999. The double-stranded RNA activated protein kinase PKR physically associates with the tumor suppressor p53 protein and phosphorylates human p53 on serine 392 in vitro. Oncogene 18, 2690-2702.

Dang, Y., Kedersha, N., Low, W.K., Romo, D., Gorospe, M., Kaufman, R., Anderson, P., Liu, J.O., 2006. Eukaryotic initiation factor 2alpha-independent pathway of stress granule induction by the natural product pateamine A. J Biol Chem 281, 32870-32878.

Eisinger-Mathason, T.S., Andrade, J., Groehler, A.L., Clark, D.E., Muratore-Schroeder, T.L., Pasic, L., Smith, J.A., Shabanowitz, J., Hunt, D.F., Macara, I.G., Lannigan, D.A., 2008. Codependent functions of RSK2 and the apoptosis-promoting factor TIA-1 in stress granule assembly and cell survival. Mol Cell 31, 722-736.

Elliott, J., Lynch, O.T., Suessmuth, Y., Qian, P., Boyd, C.R., Burrows, J.F., Buick, R., Stevenson, N.J., Touzelet, O., Gadina, M., Power, U.F., Johnston, J.A., 2007. Respiratory syncytial virus NS1 protein degrades STAT2 by using the Elongin-Cullin E3 ligase. J Virol 81, 3428-3436.

Emara, M.M., Brinton, M.A., 2007. Interaction of TIA-1/TIAR with West Nile and dengue virus products in infected cells interferes with stress granule formation and processing body assembly. Proc Natl Acad Sci U S A 104, 9041-9046.

Fearns, R., Collins, P.L., 1999. Role of the M2-1 transcription antitermination protein of respiratory syncytial virus in sequential transcription. J Virol 73, 5852-5864.

Feldman, S.A., Audet, S., Beeler, J.A., 2000. The fusion glycoprotein of human respiratory syncytial virus facilitates virus attachment and infectivity via an interaction with cellular heparan sulfate. J Virol 74, 6442-6447.

Fuentes, S., Tran, K.C., Luthra, P., Teng, M.N., He, B., 2007. Function of the respiratory syncytial virus small hydrophobic protein. J Virol 81, 8361-8366.

Gallouzi, I.E., Parker, F., Chebli, K., Maurier, F., Labourier, E., Barlat, I., Capony, J.P., Tocque, B., Tazi, J., 1998. A novel phosphorylation-dependent RNase activity of GAP-SH3 binding protein: a potential link between signal transduction and RNA stability. Mol Cell Biol 18, 3956-3965.

Garaigorta, U., Chisari, F.V., 2009. Hepatitis C virus blocks interferon effector function by inducing protein kinase R phosphorylation. Cell Host Microbe 6, 513-522.

Garcia, M.A., Gil, J., Ventoso, I., Guerra, S., Domingo, E., Rivas, C., Esteban, M., 2006. Impact of protein kinase PKR in cell biology: from antiviral to antiproliferative action. Microbiol Mol Biol Rev 70, 1032-1060.

Garcia, M.A., Meurs, E.F., Esteban, M., 2007. The dsRNA protein kinase PKR: virus and cell control. Biochimie 89, 799-811.

Gaur, U., Aggarwal, B.B., 2003. Regulation of proliferation, survival and apoptosis by members of the TNF superfamily. Biochem Pharmacol 66, 1403-1408.

Gilks, N., Kedersha, N., Ayodele, M., Shen, L., Stoecklin, G., Dember, L.M., Anderson, P., 2004. Stress granule assembly is mediated by prion-like aggregation of TIA-1. Mol Biol Cell 15, 5383-5398.

Goh, K.C., deVeer, M.J., Williams, B.R., 2000. The protein kinase PKR is required for p38 MAPK activation and the innate immune response to bacterial endotoxin. EMBO J 19, 4292-4297.

Gower, T.L., Pastey, M.K., Peeples, M.E., Collins, P.L., McCurdy, L.H., Hart, T.K., Guth, A., Johnson, T.R., Graham, B.S., 2005. RhoA signaling is required for respiratory syncytial virus-induced syncytium formation and filamentous virion morphology. J Virol 79, 5326-5336.

Gower, T.L., Peeples, M.E., Collins, P.L., Graham, B.S., 2001. RhoA is activated during respiratory syncytial virus infection. Virology 283, 188-196.

Groskreutz, D.J., Babor, E.C., Monick, M.M., Varga, S.M., Hunninghake, G.W., 2010. Respiratory syncytial virus limits alpha subunit of eukaryotic translation initiation factor 2 (eIF2alpha) phosphorylation to maintain translation and viral replication. J Biol Chem 285, 24023-24031.

Groskreutz, D.J., Monick, M.M., Powers, L.S., Yarovinsky, T.O., Look, D.C., Hunninghake, G.W., 2006. Respiratory syncytial virus induces TLR3 protein and protein

kinase R, leading to increased double-stranded RNA responsiveness in airway epithelial cells. J Immunol 176, 1733-1740.

Habjan, M., Pichlmair, A., Elliott, R.M., Overby, A.K., Glatter, T., Gstaiger, M., Superti-Furga, G., Unger, H., Weber, F., 2009. NSs protein of rift valley fever virus induces the specific degradation of the double-stranded RNA-dependent protein kinase. J Virol 83, 4365-4375.

Hanley, L.L., McGivern, D.R., Teng, M.N., Djang, R., Collins, P.L., Fearns, R., 2010. Roles of the respiratory syncytial virus trailer region: effects of mutations on genome production and stress granule formation. Virology 406, 241-252.

Harpen, M., Barik, T., Musiyenko, A., Barik, S., 2009. Mutational analysis reveals a noncontractile but interactive role of actin and profilin in viral RNA-dependent RNA synthesis. J Virol 83, 10869-10876.

Hornung, V., Schlender, J., Guenthner-Biller, M., Rothenfusser, S., Endres, S., Conzelmann, K.K., Hartmann, G., 2004. Replication-dependent potent IFN-alpha induction in human plasmacytoid dendritic cells by a single-stranded RNA virus. J Immunol 173, 5935-5943.

Hu, Y., Conway, T.W., 1993. 2-Aminopurine inhibits the double-stranded RNA-dependent protein kinase both in vitro and in vivo. J Interferon Res 13, 323-328.

Huang, S., Qu, L.K., Cuddihy, A.R., Ragheb, R., Taya, Y., Koromilas, A.E., 2003. Protein kinase inhibitor 2-aminopurine overrides multiple genotoxic stress-induced cellular pathways to promote cell survival. Oncogene 22, 3721-3733.

Iseni, F., Garcin, D., Nishio, M., Kedersha, N., Anderson, P., Kolakofsky, D., 2002. Sendai virus trailer RNA binds TIAR, a cellular protein involved in virus-induced apoptosis. EMBO J 21, 5141-5150.

Jeffree, C.E., Brown, G., Aitken, J., Su-Yin, D.Y., Tan, B.H., Sugrue, R.J., 2007. Ultrastructural analysis of the interaction between F-actin and respiratory syncytial virus during virus assembly. Virology 369, 309-323.

Johnson, S.A., Hunter, T., 2005. Kinomics: methods for deciphering the kinome. Nat Methods 2, 17-25.

Kallewaard, N.L., Bowen, A.L., Crowe, J.E., Jr., 2005. Cooperativity of actin and microtubule elements during replication of respiratory syncytial virus. Virology 331, 73-81.

Katsafanas, G.C., Moss, B., 2007. Colocalization of transcription and translation within cytoplasmic poxvirus factories coordinates viral expression and subjugates host functions. Cell Host Microbe 2, 221-228.

Kedersha, N., Anderson, P., 2002. Stress granules: sites of mRNA triage that regulate mRNA stability and translatability. Biochem Soc Trans 30, 963-969.

Kedersha, N., Anderson, P., 2007. Mammalian stress granules and processing bodies. Methods Enzymol 431, 61-81.

Kedersha, N., Chen, S., Gilks, N., Li, W., Miller, I.J., Stahl, J., Anderson, P., 2002. Evidence that ternary complex (eIF2-GTP-tRNA(i)(Met))-deficient preinitiation complexes are core constituents of mammalian stress granules. Mol Biol Cell 13, 195-210.

Kedersha, N., Stoecklin, G., Ayodele, M., Yacono, P., Lykke-Andersen, J., Fritzler, M.J., Scheuner, D., Kaufman, R.J., Golan, D.E., Anderson, P., 2005. Stress granules and processing bodies are dynamically linked sites of mRNP remodeling. J Cell Biol 169, 871-884.

Kedersha, N., Tisdale, S., Hickman, T., Anderson, P., 2008. Real-time and quantitative imaging of mammalian stress granules and processing bodies. Methods Enzymol 448, 521-552.

Kedersha, N.L., Gupta, M., Li, W., Miller, I., Anderson, P., 1999. RNA-binding proteins TIA-1 and TIAR link the phosphorylation of eIF-2 alpha to the assembly of mammalian stress granules. J Cell Biol 147, 1431-1442.

Kolobova, E., Efimov, A., Kaverina, I., Rishi, A.K., Schrader, J.W., Ham, A.J., Larocca, M.C., Goldenring, J.R., 2009. Microtubule-dependent association of AKAP350A and CCAR1 with RNA stress granules. Exp Cell Res 315, 542-555.

Korf, M., Jarczak, D., Beger, C., Manns, M.P., Kruger, M., 2005. Inhibition of hepatitis C virus translation and subgenomic replication by siRNAs directed against highly conserved HCV sequence and cellular HCV cofactors. J Hepatol 43, 225-234.

Krahling, V., Stein, D.A., Spiegel, M., Weber, F., Muhlberger, E., 2009. Severe acute respiratory syndrome coronavirus triggers apoptosis via protein kinase R but is resistant to its antiviral activity. J Virol 83, 2298-2309.

Kurt-Jones, E.A., Popova, L., Kwinn, L., Haynes, L.M., Jones, L.P., Tripp, R.A., Walsh, E.E., Freeman, M.W., Golenbock, D.T., Anderson, L.J., Finberg, R.W., 2000. Pattern recognition receptors TLR4 and CD14 mediate response to respiratory syncytial virus. Nat Immunol 1, 398-401.

Lafferty, E.I., Qureshi, S.T., Schnare, M., 2010. The role of toll-like receptors in acute and chronic lung inflammation. J Inflamm (Lond) 7, 57.

Langedijk, J.P., de Groot, B.L., Berendsen, H.J., van Oirschot, J.T., 1998. Structural homology of the central conserved region of the attachment protein G of respiratory syncytial virus with the fourth subdomain of 55-kDa tumor necrosis factor receptor. Virology 243, 293-302.

Levine, S., Klaiber-Franco, R., Paradiso, P.R., 1987. Demonstration that glycoprotein G is the attachment protein of respiratory syncytial virus. J Gen Virol 68 (Pt 9), 2521-2524.

Li, W., Li, Y., Kedersha, N., Anderson, P., Emara, M., Swiderek, K.M., Moreno, G.T., Brinton, M.A., 2002. Cell proteins TIA-1 and TIAR interact with the 3' stem-loop of the West Nile virus complementary minus-strand RNA and facilitate virus replication. J Virol 76, 11989-12000.

Lindquist, M.E., Lifland, A.W., Utley, T.J., Santangelo, P.J., Crowe, J.E., Jr., 2010. Respiratory syncytial virus induces host RNA stress granules to facilitate viral replication. J Virol.

Liu, P., Jamaluddin, M., Li, K., Garofalo, R.P., Casola, A., Brasier, A.R., 2007. Retinoic acid-inducible gene I mediates early antiviral response and Toll-like receptor 3 expression in respiratory syncytial virus-infected airway epithelial cells. J Virol 81, 1401-1411.

Lo, M.S., Brazas, R.M., Holtzman, M.J., 2005. Respiratory syncytial virus nonstructural proteins NS1 and NS2 mediate inhibition of Stat2 expression and alpha/beta interferon responsiveness. J Virol 79, 9315-9319.

Loving, C.L., Brockmeier, S.L., Ma, W., Richt, J.A., Sacco, R.E., 2006. Innate cytokine responses in porcine macrophage populations: evidence for differential recognition of double-stranded RNA. J Immunol 177, 8432-8439.

Matthews, S.P., Tregoning, J.S., Coyle, A.J., Hussell, T., Openshaw, P.J., 2005. Role of CCL11 in eosinophilic lung disease during respiratory syncytial virus infection. J Virol 79, 2050-2057.

Mazroui, R., Di Marco, S., Kaufman, R.J., Gallouzi, I.E., 2007. Inhibition of the ubiquitin-proteasome system induces stress granule formation. Mol Biol Cell 18, 2603-2618.

Mazroui, R., Sukarieh, R., Bordeleau, M.E., Kaufman, R.J., Northcote, P., Tanaka, J., Gallouzi, I., Pelletier, J., 2006. Inhibition of ribosome recruitment induces stress granule formation independently of eukaryotic initiation factor 2alpha phosphorylation. Mol Biol Cell 17, 4212-4219.

McInerney, G.M., Kedersha, N.L., Kaufman, R.J., Anderson, P., Liljestrom, P., 2005. Importance of eIF2alpha phosphorylation and stress granule assembly in alphavirus translation regulation. Mol Biol Cell 16, 3753-3763.

Minor, R.A., Limmon, G.V., Miller-DeGraff, L., Dixon, D., Andrews, D.M., Kaufman, R.J., Imani, F., 2010. Double-stranded RNA-activated protein kinase regulates early innate immune responses during respiratory syncytial virus infection. J Interferon Cytokine Res 30, 263-272.

Mokas, S., Mills, J.R., Garreau, C., Fournier, M.J., Robert, F., Arya, P., Kaufman, R.J., Pelletier, J., Mazroui, R., 2009. Uncoupling stress granule assembly and translation initiation inhibition. Mol Biol Cell 20, 2673-2683.

Mollet, S., Cougot, N., Wilczynska, A., Dautry, F., Kress, M., Bertrand, E., Weil, D., 2008. Translationally repressed mRNA transiently cycles through stress granules during stress. Mol Biol Cell 19, 4469-4479.

Monick, M.M., Yarovinsky, T.O., Powers, L.S., Butler, N.S., Carter, A.B., Gudmundsson, G., Hunninghake, G.W., 2003. Respiratory syncytial virus up-regulates TLR4 and sensitizes airway epithelial cells to endotoxin. J Biol Chem 278, 53035-53044.

Montero, H., Rojas, M., Arias, C.F., Lopez, S., 2008. Rotavirus infection induces the phosphorylation of eIF2alpha but prevents the formation of stress granules. J Virol 82, 1496-1504.

Murawski, M.R., Bowen, G.N., Cerny, A.M., Anderson, L.J., Haynes, L.M., Tripp, R.A., Kurt-Jones, E.A., Finberg, R.W., 2009. Respiratory syncytial virus activates innate immunity through Toll-like receptor 2. J Virol 83, 1492-1500.

Murphy, B.R., Sotnikov, A.V., Lawrence, L.A., Banks, S.M., Prince, G.A., 1990. Enhanced pulmonary histopathology is observed in cotton rats immunized with formalin-inactivated respiratory syncytial virus (RSV) or purified F glycoprotein and challenged with RSV 3-6 months after immunization. Vaccine 8, 497-502.

Ohn, T., Kedersha, N., Hickman, T., Tisdale, S., Anderson, P., 2008. A functional RNAi screen links O-GlcNAc modification of ribosomal proteins to stress granule and processing body assembly. Nat Cell Biol 10, 1224-1231.

Oshansky, C.M., Zhang, W., Moore, E., Tripp, R.A., 2009. The host response and molecular pathogenesis associated with respiratory syncytial virus infection. Future Microbiol 4, 279-297.

Parker, F., Maurier, F., Delumeau, I., Duchesne, M., Faucher, D., Debussche, L., Dugue, A., Schweighoffer, F., Tocque, B., 1996. A Ras-GTPase-activating protein SH3-domain-binding protein. Mol Cell Biol 16, 2561-2569.

Pastey, M.K., Crowe, J.E., Jr., Graham, B.S., 1999. RhoA interacts with the fusion glycoprotein of respiratory syncytial virus and facilitates virus-induced syncytium formation. J Virol 73, 7262-7270.

Piotrowska, J., Hansen, S.J., Park, N., Jamka, K., Sarnow, P., Gustin, K.E., 2010. Stable formation of compositionally unique stress granules in virus-infected cells. J Virol 84, 3654-3665.

Proud, C.G., 2005. eIF2 and the control of cell physiology. Semin Cell Dev Biol 16, 3-12.

Qin, Q., Hastings, C., Miller, C.L., 2009. Mammalian orthoreovirus particles induce and are recruited into stress granules at early times postinfection. J Virol 83, 11090-11101.

Raaben, M., Groot Koerkamp, M.J., Rottier, P.J., de Haan, C.A., 2007. Mouse hepatitis coronavirus replication induces host translational shutoff and mRNA decay, with concomitant formation of stress granules and processing bodies. Cell Microbiol 9, 2218-2229.

Radhakrishnan, A., Yeo, D., Brown, G., Myaing, M.Z., Iyer, L.R., Fleck, R., Tan, B.H., Aitken, J., Sanmun, D., Tang, K., Yarwood, A., Brink, J., Sugrue, R.J., 2010. Protein analysis of purified respiratory syncytial virus particles reveals an important role for heat shock protein 90 in virus particle assembly. Mol Cell Proteomics 9, 1829-1848.

Ramana, C.V., Grammatikakis, N., Chernov, M., Nguyen, H., Goh, K.C., Williams, B.R., Stark, G.R., 2000. Regulation of c-myc expression by IFN-gamma through Stat1-dependent and -independent pathways. EMBO J 19, 263-272.

Rivas-Aravena, A., Ramdohr, P., Vallejos, M., Valiente-Echeverria, F., Dormoy-Raclet, V., Rodriguez, F., Pino, K., Holzmann, C., Huidobro-Toro, J.P., Gallouzi, I.E., Lopez-Lastra, M., 2009. The Elav-like protein HuR exerts translational control of viral internal ribosome entry sites. Virology 392, 178-185.

Roberts, S.R., Compans, R.W., Wertz, G.W., 1995. Respiratory syncytial virus matures at the apical surfaces of polarized epithelial cells. J Virol 69, 2667-2673.

Rojas, M., Arias, C.F., Lopez, S., 2010. Protein kinase R is responsible for the phosphorylation of eIF2alpha in rotavirus infection. J Virol 84, 10457-10466.

Santangelo, P., Nitin, N., LaConte, L., Woolums, A., Bao, G., 2006. Live-cell characterization and analysis of a clinical isolate of bovine respiratory syncytial virus, using molecular beacons. J Virol 80, 682-688.

Santangelo, P.J., Lifland, A.W., Curt, P., Sasaki, Y., Bassell, G.J., Lindquist, M.E., Crowe, J.E., Jr., 2009. Single molecule-sensitive probes for imaging RNA in live cells. Nat Methods 6, 347-349.

Sherry, B., 2009. Rotavirus and reovirus modulation of the interferon response. J Interferon Cytokine Res 29, 559-567.

Silva, A.M., Whitmore, M., Xu, Z., Jiang, Z., Li, X., Williams, B.R., 2004. Protein kinase R (PKR) interacts with and activates mitogen-activated protein kinase kinase 6 (MKK6) in response to double-stranded RNA stimulation. J Biol Chem 279, 37670-37676.

Smith, J.A., Schmechel, S.C., Raghavan, A., Abelson, M., Reilly, C., Katze, M.G., Kaufman, R.J., Bohjanen, P.R., Schiff, L.A., 2006. Reovirus induces and benefits from an integrated cellular stress response. J Virol 80, 2019-2033.

Spangberg, K., Wiklund, L., Schwartz, S., 2000. HuR, a protein implicated in oncogene and growth factor mRNA decay, binds to the 3' ends of hepatitis C virus RNA of both polarities. Virology 274, 378-390.

Spann, K.M., Tran, K.C., Chi, B., Rabin, R.L., Collins, P.L., 2004. Suppression of the induction of alpha, beta, and lambda interferons by the NS1 and NS2 proteins of human respiratory syncytial virus in human epithelial cells and macrophages [corrected]. J Virol 78, 4363-4369.

Streitenfeld, H., Boyd, A., Fazakerley, J.K., Bridgen, A., Elliott, R.M., Weber, F., 2003. Activation of PKR by Bunyamwera virus is independent of the viral interferon antagonist NSs. J Virol 77, 5507-5511.

Tal, G., Mandelberg, A., Dalal, I., Cesar, K., Somekh, E., Tal, A., Oron, A., Itskovich, S., Ballin, A., Houri, S., Beigelman, A., Lider, O., Rechavi, G., Amariglio, N., 2004. Association between common Toll-like receptor 4 mutations and severe respiratory syncytial virus disease. J Infect Dis 189, 2057-2063.

Tekkanat, K.K., Maassab, H., Miller, A., Berlin, A.A., Kunkel, S.L., Lukacs, N.W., 2002. RANTES (CCL5) production during primary respiratory syncytial virus infection exacerbates airway disease. Eur J Immunol 32, 3276-3284.

Thorburn, J., Frost, J.A., Thorburn, A., 1994. Mitogen-activated protein kinases mediate changes in gene expression, but not cytoskeletal organization associated with cardiac muscle cell hypertrophy. J Cell Biol 126, 1565-1572.

Tourriere, H., Chebli, K., Zekri, L., Courselaud, B., Blanchard, J.M., Bertrand, E., Tazi, J., 2003. The RasGAP-associated endoribonuclease G3BP assembles stress granules. J Cell Biol 160, 823-831.

Tourriere, H., Gallouzi, I.E., Chebli, K., Capony, J.P., Mouaikel, J., van der Geer, P., Tazi, J., 2001. RasGAP-associated endoribonuclease G3Bp: selective RNA degradation and phosphorylation-dependent localization. Mol Cell Biol 21, 7747-7760.

Utley, T.J., Ducharme, N.A., Varthakavi, V., Shepherd, B.E., Santangelo, P.J., Lindquist, M.E., Goldenring, J.R., Crowe, J.E., Jr., 2008. Respiratory syncytial virus uses a Vps4-independent budding mechanism controlled by Rab11-FIP2. Proc Natl Acad Sci U S A 105, 10209-10214.

Virgin, H.W.t., Bassel-Duby, R., Fields, B.N., Tyler, K.L., 1988. Antibody protects against lethal infection with the neurally spreading reovirus type 3 (Dearing). J Virol 62, 4594-4604.

White, J.P., Cardenas, A.M., Marissen, W.E., Lloyd, R.E., 2007. Inhibition of cytoplasmic mRNA stress granule formation by a viral proteinase. Cell Host Microbe 2, 295-305.

Xie, X.H., Law, H.K., Wang, L.J., Li, X., Yang, X.Q., Liu, E.M., 2009. Lipopolysaccharide induces IL-6 production in respiratory syncytial virus-infected airway epithelial cells through the toll-like receptor 4 signaling pathway. Pediatr Res 65, 156-162.

Yoon, C.H., Lee, E.S., Lim, D.S., Bae, Y.S., 2009. PKR, a p53 target gene, plays a crucial role in the tumor-suppressor function of p53. Proc Natl Acad Sci U S A 106, 7852-7857.

Zhang, P., Samuel, C.E., 2007. Protein kinase PKR plays a stimulus- and virus-dependent role in apoptotic death and virus multiplication in human cells. J Virol 81, 8192-8200.